

Ninevah University  
College of Electronics Engineering



# **Metal Object Detection Using Deep Learning Algorithms for Medical Microwave Imaging**

**Narmeen Hussein Fathi AL\_Goyani**

**M.Sc. Dissertation in  
Communication Engineering**

**Supervised by**

**Ass. Prof. Dr. Dia M. Ali**

**Ass. Prof. Dr. Younis M. Abbosh**

# **Metal Object Detection Using Deep Learning Algorithms for Medical Microwave Imaging**

**Dissertation Submitted by**

**Narmeen Hussein Fathi AL\_Goyani**

To

The Council of College of Electronic Engineering

Ninevah University

In Partial Fulfillment of the Requirements for the Degree

of Master of Sciences

**In Communication Engineering**

**Supervised by**

**Ass. Prof. Dr. Dia M. Ali**

**Ass. Prof. Dr. Younis M. Abbosh**

2023 A.D.

1445 A.H

## ***Supervisor's Certification***

We certify that the dissertation entitled (**Metal Object Detection Using Deep Learning Algorithms for Medical Microwave Imaging**) was prepared by **Narmeen Hussein Fathi** under our supervision at the Department of Communication Engineering, Ninevah University, as a partial requirement for the Master of Science Degree in Communication En

Signature:

**Name:** Ass. Prof. Dr. Dia M. Ali

**Date:** / /2023

Signature:

**Name:** Ass. Prof. Dr. Younis M. Abbosh

**Date:** / /2023

## **Report of the Head of Department**

I certify that this dissertation was carried out in the Department of Communication Engineering. I nominate it to be forwarded for discussion.

Signature:

**Name:** Dr. Mahmud A. Mahmud

**Date:** / /2023

## **Report of Linguistic Reviewer**

I certify that the linguistic reviewer of this dissertation was carried out by amending is accepted linguistically and in expression.

Signature:

**Name:**

**Date:** / /2023

## **Report of the Head of Postgraduate Studies Committee**

According to the recommendations presented by the supervisors of this dissertation and the linguistic reviewer, I nominate this dissertation to be forwarded to the discussion.

Signature:

**Name:**

**Date:**   /   /2023

## **Acknowledgments**

Before anything, praise be to Allah, who has given me the fortitude and capacity to finish my thesis.

My best and deep gratitude to my supervisors Dr. Younis M. Abbosh and Dr. Dia M. Ali, for all of their help and support during the study process. They provided me with continual direction, helpful recommendations, consistent encouragement, and aid to me throughout the research time.

Additionally, I would like to thank the Communication Engineering department staff for teaching me the courses of post-graduate studies.

Last but not least, my sincere thanks also go to my family for their understanding, patience, and continuing support in every aspect of my life.

## **Abstract**

The detection of shrapnel in the human body is a medical imaging task that is typically performed using X-ray, computed tomography (CT), Ultrasounds, or magnetic resonance imaging (MRI) scans. These imaging techniques can provide detailed images of the internal organs and bones. However, those methods suffer from not distinguishing non-metallic shrapnel, causing ionizing radiation, not distinguishing between shrapnels and bones, and being time-consuming, respectively.

Medical microwave imaging is the method that involves the use of microwave electromagnetic waves to create images of the internal structures of the human body. It has the advantage of being non-invasive and safe. Microwave imaging can be combined with neural networks to enhance the analysis and interpretation of the collected microwave data.

In this research, the deep neural network was employed to identify the presence or absence, size, and location of shrapnel. To build a model, an electromagnetic simulator CST Microwave Studio is employed. The model consists of four layers (skin-fat- muscle- bone) with different conductivity and relative permittivity. Spherical shrapnel of different radii (5mm, 10mm, and 15mm) is supposed to be at various places in the model. The signal is directed at the model using a monopole ultra-wideband antenna, which is also used to pick up reflected signals. The transmitted signal operates in the frequency range of 1 GHz to 6 GHz. In order to determine whether shrapnel is present or not, its size, and where it is located, the collected signals are analyzed using a deep neural network.

It is important to select an appropriate design and learning algorithm for the neural network to produce the best results. MATLAB can be used to test various neural network designs and sizes and conclude on the best model.

The results were acquired utilizing the neural network with 90% success in shrapnel identification, 86% success in shrapnel sizing, and 78% success in shrapnel depth. Better results were obtained using CNN, where 99% success was reached in

determining the presence of the fragment and 88% in determining its size and location.

Overall, the combination of microwave imaging and neural networks, specifically CNNs, shows great potential in improving the accuracy and reliability of shrapnel detection systems, especially with a large amount of trained data. Further research and advancements in this field can lead to enhance medical imaging techniques and improved patient care.

## **Published Research**

N. H. Fathi, Y. M. Abbosh and D. M. Ali, "Hidden Object Recognition using Convolutional Neural Network," 2022 2nd International Seminar on Machine Learning, Optimization, and Data Science (ISMODE), Jakarta, Indonesia, 2022, pp. 596-600, doi: 10.1109/ISMODE56940.2022.10180920.

## TABLE OF CONTENTS

<b>Subject</b>		<b>Page</b>
Acknowledgments		<b>V</b>
Abstract		<b>VI</b>
Published Research		<b>VIII</b>
Table of Contents		<b>IX</b>
List of Tables		<b>XIII</b>
List of Figures		<b>XIV</b>
List of Abbreviations		<b>XVII</b>
List of Symbols		<b>XVIII</b>
<b>CHAPTER ONE – INTRODUCTION</b>		<b>1</b>
<b>1.1</b>	<b>Overview</b>	<b>1</b>
<b>1.2</b>	<b>Some Hidden Object Detection Techniques</b>	<b>1</b>
<b>1.2.1</b>	<b>X-rays</b>	<b>1</b>
<b>1.2.2</b>	<b>Magnetic Resonance Imaging</b>	<b>2</b>
<b>1.2.3</b>	<b>Computed Tomography</b>	<b>3</b>
<b>1.2.4</b>	<b>Ultrasound Imaging</b>	<b>3</b>
<b>1.2.5</b>	<b>Microwave Imaging</b>	<b>4</b>
<b>1.3</b>	<b>Literature Review</b>	<b>4</b>
<b>1.4</b>	<b>Aims of the Dissertation</b>	<b>7</b>
<b>1.5</b>	<b>Dissertation Layout</b>	<b>8</b>

<b>CHAPTER TWO – NEURAL NETWORKS AND MICROWAVE IMAGING SYSTEM</b>		<b>9</b>
<b>2.1</b>	<b>Neural Networks</b>	<b>9</b>
<b>2.2</b>	<b>Transfer Function</b>	<b>13</b>
<b>2.3</b>	<b>Feed-Forward Back Propagation</b>	<b>14</b>
<b>2.4</b>	<b>The Architecture of Neural Network</b>	<b>14</b>
<b>2.5</b>	<b>Training process</b>	<b>15</b>
<b>2.6</b>	<b>Deep Neural Network</b>	<b>16</b>
<b>2.7</b>	<b>Convolutional Neural Network</b>	<b>17</b>
<b>2.7.1</b>	<b>Convolutional Layer</b>	<b>17</b>
<b>2.7.2</b>	<b>Pooling Layer</b>	<b>18</b>
<b>2.7.3</b>	<b>Fully Connected Layer</b>	<b>19</b>
<b>2.7.4</b>	<b>Rectified Linear Unit Layer (RELU)</b>	<b>20</b>
<b>2.8</b>	<b>Deep Neural Network Structure Design</b>	<b>20</b>
<b>2.9</b>	<b>Microwave Imaging System</b>	<b>20</b>
<b>2.9.1</b>	<b>Microwave Imaging Methods</b>	<b>22</b>
<b>2.9.1.1</b>	<b>Matching Interface Imaging</b>	<b>23</b>
<b>2.9.1.2</b>	<b>Quantitative Imaging</b>	<b>23</b>
<b>2.9.1.3</b>	<b>Qualitative Imaging</b>	<b>24</b>
<b>2.9.2</b>	<b>Fundamentals of Microwave Imaging</b>	<b>24</b>
<b>2.9.2.1</b>	<b>Propagation of Electromagnetic Waves</b>	<b>24</b>
<b>2.9.2.2</b>	<b>Attenuation Constant</b>	<b>27</b>
<b>2.9.2.3</b>	<b>Skin Depth</b>	<b>27</b>
<b>2.9.2.4</b>	<b>Wave Impedance</b>	<b>27</b>

<b>2.9.3</b>	<b>Dielectric Properties of Biological Tissues</b>	<b>28</b>
<b>2.9.3.1</b>	<b>Debye Model</b>	<b>28</b>
<b>2.9.3.2</b>	<b>Cole - Cole Model</b>	<b>29</b>
<b>2.9.4</b>	<b>Microwave Energy Radiation Safety Issues</b>	<b>29</b>
<b>2.10</b>	<b>Types of Signals</b>	<b>29</b>
<b>2.10.1</b>	<b>Frequency Domain System</b>	<b>30</b>
<b>2.10.2</b>	<b>Time Domain Systems</b>	<b>30</b>
<b>2.11</b>	<b>UWB Imaging Technique</b>	<b>31</b>
<b>CHAPTER THREE – SIMULATIONS AND RESULTS OF MICROWAVE IMAGING SYSTEM</b>		<b>33</b>
<b>3.1</b>	<b>Introduction</b>	<b>33</b>
<b>3.2</b>	<b>UWB Antenna</b>	<b>33</b>
<b>3.3</b>	<b>CST Microwave Studio Software</b>	<b>36</b>
<b>3.4</b>	<b>Planar Monopole Antenna Design</b>	<b>37</b>
<b>3.5</b>	<b>Modeling Human Body Layers</b>	<b>42</b>
<b>3.6</b>	<b>Human Model Effect on Antenna Parameters</b>	<b>44</b>
<b>CHAPTER FOUR – NEURAL NETWORKS IMPLEMENTATION AND RESULTS</b>		<b>55</b>
<b>4.1</b>	<b>Introduction</b>	<b>55</b>
<b>4.2</b>	<b>Dataset Preparation for Homogenous Model</b>	<b>58</b>
<b>4.3</b>	<b>Deep Network Designer in MATLAB</b>	<b>59</b>
<b>4.4</b>	<b>One-Dimensional Locating of Shrapnel Using ANN</b>	<b>61</b>
<b>4.5</b>	<b>Two-Dimensional Locating of Shrapnel Using ANN</b>	<b>70</b>
<b>4.6</b>	<b>Convolutional Neural Network (CNN) Training Results for Shrapnel Detection</b>	<b>72</b>

<b>CHAPTER FIVE - CONCLUSIONS AND FUTURE WORK</b>		<b>79</b>
<b>5.1</b>	<b>Conclusions</b>	<b>79</b>
<b>5.2</b>	<b>Future Works</b>	<b>80</b>
<b>REFERENCES</b>		<b>81</b>
<b>Arabic Abstract</b>		

## LIST OF TABLES

<b>CHAPTER THREE – SIMULATIONS AND RESULTS OF MICROWAVE IMAGING SYSTEM</b>		
<b>Table</b>	<b>Title</b>	<b>Page</b>
<b>3.1</b>	Material properties of antenna design	<b>38</b>
<b>3.2</b>	Design parameters of the proposed antenna	<b>39</b>
<b>3.3</b>	The dimensions of the homogenous model	<b>44</b>
<b>3.4</b>	The electrical properties of a homogenous model	<b>44</b>
<b>CHAPTER FOUR – NEURAL NETWORKS IMPLEMENTATION AND RESULTS</b>		
<b>4.1</b>	Hypotheses and Rationale for shrapnel detection using a neural network.	<b>56</b>

## LIST OF FIGURES

<b>CHAPTER ONE–INTRODUCTION</b>		
<b>Figure</b>	<b>Title</b>	<b>Page</b>
<b>1.1</b>	Magnetic resonance imaging system	<b>2</b>
<b>CHAPTER TWO – NEURAL NETWORKS AND MICROWAVE IMAGING SYSTEM</b>		
<b>Figure</b>	<b>Title</b>	<b>Page</b>
<b>2.1</b>	Principle of an artificial neuron	<b>10</b>
<b>2.2</b>	(a) Single layer network, (b) Multiple layers network	<b>12</b>
<b>2.3</b>	(a) Recurrent network, (b) Mesh network	<b>13</b>
<b>2.4</b>	Common activation functions of neural networks	<b>13</b>
<b>2.5</b>	Architecture of CNN	<b>17</b>
<b>2.6</b>	Operation of the convolutional layer	<b>18</b>
<b>2.7</b>	Operation pooling layer	<b>19</b>
<b>2.8</b>	A schematic illustration of the microwave imaging system's components.	<b>21</b>
<b>CHAPTER THREE – SIMULATIONS AND RESULTS OF MICROWAVE IMAGING SYSTEM</b>		
<b>Figure</b>	<b>Title</b>	<b>Page</b>
<b>3.1</b>	The suggested antenna's geometry in (a) front and(b) back views. All measurements are in millimeters.	<b>38</b>
<b>3.2</b>	Simulated reflection coefficient results of UWB monopole antenna.	<b>40</b>
<b>3.3</b>	Simulated VSWR with frequency	<b>40</b>
<b>3.4</b>	3D Radiation plot at 2.2 GHz	<b>41</b>
<b>3.5</b>	The proposed antenna's radiation patterns, (a) H-plane, and (b)E-plane	<b>42</b>
<b>3.6</b>	The model (a) side view in CST, (b) cross-sectional view	<b>43</b>

<b>3.7</b>	Block representation of monopole antenna near simplified skin layer	<b>48</b>
<b>3.8</b>	Return loss of the monopole antenna in free space and with skin layer	<b>48</b>
<b>3.9</b>	Block representation of monopole antenna near simplified fat layer	<b>49</b>
<b>3.10</b>	Return loss of the monopole antenna in free space and with fat layer	<b>49</b>
<b>3.11</b>	Block representation of monopole antenna near simplified muscle layer	<b>50</b>
<b>3.12</b>	Return loss of the monopole antenna in free space and with muscle layer	<b>50</b>
<b>3.13</b>	Block representation of monopole antenna near simplified bone layer	<b>51</b>
<b>3.14</b>	Return loss of the monopole antenna in free space and with bone layer	<b>51</b>
<b>3.15</b>	Monopole antenna return loss in multilayer tissues (skin, fat, muscle and bone)	<b>52</b>
<b>3.16</b>	Block diagram of monopole antenna near layer of body model	<b>53</b>
<b>3.17</b>	Return loss of the monopole antenna with absence of body model	<b>53</b>
<b>3.18</b>	3D radiation pattern received from the model.	<b>54</b>
<b>3.19</b>	Received radiation pattern from the model (a) H-plane (b) E-plane	<b>54</b>
<b>CHAPTER FOUR – NEURAL NETWORKS IMPLEMENTATION AND RESULTS</b>		
<b>Figure</b>	<b>Title</b>	<b>Page</b>
<b>4.1</b>	The flow chart of process steps	<b>57</b>
<b>4.2</b>	Simulated reflection loss for three different sizes	<b>59</b>
<b>4.3</b>	Neural network start in MATLAB	<b>60</b>
<b>4.4</b>	Pattern recognition neural network to predict the presence of shrapnel	<b>63</b>
<b>4.5</b>	Cross entropy loss in training	<b>63</b>

<b>4.6</b>	Fitting neural network to predict the size of shrapnel	<b>65</b>
<b>4.7</b>	MSE in training process to predict size of shrapnel	<b>65</b>
<b>4.8</b>	MSE in training process to predict depth of shrapnel	<b>66</b>
<b>4.9</b>	Feedforward neural network construction	<b>67</b>
<b>4.10</b>	Error curves of training set and validation Set performance across epochs	<b>68</b>
<b>4.11</b>	Regression in feedforward neural network	<b>69</b>
<b>4.12</b>	Training performance of pattern recognition neural network	<b>70</b>
<b>4.13</b>	Training performance for predicting the size of shrapnel	<b>71</b>
<b>4.14</b>	Training performance for predicting the depth of shrapnel	<b>71</b>
<b>4.15</b>	Samples from the labeled data set in Excel	<b>75</b>
<b>4.16</b>	Training process for classification using CNN	<b>76</b>
<b>4.17</b>	Training process for prediction size and location using CNN	<b>78</b>

## LIST OF ABBREVIATIONS

Abbreviation	Name
ANN	Artificial Neural Network
AVA	Antipodal Vivaldi Antenna
CT	Computer tomography
CNN	Convolutional Neural Network
CST	Computer Simulation Technology
DL	Deep Learning
DNN	Deep Neural Network
EM	ElectroMagnetic
FFBPN	Feed Forward Back Propagation Network
FCC	Federal Communications Commission
GPR	Ground Penetrating Radar
GUI	Graphical User Interface
HPBW	Half Power Beam Width
IO	Imaging Object
MSE	Mean Square Error
ML	Machine Learning
MRI	Magnetic Resonance Imaging
NN	Neural Network
S11	Reflection coefficient
RELU	Rectified Linear Unit Layer
RCNN	Region-based Convolutional Neural Network
SAR	Specific Absorption Rate
UWB	Ultra-Wide Band
VNA	Vector Network Analyzer
VSWR	Voltage Standing Wave Ratio
YOLOv3	You Only Look Once version 3

## LIST OF SYMBOLS

Symbols	Name
$E$	Electric Field
$H$	Magnetic Field
$D$	Electric Flux Density
$B$	Magnetic Flux Density
$J$	Electric Current Density
$\rho$	Electric Charge Density
$\sigma$	Conductivity
$k$	Wave Number
$w$	Angular Frequency
$\alpha$	Attenuation
$\beta$	Phase Constant
$\gamma$	Propagation Constant
$dB$	Decibel
$v_p$	Phase Velocity
$\lambda$	Wave Length
$\delta_s$	Skin Depth
$GHz$	Giga Hertz
$THz$	Tera Hertz
$\eta$	Wave Impedance
$\eta_0$	Intrinsic Wave Impedance
$\epsilon_\infty$	Saturated Permittivity
$\epsilon_s$	Static Permittivity
$\tau'$	Relaxation Time Constant
$\rho_m$	Tissue Density
$f_h$	Upper Frequency
$f_L$	Lower Frequency
$f_c$	Center Frequency
$\phi$	Phi Component
$\theta$	Theta Component
$D_0$	Directivity
$p_{in}$	Input Power
$p_{rad}$	Radiated Power
$L$	Length of Cylindrical Monopole Antenna
$r$	Radius of Cylindrical Monopole Antenna
$c$	Speed of Light
$mm$	Millimeter (1 meter * $10^{-3}$ )

$p$	Gap Between Ground Plane & Radiating Patch
$S_{11}$	Reflection Coefficient
$\Gamma$	Tissue Reflection Coefficient
$\Pi$	Pi
$P$	Power
$G$	Gain
$ML$	Mismatch Loss
$LP$	Path Loss
$eP$	Polarization Mismatch Factor
$TX$	Transmitter
$RX$	Receiver
$S$	Random Scatter
$d_0$	Distance
$G_{con}$	Conductive Gain
$R_r$	Radiation Resistance
$R$	Intrinsic Resistance
$I_i$	Input Current
$P_{abs}$	Absorbed Power
$\epsilon_{eff}$	Effective Dielectric Constant
$\epsilon_0$	Permittivity of Vacuum
$\epsilon_r$	Relative Dielectric Constant
$\epsilon_m$	Permittivity of Medium
$\mu_r$	Relative Permeability
$\mu_0$	Permeability of Vacuum
$a$	Major Axis of Radiating Patch
$b$	Minor Axis of Radiating Patch
$f_r$	Resonant Frequency
$L(m)$	Distance Travelled through the body

# CHAPTER ONE

## INTRODUCTION

### 1.1 Overview

Whether in peacetime or wartime, metal may enter the human body in numerous ways, including trauma, medical accidents, medical implants, and misuse. The most common injuries are gunshot wounds, shrapnel, and metal fragments remaining in the human body. It is important to locate the metal in the body quickly and accurately with effective imaging methods such as X-ray, CT scan, MRI, or ultrasound. This will help to determine the size, shape, and location of the metal, which is important for planning any necessary surgery or treatment. Additionally, this can help in reducing the pain of the patient [1].

Typically, shrapnel material is either steel, copper, or aluminum. This shrapnel is frequently moves inside the patient's body for a variety of reasons. A surgeon must find the shrapnel and surgically remove it in order to treat injuries [2].

### 1.2 Some Hidden Object Detection Techniques

Hidden object-detecting techniques are used to detect concealed items or objects in various scenarios, such as security checkpoints, baggage screening, or medical imaging. Here are some commonly used hidden object-detecting techniques

#### 1.2.1 X-Rays

X-rays are a type of electromagnetic radiation that can pass through many materials, including soft tissue, bones, and metal. They are used to detect hidden objects in the human body, such as shrapnel, bullets, or other metallic objects that may be present inside the body in some circumstances. X-rays work by passing through the body and being absorbed by different materials at different rates. Dense materials like bone absorb more X-rays, while less dense materials like soft tissue absorb fewer.

Metals, such as those used in shrapnel, are highly dense, and therefore absorb

a significant number of X-rays, making them visible on an X-ray image. X-ray imaging is a non-invasive procedure, it can be done quickly and easily, and it does not require the patient to have anesthesia. However, X-ray imaging exposes the patient to ionizing radiation, which can have potential long-term health effects [3].

### 1.2.2 Magnetic Resonance Imaging

Magnetic Resonance Imaging (MRI) is often used to detect hidden objects in the human body. The technique uses a powerful magnetic field, radio waves, and computer technology to produce detailed images of internal organs, bones, and other structures. The MRI system is shown in Figure (1.1). MRI can be used to detect a variety of foreign objects, such as bullets, shrapnel, and other metallic fragments, as well as non-metallic objects like glass, wood, and plastic. It can also be used to detect tumors. The high resolution and contrast of MRI make it a valuable tool for detecting objects that may not be visible using other imaging techniques. However, there are a few challenges associated with MRI. One problem is the time-consuming nature of MRI scans, which can limit their use in emergency situations [4]. The MRI technique exploits the behavior of hydrogen protons in a magnetic field and their response to RF pulses to create detailed and informative images of the body's internal structure[5].



Figure 1.1: Magnetic resonance imaging system

### **1.2.3 Computed Tomography**

Computed tomography (CT) can be an effective tool for detecting shrapnel in the human body. CT scans use X-rays to produce detailed images of the body's internal structures, including bones and soft tissue. The metal of shrapnel shows up in white on a CT scan, which makes it easy to be identified and located. In addition, CT scans can also be used to detect any internal injuries or bleeding that may have been caused by the shrapnel. CT scans are fast and non-invasive, and they can provide important information to help guide treatment decisions.

CT can offer more detailed imaging data, and accurate three-dimensional placement and location are both possible. The cost is a drawback because it is high. In addition, it cannot be effectively used in the complex environment seen on the battlefield due to its big size, awkward carrying, and high environmental requirements.

### **1.2.4 Ultrasound Imaging**

The high-frequency sound waves of ultrasound can create images of internal organs and tissues, allowing healthcare providers to locate and identify foreign objects such as shrapnel. It is a non-invasive and relatively safe method for detecting shrapnel in the body.

During the ultrasound imaging, the sonographer will apply a water-based gel to the skin and move a handheld transducer over the area of concern. The transducer sends out sound waves that bounce off of internal structures and return to the transducer to create an image. The sonographer can adjust the frequency and intensity of the sound waves to optimize the image for the specific type and size of shrapnel. Under ultrasound supervision, metallic bodies can be removed safely and without radiation harm. However, the metallic body appears identical to the bone in ultrasonic pictures, making it impossible to distinguish between the two [6].

### **1.2.5 Microwave Imaging**

Microwave imaging is one promising technology for seeing internal human structure by subjecting it to electromagnetic waves at microwave frequencies between 300MHz and 30GHz [7]. In general microwave technology is reliable, affordable, and portable, and it can provide the initial diagnosis of a number of serious medical disorders. The necessary hardware for a microwave-based diagnosis system typically consists of a transmitter, such as a portable vector network analyzer (VNA), an array of antennas (or occasionally just one antenna in sensing applications), and some switching networks to switch between multiple antennas. This necessary hardware can be made for a small portion of the cost of other traditional diagnosis tools [8].

Microwave imaging techniques utilize the interaction between microwave signals and biological tissues to provide information about their composition and properties. It can provide valuable information about tissue properties, such as electrical conductivity and permittivity.

This technology is especially relevant in military medicine, as it can detect and locate shrapnel in soldiers who have been injured by explosive devices, without the need for invasive surgery. It can also be used in emergency rooms and trauma centers to quickly identify and locate shrapnel in the bodies of civilians who have been injured in bombings or other explosions.

## **1.2 Literature Review**

In 2018, Mohammad T. et al. presented a review of concepts and electromagnetic techniques for microwave breast imaging, with a specific emphasis on the use of ultra-wideband (UWB) antenna sensors [9]. The use of UWB sensor-based microwave energy in various imaging applications for breast tumor-related diseases, tumor detection, and breast tumor detection. In microwave imaging, the back-scattered signals radiating by sensors from a human body are analyzed for changes in the electrical properties of tissues. Tumorous cells exhibit higher dielectric

constants because of their high-water content.

In 2018, Oleksandr D. et al. developed an impulse electromagnetic wave that is used to irradiate the surface, and the reflected field characteristics are analyzed using an ANN [10]. This data is used to train the ANN to recognize specific objects based on the characteristics of the reflected field. The ANN is then able to identify objects based on the input data it receives during testing. This method can be used to detect and identify a wide range of hidden objects. also investigated the effect of the number of hidden layers in the ANN on the precision of recognition.

In 2019, Chen H. et al. presented a unified approach that performs thoracic disease identification and localization using deep learning techniques [11]. The proposed method is to build an accurate prediction model that can effectively identify and locate thoracic diseases in radiology images. The method is based on deep learning techniques, which have shown significant success in medical image analysis tasks. Deep learning models can automatically learn relevant features from the data, making them well-suited for complex image recognition tasks. the proposed method shows promising results in accurately identifying and localizing thoracic diseases in radiology images, making it a potentially valuable tool for clinical diagnosis and treatment planning.

In 2020, Ahmed J. et al. presented a small-size UWB monopole antenna to accurately locate and identify kidney stones within the body [12]. The low profile, simple structure, and lightweight nature of the antenna design are intended to make it easy to manufacture and to be comfortable for patients to use during the scanning process. The UWB antenna was simulated, measured, and tested at an ultra-wideband frequency range of 3-11 GHz to detect kidney stones. The test results showed that when a stone is present, the Reflection coefficient ( $S_{11}$ ) increases.

In 2020, Gennadiy P. et al. proposed UWB antenna systems that can be used for detection and classification by sending out UWB pulses and analyzing the reflections [13]. The reflections can be analyzed using artificial neural networks (ANNs) to

classify the object, The ANNs can then be trained to recognize the characteristics of hidden objects and differentiate them from other objects in the environment.

In 2021, Vikesh S. et al. proposed automated microwave monitoring a technique that utilizes microwave signals to detect hidden objects in strategic and security applications [14]. The technique works by emitting microwave signals and measuring the reflections, which can reveal the presence of hidden objects. By measuring the S-parameters of the test region using a horn-lens antenna and a network analyzer in the wide frequency range of 2-10 GHz, it is possible to detect hidden objects. The proposed scheme allows for the calculation and comparison of the objects' shape, size, and depth profile with their actual values in addition to determine their dielectric properties.

In 2021, Amran H. et al. investigated A YOLOv3 deep neural network to detect brain tumors in portable electromagnetic imaging systems [15]. a nine-antenna array setup and a phantom that mimics tissue are used, and the portable head imaging system can collect detailed scattering data to produce high-resolution images of the head and brain. These images can be analyzed using a YOLOv3 deep neural network model to detect and locate brain tumors. A final image data set is created by combining fifty sample images, that were gathered from various EM head imaging system development scenarios. The data set is made up of 1000 images, including 50 samples, of which 80% are used for training and the remaining 20% for validation and testing. The results of the proposed architecture demonstrate great training, and validation accuracy with low training and validation loss.

In 2022, Sofia I. et al. proposed a YOLOv3 deep neural network for the identification of shrapnel in different sizes and locations with respect to a neurovascular bundle [16]. This makes it possible to employ automated methods to determine how close shrapnel is near tissue's critical features, which can then be used to determine whether evacuation or surgical intervention is necessary.

In 2022, Emily N. et al. developed a deep learning neural network model

specifically designed to identify shrapnel in ultrasound images, termed ShrapML (ML)[17]. It is faster than traditional deep learning models, ShrapML can minimize the cognitive burden for medical professionals in high-stress emergency, or military medicine scenarios by automating some tasks and providing real-time help and analysis.

In 2022, Gokul N. et al. introduced a UWB Antipodal Vivaldi Antenna (AVA) for microwave imaging applications [18]. The AVA accomplishes high transmission capacity from 1.2–14 GHz with a maximum gain of 13 dBi at 10 GHz. The antenna is utilized for the identification of a metal object located inside a human stomach cross-section modeled in the simulator. A suitable imaging algorithm is devised to identify the material inside the stomach. The algorithm can locate the exact coordinates of the metallic objects along with their actual dimensions used in the simulations. Further, the resolution of the image has been improved.

### **1.3 Aims of the Dissertation**

The aim of this dissertation is to detect the existence of shrapnel in the human body and determine its size and its location using microwave imaging and neural networks (NN). To do that the following steps are to be taken:

1. Constructing a model that mimics the layers of the human body, then apply an electromagnetic signal to the model.
2. Creating a planar monopole antenna for UWB microwave imaging.
3. Analyzing the backscattered signals from the model.
4. Collecting the signal sets, and prepare the data for use in the neural network.
5. Utilizing the data as input, a neural network can be employed to identify the presence of shrapnel, estimate its size, and determine its location.
6. By analyzing the input data, the neural network learns patterns and correlations that correspond to the presence, size, and location of shrapnel.

## **1.4 Dissertation Layout**

This dissertation includes the following chapters. Chapter one contains background about the shrapnel, hidden object detection techniques, and a literature review about the subject. Chapter Two states the theory of neural networks, the theory of microwave imaging, and the fundamentals of microwave imaging. Chapter three includes the theory of Ultra-Wideband Antenna, a planar monopole antenna that has been developed for this purpose, building a simple two-dimensional homogeneous model of the human body using CST studio, theory of human model effect on antenna parameters. Chapter four includes the theory and simulation of dataset reparation for a homogenous Model, the architecture of neural networks, results and analysis of one-dimensional locating using artificial neural networks (ANN), results and analysis of two-dimensional locating using artificial neural networks (ANN), and results of training Convolutional Neural Network (CNN). Finally, chapter five presents' conclusions and some suggestions for future work.

## CHAPTER TWO

### NEURAL NETWORKS AND MICROWAVE IMAGING

#### 2.1 Neural Network

An Artificial Neural Network (ANN) is a machine learning model that draws inspiration from the structure and function of biological neural networks, which are found in the human brain. It is composed of layers of interconnected nodes, called artificial neurons, which process and transmit information. The neurons in each layer are connected to the neurons of the previous and next layers via pathways called synapses. The neurons and synapses are used to learn and make predictions or decisions based on input data. ANNs are widely used for medical applications in various disciplines of medicine. ANNs have been extensively applied in diagnosis, electronic signal analysis, medical image analysis, and radiology [19].

ANNs can be trained using supervised, or unsupervised methods. In supervised learning, the neural network is trained on a labeled dataset, where both input data and corresponding target outputs are provided. During training, the network learns to map inputs to desired outputs by adjusting its internal parameters through an optimization process, typically using techniques like backpropagation and gradient descent. The goal is to minimize the difference between the network's predictions and the actual targets.

In unsupervised learning, the neural network is trained on an unlabeled dataset, where only the input data is provided without any corresponding target outputs. The network tries to find patterns or structures in the data without explicit guidance. Common unsupervised learning tasks include clustering (grouping similar data points) and dimensionality reduction (finding a lower-dimensional representation of the data) [20].

An artificial neural network is a nonlinear function, represented by a collection of interconnected artificial neurons, in which an input vector ( $x$ ) multiplied by a weights vector ( $w$ ) summed, and then inserted into a certain activation function

which determines if the neuron is activated, and an output is generated. These weights are typically adjusted during a training process, where the network is presented with a set of input-output examples, and the weights are adjusted to minimize the difference between the network's output, and the target output. The output can be unidimensional or multidimensional, depending on the problem, and the architecture of the network. The working principle of an artificial neuron is shown in Figure (2.1). The mathematical explanation of the artificial neuron model is below [21].

$$y(k) = f(\sum_{i=0}^m w_i(k) \cdot x_i(k) + b) , \quad (2.1)$$

where:

$x_i(k)$  is input value in a discrete-time  $k$  where  $i$  goes from 0 to  $m$ ,

$w_i(k)$  is weight value in a discrete-time  $k$  where  $i$  goes from 0 to  $m$ ,

$b$  is bias,

$F$  is a transfer function,

$y_k(k)$  is output value in discrete time  $k$ .

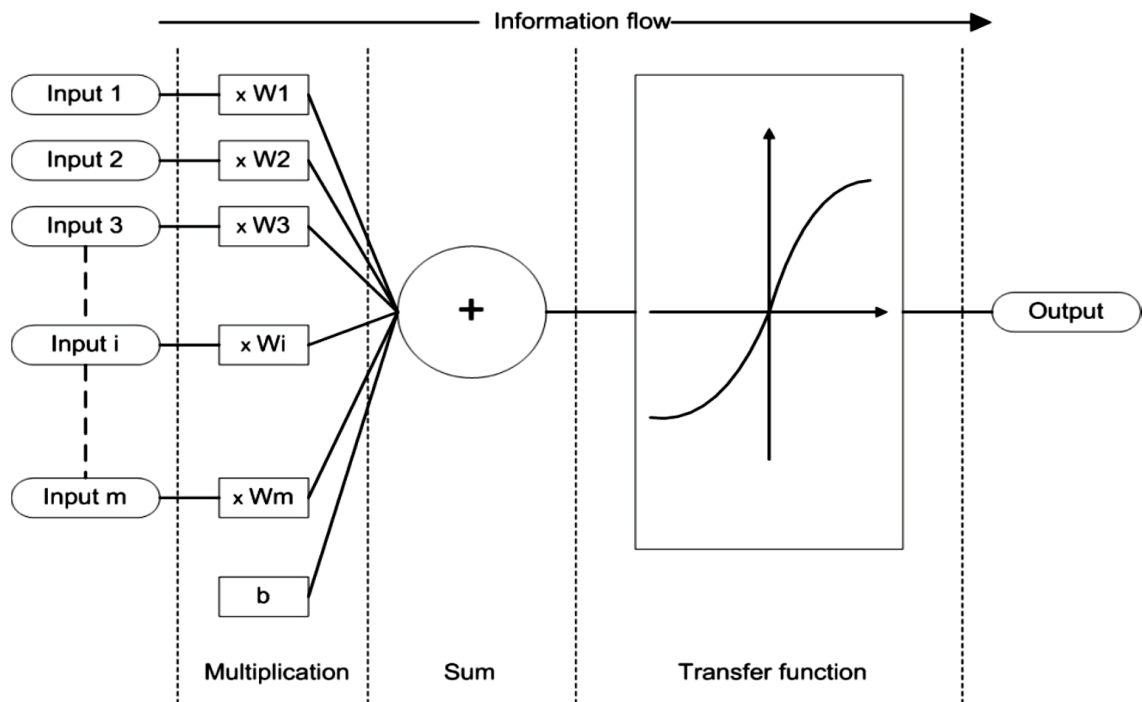


Figure 2.1: Principle of an artificial neuron[21]

In an ANN, weights, and biases are the learnable parameters that enable the network to make predictions and learn from data during the training process. These parameters are crucial for the network's ability to approximate complex functions and generalize to new data.

A weight is a scalar value associated with each connection between neurons in adjacent layers. Each connection represents the flow of information from one neuron to another. The weight determines the strength and direction of the signal being passed from one neuron to the next. During the training process, the network adjusts the weights to find the optimal values that minimize the prediction error on the training data.

A bias is a scalar value associated with each neuron in the network, including the input layer and all hidden layers. The bias provides an offset or threshold for the neuron's activation function. It allows the network to adjust the decision boundary and control the neuron's responsiveness to the input.

The bias term is essential because without it, the output of a neuron would be solely determined by the weights and inputs, which may not be sufficient to model complex relationships in the data. The bias allows the network to shift and adjust the activation function, making it more flexible and adaptable [22].

The main artificial neural network architectures fall into the following categories, taking into account the neuron disposition, their connectivity, and the makeup of their layers:

- **Single-layer feedforward network:** This type of network is also known as a perceptron, which consists of only one layer of neurons, where each neuron receives input from the layer, processes it, and sends it to the output layer. These networks are usually employed in pattern classification, and linear filtering problems.
- **Multilayer feedforward networks:** These networks consist of multiple layers of neurons, where each layer receives input from the previous layer, processes it, and sends it to the next layer. These networks are also known as multi-layer

perceptron, as seen in Figure (2.2). They are used to solve a variety of issues, including those involving function approximation, pattern classification, system identification, process control, optimization, and more.

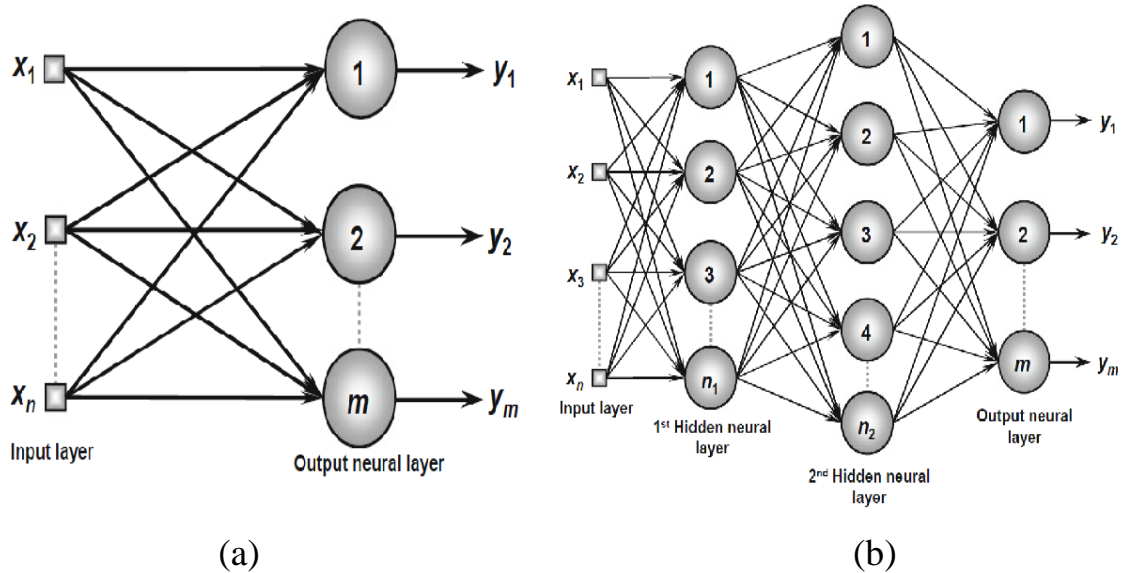


Figure 2.2: (a) Single layer network, (b) Multiple layers network.

- Recurrent networks: In these networks, the output of a neuron is fed back to itself, and to the other neurons in the same layer. This creates a feedback loop, allowing the network to maintain a certain level of internal state, and process sequential data.
- Mesh networks: These networks are composed of multiple processing nodes connected by directed edges, where each node can represent a single or multiple neurons, and the edges represent the connections between them as seen in Figure (2.3). These networks are utilized for a variety of tasks, including data clustering, pattern recognition, and system optimization [23].

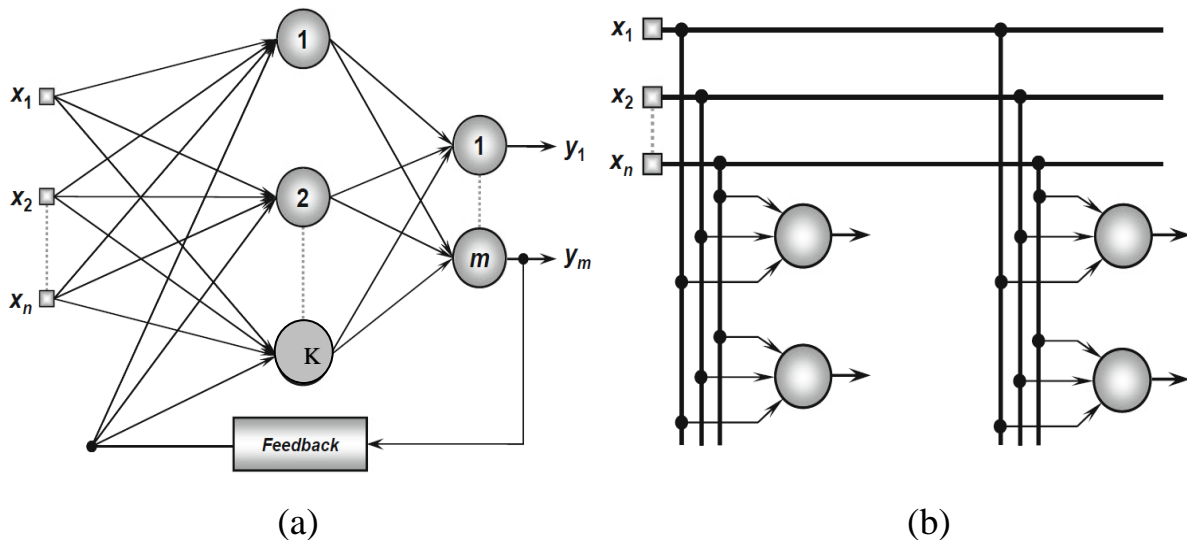


Figure 2.3: (a) Recurrent network, (b) Mesh network [23].

## 2.2 Transfer Functions

The transfer function is a crucial component of an artificial neuron in a neural network. It maps the input signal to an output signal, and its properties determine the behavior of the neuron. A transfer function can be either linear or nonlinear. A linear transfer function produces an output that is directly proportional to the input, while a nonlinear transfer function produces an output that is not directly proportional to the input. The choice of a linear, or nonlinear transfer function depends on the specific problem that the neuron or system is trying to solve. Figure (2.4) illustrates several of the typical activation functions, command used [24].

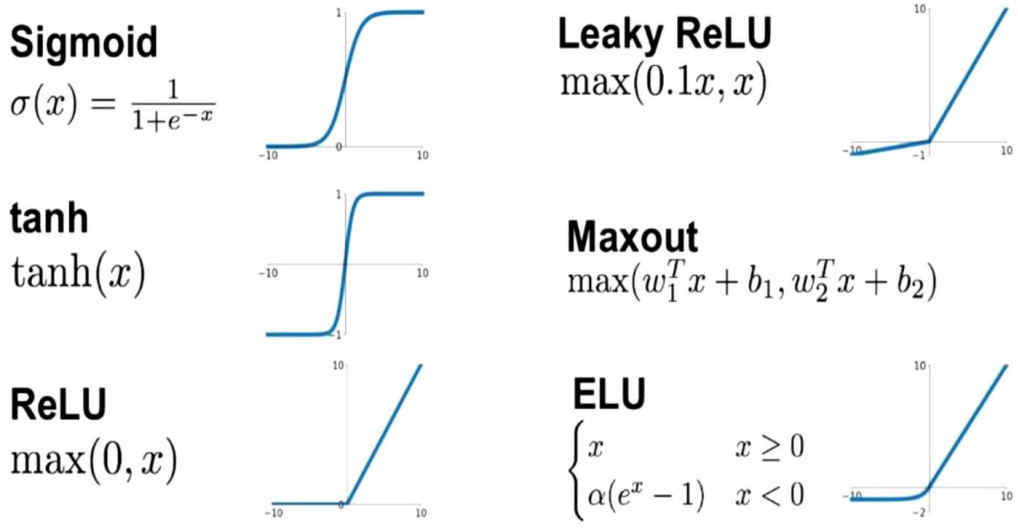


Figure 2.4: Common activation functions of NN [24].

### **2.3 Feed-Forward Back Propagation**

The FFBN method is used to train a model that represents the results of two-way iterations. The feed-forward aspect of the process refers to the flow of data through the network, moving from the input layer to the output layer, without looping back. The backpropagation aspect of the process refers to the flow of error information, moving from the output layer to the input layer, and adjusting the weights of the connections between the layers in order to minimize the error. This process is repeated many times, also known as an "epoch," until the network reaches a satisfactory level of accuracy. The number of iterations or epochs required to train a neural network can vary depending on factors, such as the complexity of the network, the size of the dataset, and the learning rate [25].

### **2.4 The Architecture of Neural Network**

The best method for recognizing and distinguishing between various signal sets is a neural network. It is important to select an appropriate design and learning algorithm for the neural network to produce the best outcomes. The simplest approach to achieve that is to decide what is projected to be appropriate based on prior experience, and then to increase or decrease the size of the neural network until a suitable output is generated.

Neural networks are typically trained using a process called backpropagation, where the network is adjusted based on the difference between its output and the expected target output. During training, the neural network is repeatedly presented with input/target pairs, and the weights and biases of the network are updated so as to minimize the difference between the network's output and the target output.

During the implementation of neural networks, it is a common practice to divide the available data into three sets: training data, validation data, and testing data.

The training data set is used to teach the network how to map input data to output data by adjusting the network's parameters based on the errors between the

predicted outputs and the true outputs. The training process continues until the network's error on the training data set is minimized and the network has learned to generalize to new unseen data.

The validation data set is used to evaluate the performance of the network during training and to prevent overfitting. Overfitting occurs when the network becomes too specialized in the training data and fails to generalize to new data. The network is evaluated on the validation data set after each training epoch, and training is stopped when the error on the validation data set starts to increase, indicating that the network has started to overfit.

The testing data set is used to provide an independent measure of the network's performance after training. The testing data set is not used during training or validation, and the network has not seen this data before. By evaluating the network on the testing data set, we can estimate the generalization performance of the network, i.e., how well it can perform on new, unseen data.

It may be possible to use an artificial neural network (ANN) with reflection coefficient data inputs to predict the depth of shrapnel in a human. Reflection coefficient data can be used to estimate the dielectric properties of tissues, which can in turn be used to estimate the depth of penetration of shrapnel.

## **2.5 Training Process**

The training process of a neural network is guided by a learning algorithm, which is responsible for adjusting the weights, and biases of the neurons in the network. The goal of the learning algorithm is to find a set of weights and biases that minimize the error between the predicted output, and the true output. This process is iterative, and typically uses a dataset of labeled examples, called the training set, to update the weights and biases. As the training progresses, the network extracts discriminant features from the input data, that are useful for solving the problem at hand. These features are learned by the network in the form of weights, and biases which then can be used to make predictions on unseen data, known as the test set.

A training epoch is also the term used to describe each complete presentation of all the samples from the training set during the training of artificial neural networks in order to modify the synaptic weights and thresholds. Before the training process begins, the number of training epochs must be set as a hyperparameter. The training process ends when performance on the validation set stops advancing, or after a predetermined number of training epochs [26].

In training a backpropagation neural network, the mean squared error (MSE) function is commonly used as the cost function. It calculates the average squared difference between the predicted output and the actual output for all training samples [26].

$$\text{MSE} = \frac{1}{N} \sum_{i=1}^N (d_i - y_i)^2 = \frac{1}{N} \sum_{i=1}^N e_i^2 \quad , \quad (2.2)$$

where:

MSE is the mean square error.

N training samples were generated using an EM simulator.

$d_i$  the expected output.

$y_i$  the corresponding output of neural networks.

$e_i$  the sample errors.

## 2.6 Deep Neural Network

A DNN is a type of ANN that has multiple layers of artificial neurons, also known as hidden layers. The added layers in a deep neural network can make it more powerful and capable of solving more complex problems, but they can also lead to certain issues. The vanishing gradient problem is one such issue. It occurs when the gradients of the weights in the network become very small, as they are backpropagated through the layers, causing the weights to update very slowly. As a result, the network may take a very long time to converge, or may not converge at all. This can make it difficult to train DNNs. Overfitting is another issue that can occur when the model becomes too complex and starts to memorize the training data,

rather than generalizing to new unseen data. This can lead to poor performance on unseen data or validation set [27].

## 2.7 Convolutional Neural Network (CNN)

CNN is a type of deep learning model. It consists of multiple layers, including convolutional layers, pooling layers, and fully connected layers, which work together to extract features from the input data and make predictions [28]. The training, and testing of the input data is performed by passing the data through a series of convolution layers with filters. These filters are also known as kernels. Because of their ability to automatically learn features from data, CNNs have been widely used in computer vision tasks such as object detection, image segmentation, and image classification. A general CNN architecture is shown in Figure (2.5). It consists of Convolutional Layer, Pooling Layer, Fully connected layer (FC), and Rectified Linear Unit Layer.

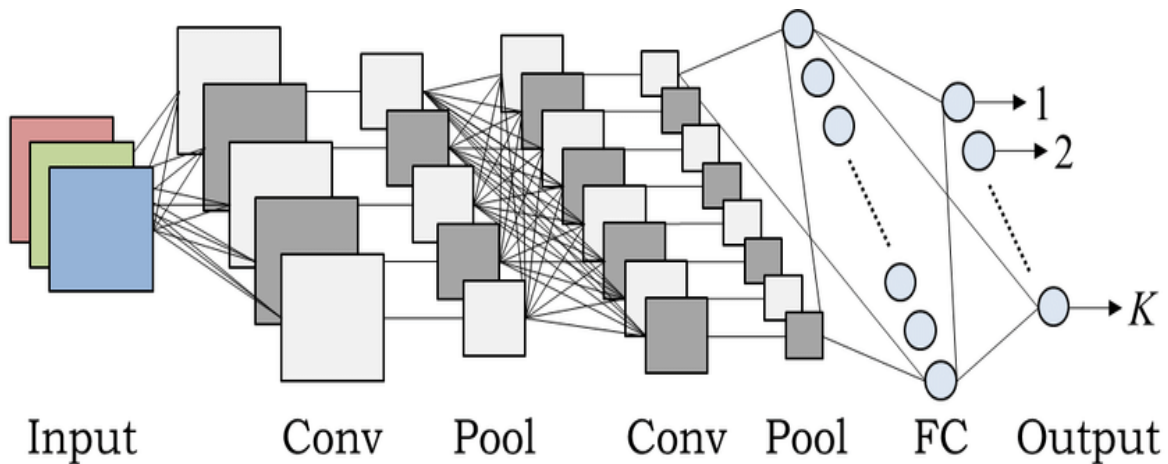


Figure 2.5: Architecture of CNN.

### 2.7.1 Convolutional Layer

The main purpose of a convolution layer is to detect local features, or combinations of local features by applying filters to the input. The convolutional layer takes the input data  $x$  and a set of filters  $F = \{f_1, f_2, \dots, f_{N_k}\}$ , and applies the convolution operation  $\otimes$  between them. This operation produces a set of  $N_k$  feature maps  $h$ :

$$h_k = f_k \otimes x . \tag{2.3}$$

By sliding the filter over the data, it performs a dot product with the local region of the data, producing a response that indicates the presence or absence of a certain feature. This response is then transformed into a feature map, which can be used as input for the next stage of processing [29].

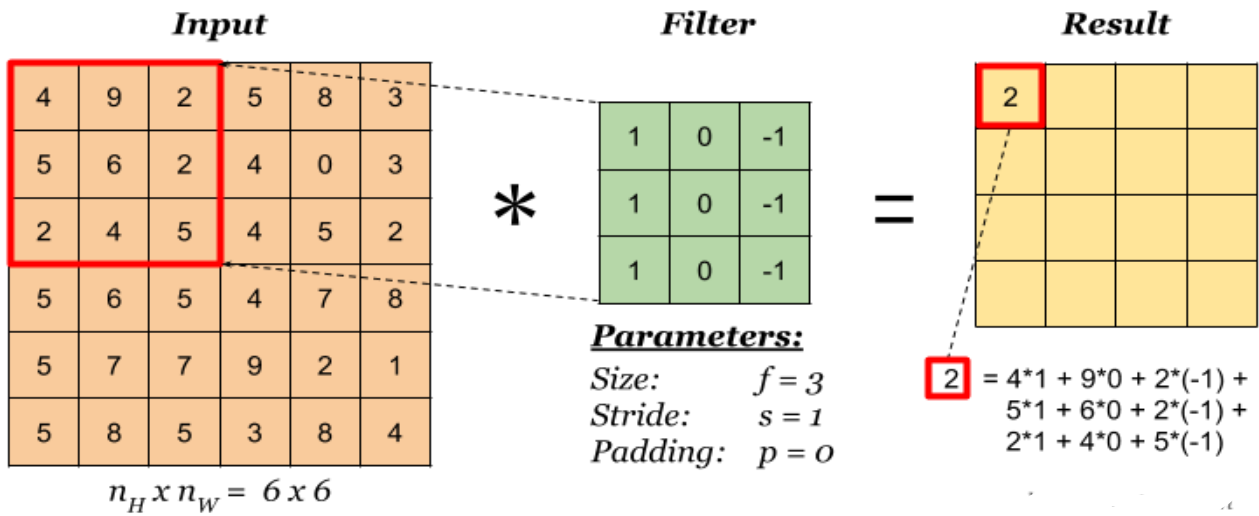


Figure 2.6: Operation of the convolutional layer.

### 2.7.2 Pooling Layer

The main purpose of pooling layers is to down-sample the spatial dimensions of the input feature map, reducing their size, and the number of parameters in the network. This can help to reduce overfitting, improve computation efficiency, and control the size of the feature maps. The most commonly used pooling operations are Max Pooling and Average Pooling.

Max pooling takes the maximum value among the data in a pooling field, and average pooling takes the average of all the values in the same field. Figure (2.7) shows the operation of the pooling layer. The choice between max pooling and average pooling depends on the characteristics of the data, the task at hand, and the network architecture. By taking the maximum value, max-pooling preserves the most prominent feature in that region, making it robust to small variations or noise. This

property helps the network focus on the most important and discriminative features while discarding less relevant information. In situations where extreme values exist in the data, max pooling may emphasize these outliers, potentially leading to a loss of information about the majority of the data points. In contrast, average pooling computes the mean value within the pooling window, which can help mitigate the influence of extreme values and provide a more stable representation of the data. [30].

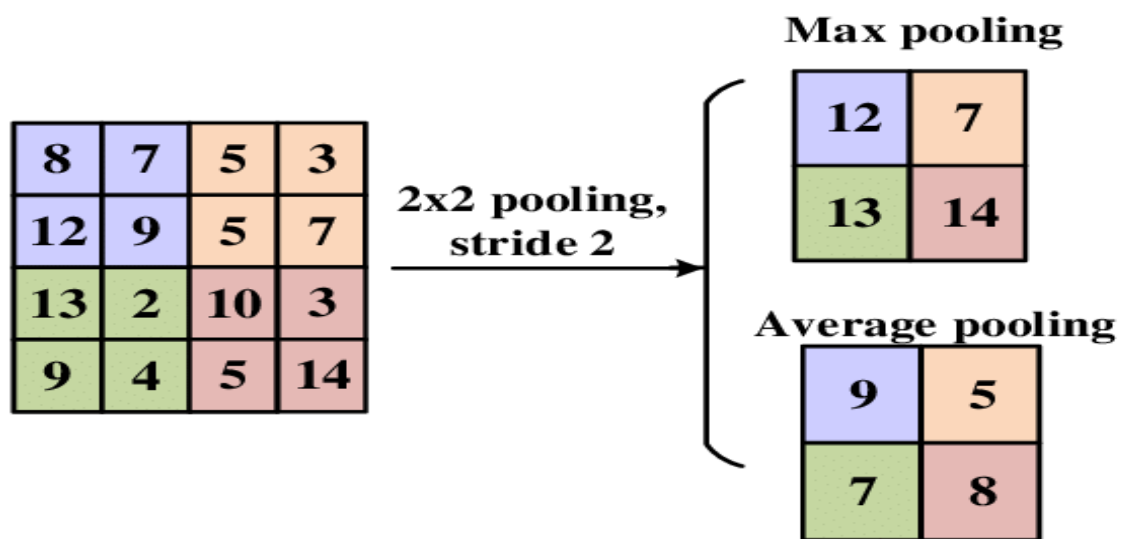


Figure 2.7: Operation of pooling layer.

### 2.7.3 Fully Connected Layer

The fully connected (FC) layer is used to perform the final classification of the input data into different classes. The FC layer takes the output from the convolutional and pooling layers, which have learned high-level features from the input data, and performs a dot product with a set of weights and biases to produce the final classification scores. The weights and biases in the FC layer are learned through the training process, allowing the model to recognize and classify new, unseen data.

### 2.7.4 Rectified Linear Unit Layer (RELU)

Typically, CNN employs the nonlinear RELU activation function. Values greater than zero remain unaffected by RELU, while values less than zero are transformed to zero (1) [31].

$$f(x) = \begin{cases} 0, & \text{if } x < 0. \\ x, & \text{otherwise.} \end{cases} \quad (2.4)$$

## 2.8 Deep Neural Network Structure Design

The design of a DNN involves choosing the number, and type of layers, the number of neurons in each layer, the activation functions, and the type of connectivity between the layers. The number of hidden layers in a deep neural network is a key factor in determining its performance. The right number of hidden layers depends on the complexity of the problem, the size of the input and output layers, and the amount of training data available. If the network has too few hidden layers it may not be able to capture the complexity of the problem, and may result in underfitting. If the network has too many hidden layers, it may become too complex and may result in overfitting. Therefore, the neural network that will be used in this dissertation has two hidden layers.

## 2.9 Microwave Imaging System

The physical basis of microwave imaging techniques is the significant dielectric between the various tissues of the human body and its surroundings in the microwave frequency region [32].

Different imaging algorithms have been developed to extract the data from measurements of the scattered fields depending on the imaging system design. There are primarily two types of configurations (monostatic and multistatic), which use one or more spatially varied antennas as transmitters and receivers. In the monostatic technique, a single antenna serves both the transmitter and receiver. To gather more details about the imaging domain, the antenna can be shifted to various places. At

least two antennas are used in multistatic. Each antenna in this setup sends out a microwave signal, which is then picked up by all the other antennas. To record every signal required, this procedure is done for each antenna. While the multistatic arrangement is more complex than the monostatic method, it can provide more details about the photographed domain by sending and receiving signals to, and from every area of the pictured domain.

An Ultra-Wideband (UWB) imaging systems typically consist of two main parts: a hardware component, usually an antenna, that illuminates the target object with microwave signals, and collects the signals that are reflected, and a software or post-processing component that uses these signals to reconstruct an image of the target object. The image can then be used for visualization and analysis of the target's internal structure as shown in Figure (2.8) [33].

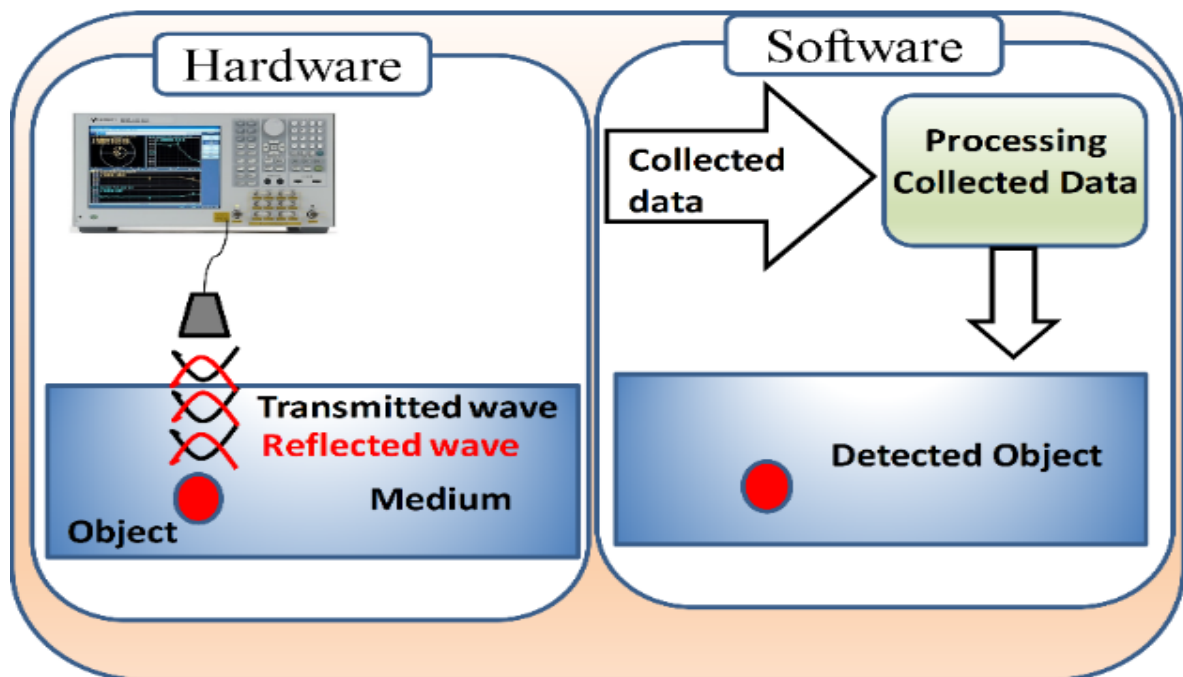


Figure 2.8: A schematic illustration of the microwave imaging system's components.

Microwave imaging can be divided into three main categories:

- **Passive microwave imaging:** The operation principle of passive microwave imaging is based on the measurement of microwave radiation emitted by

objects. The emitted radiation is typically in the form of thermal emission or scattered radiation. The passive microwave sensor detects the emitted or scattered microwave radiation, and converts it into an electrical signal, which is then processed to produce an image.

- **Active microwave imaging:** It works by transmitting microwave signals into human tissue, and measuring the reflected signals. The differences in the reflected signals can then be used to construct an image of the object. The image represents the distribution of material properties within the object such as permittivity and conductivity, which affect the reflection of the transmitted signals. The process is repeated many times to increase the accuracy of the image.
- **Hybrid microwave imaging:** The operation principle of hybrid microwave imaging is based on the difference in electrical properties between normal and abnormal tissues. Microwave signals are transmitted into the body, and the energy from these signals is absorbed and scattered by the tissue. The amount of energy absorbed and scattered by the tissue depends on its electrical properties, such as conductivity and permittivity. Abnormal tissue has different electrical properties compared to normal tissue, and therefore, it absorbs and scatters microwave energy differently. The expansion of the abnormal tissue due to the absorbed energy creates pressure waves, which are then detected by an ultrasound transducer [34].

### 2.9.1 Microwave Imaging Methods

Microwave imaging methods refer to techniques used to create images or maps of objects or scenes using microwave radiation. These methods utilize the interaction of microwaves with the target to extract information about its properties and structure

### 2.9.1.1 Matching Interface Imaging

Utilizing a matching medium is designed to efficiently couple EM radiation to the body and reduce reflections at the air-body interface. Additionally, because the resolution of a microwave imaging system depends on wavelength, using a matching medium increases the imaging resolution in accordance to:

$$\lambda_m = \frac{\lambda_0}{\sqrt{\epsilon_m}} . \quad (2.5)$$

Where  $\lambda_m$  is the wavelength of an electromagnetic wave in a material medium,  $\lambda_0$  is the wavelength in free space, and  $\epsilon_m$  is the permittivity of the medium.

Additionally, the reflections off the boundaries will be limited by a lossy matching medium. Assure that the scattering from the imaging item dominates the signals picked up by the receivers and that all other multi-paths are negligible. The matching medium is considered the best way to transfer microwave energy into an Imaging Object (IO) because it reduces losses at the air-body interface. This is due to the higher permittivity of biological tissues compared to air, which causes high losses when coupling microwave energy directly into the tissue. The matching medium helps to match the permittivity of the tissue and air, reducing these losses and improving the coupling efficiency of the microwave energy into the IO [35].

### 2.9.1.2 Quantitative Imaging

Quantitative imaging techniques, also known as microwave tomography, create the image based on the electrical conductivity, and relative permittivity values of the various human tissues. The generated image demonstrates the distribution of tissues inside the body with various electrical characteristics. In medical applications, the large differences in the dielectric characteristics of various biological tissues can lead to an extremely ill-posed inverse scattering problem, making it challenging to estimate accurately the dielectric permittivity map of the imaged domain. Nonlinear iterative techniques must be used to solve the inverse

scattering problem. A large number of transmit, and receive antennas surround the body that has to be scanned. At a given time, each transmitter antenna illuminates the body with a microwave signal, and all receive antennas to collect the signal that the body scatters. This complete setup is typically placed in a homogenous medium with permittivity, which serves as a matching medium for coupling the microwave energy delivered to the body, and minimizing any reflection that may have happened at the air-body contact in the absence of it.

### 2.9.1.3 Qualitative Imaging

The goal of imaging in some medical applications is not to determine the electrical characteristics of the tissues, but rather to find and locate the hidden object. These methods utilize an ultra-wideband (UWB) signal for good time resolution. However, each antenna only sends out short pulses at a time (UWB in the frequency domain), and the same antenna only receives the backscatter return [36]

## 2.9.2 Fundamentals of Microwave Imaging

The use of microwave frequencies for non-ionizing electromagnetic (EM) waves is regarded as an economical, and low-risk imaging technique. The dispersive nature of human tissues at RF frequencies leads to signal attenuation, and distortion, making it crucial to understand the electromagnetic (EM) properties of these tissues for medical imaging purposes.

### 2.9.2.1 Propagation of Electromagnetic Waves

The propagation of electromagnetic waves is best described using Maxwell equations. When the medium is linear ( $\epsilon$  and  $\mu$  independent of  $\vec{E}$  and  $\vec{H}$ ), the Maxwell equation can be written as [37]:

$$\nabla \times \vec{E} = -j\omega\mu\vec{H} , \quad (2.6a)$$

$$\nabla \times \vec{H} = j\omega\epsilon\vec{E} + \vec{j} , \quad (2.6b)$$

$$\nabla \cdot \vec{D} = \rho , \quad (2.6c)$$

$$\nabla \cdot \vec{B} = 0 , \quad (2.6d)$$

$$\vec{D} = \varepsilon \vec{E} , \quad (2.6e)$$

$$\vec{B} = \mu \vec{H} , \quad (2.6f)$$

where:

$\nabla$ . is the divergence operator, which is represented by a vector symbol ( $\nabla$ ) followed by a dot ( $\cdot$ )

$\vec{E}$  is the electric field, in volts per meter (V/m).

$\vec{H}$  is the magnetic field, in amperes per meter (A/m).

$\vec{D}$  is the electric flux density, in coulombs per meter squared (Coul/m<sup>2</sup>).

$\vec{B}$  is the magnetic flux density, in webers per meter squared (Wb/m<sup>2</sup>).

$J$  is the electric current density, in amperes per meter squared (A/m<sup>2</sup>).

$\rho$  is the electric charge density, in coulombs per meter cubed (Coul/m<sup>3</sup>).

$\varepsilon$  and  $\mu$  are the permittivity and permeability of the medium.

$$\varepsilon = \varepsilon_0 \varepsilon_r . \quad (2.7)$$

$$\mu = \mu_0 \mu_r . \quad (2.8)$$

$\varepsilon_0 = 8.85 \times 10^{-12}$  and  $\mu_0 = 4\pi \times 10^{-7}$  are the intrinsic permittivity and permeability of the vacuum.

The conductive currents in human tissues are typically dominant, due to their high electrical conductivity. The relative permittivity of a medium is a measure of its ability to store electrical energy, and is generally represented as a complex value. The relative permittivity helps to determine the behavior of electromagnetic waves in a medium, such as how they are transmitted, reflected, and absorbed. It is assumed

that biological tissues do not have magnetic properties, and therefore the magnetic permeability  $\mu$  is considered to be zero.

For a medium conductivity  $\sigma$ , a corresponding conduction current density  $\vec{j}$  exists that is proportional to the  $\vec{E}$  vector according to [37]:

$$\vec{j} = \sigma \vec{E} . \quad (2.9)$$

Equation (2.7) can be re-written as:

$$\begin{aligned} \nabla \times \vec{H} &= j\omega \varepsilon \vec{E} + \vec{j} \\ \nabla \times \vec{H} &= j\omega \varepsilon_0 \varepsilon_r \vec{E} + \sigma \vec{E} \\ &= j\omega \varepsilon_0 \left[ \varepsilon_r - j \frac{\sigma}{\omega \varepsilon_0} \right] \vec{E} . \end{aligned} \quad (2.10)$$

Therefore, the modified complex permittivity can be expressed as:

$$\varepsilon = \varepsilon_0 \left( \varepsilon_r - j \frac{\sigma}{\omega \varepsilon_0} \right) . \quad (2.11)$$

The wave equation is required to specify other crucial propagation parameters.

$$\nabla \times \vec{E} = -j\omega \mu_0 \vec{H}$$

$$\nabla \times \nabla \times \vec{E} = -j\omega \mu_0 \nabla \times \vec{H}$$

$$\nabla(\nabla \cdot \vec{E}) - \nabla^2 \vec{E} = \omega^2 \mu_0 \varepsilon_0 \left[ \varepsilon_r - j \frac{\sigma}{\omega \varepsilon_0} \right] \vec{E} . \quad (2.12)$$

$$\nabla^2 \vec{E} + \omega^2 \mu_0 \varepsilon_0 \left[ \varepsilon_r - j \frac{\sigma}{\omega \varepsilon_0} \right] \vec{E} = 0 . \quad (2.13)$$

The wave number in a lossy medium is defined as:

$$k = \omega \sqrt{\mu_0 \varepsilon_0 \left[ \varepsilon_r - j \frac{\sigma}{\omega \varepsilon_0} \right]} . \quad (2.14)$$

The complex wave propagation constant in the medium is given by the following equation:

$$\gamma = \alpha + j\beta = jk = j\omega \sqrt{\mu_0 \varepsilon_0 \left[ \varepsilon_r - j \frac{\sigma}{\omega \varepsilon_0} \right]} . \quad (2.15)$$

$\alpha$  and  $\beta$  are the attenuation, and phase constants, respectively.

### 2.9.2.2 Attenuation Constant

Conductive losses in a medium can lead to signal attenuation, and result in a reduction of the amplitude, and energy of the propagating signal. This occurs because some of the energy is absorbed, and dissipated as heat in the medium. The magnitude of the conductive losses, and the resulting signal attenuation is dependent on the conductivity of the medium, and the frequency of the signal. The propagation factor for the positive traveling wave is then as follows:

$$e^{-\gamma z} = e^{-\alpha z} e^{-j\beta z} \quad . \quad (2.16)$$

This indicates that a wave moving in the +z direction with a phase velocity  $v_P = \omega/\beta$ , Wavelength  $\lambda = 2\pi / \beta$ . The wave's rate of decay is controlled by the attenuation constant. It can be represented as follows in dB, assuming a 1-meter distance:

$$D_{(dB/m)} = 20 \log_{10}(e^{-\alpha}) = -20. \alpha. \log_{10}(e) = 8.686. \alpha \quad . \quad (2.17)$$

### 2.9.2.3 Skin Depth

The skin depth, or penetration depth is a crucial parameter in electromagnetism, and is defined as the depth at which the magnitude of the electromagnetic field decreases to 1/e (37%) of its original value at the surface of the medium. This concept is useful in understanding the interaction of electromagnetic waves with materials.

$$\delta_s = \frac{1}{\alpha} = \sqrt{\frac{2}{\omega\mu\sigma}} \quad . \quad (2.18)$$

### 2.9.2.4 Wave Impedance

The wave impedance in a lossy medium can be estimated using the relationship between the wave's electric field (E), magnetic field (H), the complex permittivity ( $\epsilon$ ), and complex permeability ( $\mu$ ) of the medium. The wave impedance (Z) can be expressed as [37]:

$$\eta = \sqrt{\frac{\mu}{\epsilon}} = \sqrt{\frac{\mu_0\mu_r}{\epsilon_0\epsilon_r}} = \eta_0 \sqrt{\frac{\mu_r}{\epsilon_r}} \quad . \quad (2.19)$$

where  $\eta_0$  is the intrinsic wave impedance of vacuum and is equal to  $120\pi$ ,  $\mu_r$  is the relative permeability of the material,  $\epsilon_r$  is the relative permittivity of the material.

The discussion above, and the introduction of the key wave propagation parameters lead to the conclusion that it is theoretically possible to estimate the phase constant, attenuation, penetration depth and wave impedance by knowing the complex relative permittivity of a medium (the medium's dielectric properties). As a result, the analysis of wave propagation and its interactions with the human body is based on the dielectric characteristics of biological human tissues.

### **2.9.3 Dielectric Properties of Biological Tissues**

Dielectric properties of biological tissues play a crucial role in understanding the interactions of electromagnetic (EM) waves with the human body. These properties include the ability of a tissue to store electrical energy and the ease with which it allows the flow of electrical currents. Understanding these properties is important in fields such as medical imaging and therapeutic applications of EM waves, that operate in the frequency range of biological tissues.

Different types of tissues have different electrical properties that affect how they scatter electromagnetic waves. The two most commonly studied dielectric properties are relative permittivity and conductivity. Relative permittivity is a measure of a material's ability to store electrical energy, and conductivity is a measure of its ability to allow electrical current flow. These properties can vary between different tissues, and even within a single tissue depending on the frequency of the electromagnetic wave.

#### **2.9.3.1 Debye Model**

The Debye model is one commonly used method for predicting the frequency-dependent dielectric properties of biological tissues. The Debye model provides a first-order approximation for the complex relative permittivity of a single tissue as a function of frequency. The equation for the Debye model describes the relationship between the complex relative permittivity, the frequency of the electromagnetic wave and a single relaxation time constant which characterizes the electrical properties of the tissue. This model provides a simple and intuitive way to describe the frequency-dispersive nature of biological tissues and is used in the field of medical imaging.

$$\varepsilon = \varepsilon_{\infty} + \frac{\varepsilon_s - \varepsilon_{\infty}}{1 + j\omega\tau'} \quad (2.20)$$

where  $\varepsilon_{\infty}$  is the saturated permittivity at very high frequencies,  $\varepsilon_s$  is the static permittivity at very low frequencies.  $\Delta\varepsilon = \varepsilon_s - \varepsilon_{\infty}$  is described as the magnitude of the dispersion and finally  $\tau'$  is a relaxation time constant.

### 2.9.3.2 Cole - Cole Model

The Cole-Cole model is a higher-order approximation compared to the Debye model, and provides a more accurate description of the electrical properties of biological tissues, including their frequency-dependent.

### 2.9.4 Microwave Energy Radiation Safety Issues

The known risks associated with electromagnetic radiation exposure are thermal impacts. Radio frequency (RF) and microwave radiation are absorbed by the body and converted to heat.

Since the heating takes place inside the body, it cannot be sensed from the outside. To avoid exposure to dangerous power levels, it is crucial to establish acceptable safety levels when using EM waves for medical applications.

Specific Absorption Rate (SAR) measures the amount of dissipated power (heat) in a unit of tissue mass and is expressed in watts per kilogram (W/kg) of tissue. SAR is defined as [37]:

$$SAR = \frac{\sigma}{2\rho_m} |\vec{E}|^2 \quad (2.21)$$

where  $\sigma$  is the conductivity of the tissue ( $S/m$ ),  $\rho_m$  is the tissue density ( $K_g/m^3$ ) and  $|\vec{E}|$  is the electric field inside the tissue.

## 2.10 Types of Signals

Microwave measurements can be conducted either in the frequency domain or in the time domain. Both approaches have their advantages and disadvantages and the choice between them depends on the nature of the system under investigation and the goals of the measurement.

### **2.10.1 Frequency Domain System**

Frequency domain systems in microwaves are based on inverse scattering techniques, which involve the measurement of scattered fields produced by an object, or a system when it is illuminated by a microwave transmitter. The scattered fields are then used to determine the object's properties, such as its size, shape and electrical characteristics. In inverse scattering techniques, the incident field is first measured, and then subtracted from the total field to obtain the scattered field.

The inverse problem in microwave inverse scattering techniques is to determine the position and permittivity (or dielectric constant) of a scatterer from the measurement of the scattered fields. The solution to this problem is often carried out by using an optimization procedure in which aims to minimize the difference between the measured and calculated data. The field measurements in the inverse scattering problem can be carried out either by using a bistatic configuration with mechanical scanning or an array of antennas with electronic scanning.

In the case of mechanical scanning, the scattered signal data is recorded at each antenna position and stored in the data processor, which can result in a long data acquisition time. In the case of electronic scanning, the array of antennas can provide high-speed data acquisition, potentially reducing the data acquisition time compared to mechanical scanning. However, the use of electronic scanning requires advanced signal processing techniques to estimate the scattered field from the measured data.

### **2.10.2 Time Domain Systems**

Time domain systems are commonly used in Ultra-Wideband (UWB) radar techniques. In medical imaging, UWB radar can be used to obtain images of internal structures of the body, including highly reflective objects such as shrapnel. The technique involves transmitting low-power short pulses of radar energy into the body and detecting the scattered signals with a probe antenna or an array of antennas. The time delay and shape of the received signals are analyzed to obtain information about the location of the scatterers. The processed signals from multiple locations can then be combined to form a 2D or 3D image. In comparison to frequency-domain

measurements, time-domain measurements could have shorter scan times, and more cost-effective measurement equipment [38].

## 2.11 UWB Imaging Technique

Ultra-Wide Band (UWB) technology is preferred for its good range resolution and penetration through materials, due to the high bandwidth of UWB radar. The high bandwidth results in better separation of multiple targets, making UWB a popular choice for various applications such as real-time location tracking, imaging and communication [39].

UWB is a type of microwave imaging technique that uses short pulses to probe a target and gather information about its position, size and composition. The time delay between the transmitted and scattered signals provides information about the distance to the target, while the amplitude of the scattered signals provides information about its reflectivity and composition.

Compared to microwave tomography, UWB radar is considered to be less computationally complex, as it focuses on detecting and localizing regions with highly scattered signals, rather than reconstructing the dielectric properties of the tissues. This makes UWB radar a faster and more efficient method for detecting certain targets such as abnormal tissues and objects, but it provides less detailed information about the composition and structure of the target compared to microwave tomography [34].

UWB systems are known for their ability to transmit large amounts of data with high accuracy, and low power consumption [41].

$$\textit{Fractional Bandwidth} = 2 \frac{(f_h - f_L)}{(f_h + f_L)} . \quad (2.22)$$

where  $f_h$  and  $f_L$  are used to describe the frequency limits of the -10 dB emission limit in the field of radio frequency. The -10 dB emission limit refers to the maximum level of radio frequency energy that can be emitted from a device and still be considered compliant with regulatory standards. The frequency range between  $f_h$

and  $f_L$  defines the frequency band within which the device must meet the -10 dB emission limit.

$$\text{Center Frequency } (f_c) = \frac{f_h + f_L}{2} . \quad (2.23)$$

Lower-frequency electromagnetic waves have better penetrating properties compared to higher-frequency waves. This property makes them suitable for UWB applications where the ability to penetrate through objects is important.

UWB radar uses a wide bandwidth of low-frequency signals which increases its ability to detect hidden objects and provide precise location information. The wavelength of an electromagnetic wave is inversely proportional to its frequency. This means that, as the frequency of an electromagnetic wave increases, its wavelength decreases, making it possible to use smaller receive and transmit antennas.

On the other hand, increasing the center wavelength of the signal results in a lower frequency, making it more suitable for penetrating through layers. This makes the longer wavelength, lower frequency signals more desirable for applications that require the ability to penetrate through objects [34], [40].

# **CHAPTER THREE**

## **SIMULATIONS AND RESULTS OF MICROWAVE IMAGING SYSTEM**

### **3.1 Introduction**

In 2002, the Federal Communications Commission (FCC) approved the use of UWB technology used within the range of 3.1 to 10.6 GHz [41]. UWB imaging systems require specially designed antennae to transmit electromagnetic energy and receive the reflected signal from the human body and any objects within it, such as a shrapnel. The received signals are then processed to determine the location and size of the objects including shrapnel. The human body has unique electrical properties that affect the scattering of electromagnetic (EM) waves, leading to differences in the way that EM waves are reflected, absorbed and transmitted by the body. Therefore, it is important to take into account the electrical properties of the human body when designing UWB antennas for this application. A planar monopole antenna is one type of antenna that has been developed for this purpose. CST Microwave Studio is a powerful software tool for designing the antenna. Exporting the design from CST Microwave Studio allows the user to take the scattered signals as input to the deep neural network when it is used as a tool in recognition and discrimination in this work.

In this chapter a simple two-dimensional homogeneous model of the human body has been built. The model can be created by dividing the body into different layers, each with its electrical properties, such as conductivity and permittivity. The main layers typically include the skin, fat, muscle and bone.

### **3.2 UWB Antenna**

The antenna is a critical component for UWB systems. The UWB antenna technology is based on the transmission of short, low-power pulses over a wide bandwidth, which allows for the detection of hidden objects. This is because the short

pulses can penetrate through materials and bounce back from the hidden object, providing information about its location, and composition. The wide bandwidth of UWB signals also enables high-resolution imaging, making it a promising technology for microwave hidden object detection. Several fundamental parameters are used to describe the performance of UWB antenna, including:

- **Radiation Pattern**

The radiation pattern is a representation of the relative distribution of the electric and magnetic fields generated by an antenna in space. This space can be divided into three regions: reactive near field, radiating near field, and far field. The region in which an antenna operates depends on its physical size compared to the wavelength of the electromagnetic waves.

When the antenna size is much smaller than the wavelength ( $D/\lambda \ll 1$ ), the antenna operates in the reactive near field region. In this region, the electromagnetic fields have both reactive and radiating components, and the behavior of the antenna is strongly influenced by its immediate surroundings.

When the antenna size is comparable to the wavelength ( $D/\lambda \sim 1$ ), the antenna operates in the radiating near field region. In this region, the antenna starts to exhibit more radiating properties, and the reactive components diminish as the distance from the antenna increases.

When the antenna size is much larger than the wavelength ( $D/\lambda \gg 1$ ), the antenna operates in the far field region. In this region, the electromagnetic fields are predominantly radiating, and the antenna behaves as a traditional electromagnetic radiator.

Radiation patterns are defined in spherical coordinates. The x-y plane contains the phi component where the theta-component is 90 degrees ( $\phi = 0$  where  $\theta = 90^\circ$ ), and is usually referred to as the azimuthal plane. The x-z plane contains the theta-component where phi is zero degrees, and usually indicates the elevation plane ( $\theta = 0$  where  $\phi = 90^\circ$ ). A linearly polarized antenna is often described in terms of its principal E-field (electric field), and H-field (magnetic field) patterns. The E-field

pattern represents the distribution of the electric field in the direction of polarization, while the H-field pattern represents the distribution of the magnetic field perpendicular to the direction of polarization [42].

- **Bandwidth**

The bandwidth (BW) is the range of frequencies where an antenna's performance complies with a given specification. The antenna must typically offer a return loss of less than -10 dB over its bandwidth [42].

- **Radiation Pattern Lobes**

The radiation pattern of a directional antenna is represented by multiple lobes or peaks, where the main lobe has the highest field intensity, and the other lobes are called minor or back lobes. The direction of the main lobe determines the direction of maximum radiation, and sensitivity of the antenna. The HPBW is defined as the angular separation between the points on the main lobe where the power drops to half of its maximum value [42].

- **Gain and Directivity**

The Gain of an antenna is a measure of its ability to direct the radio waves in a specific direction, rather than distributing it uniformly in all directions. It is expressed as the ratio of the power density (intensity) in a particular direction to the power density, that would be obtained if the power were equally distributed in all directions (isotropic). The gain is usually expressed in decibels (dB) relative to an isotropic radiator.

$$Gain = \frac{\text{radiation intensity}}{\text{total input(accepted) power}} = 4\pi \frac{U(\theta,\phi)}{P_{in}} . \quad (3.1)$$

Directivity is defined as the maximum gain of an antenna in a particular direction, relative to the gain of an isotropic radiator, which has equal power output in all directions. Directivity is a measure of the ability of an antenna to concentrate its radiated power in a specific direction, and is usually expressed in dB [42].

$$D_0 = \frac{U_{max}}{U_0} = \frac{4\pi U_{max}}{P_{rad}} . \quad (3.2)$$

### 3.3 CST Microwave Studio Software

CST Microwave Studio (CST MWS) is a component of CST Studio Suite that provides fast and accurate 3-D electromagnetic simulation tools for high-frequency problems. It offers a variety of different solvers that operate in both time and frequency domains. The software offers advanced solvers, visualization tools, and an extensive library of materials and components to help users in the design and analysis of complex electromagnetic systems [43].

CST Microwave Studio is a software tool used to design antennas by simulating their electromagnetic behavior. The tool can evaluate various performance parameters such as reflection coefficient, impedance matching, gain, radiation efficiency, and radiation pattern. This helps in analyzing the antenna's performance and improving its design.

The transient solver gives appropriate results of homogeneous human layers imaging. An antenna that transmits and receives the signal, known as a wideband planner, has been used to collect data. The decisive parameter S11 is used for detecting a hidden object. S11 refers to the ratio of signal that reflects from the port for a signal incident on that port.

In the design of antenna, several important factors are needed to be considered to ensure that the antenna works effectively and safely:

- Resonant frequency: In medical applications, the resonant frequency must be chosen to ensure that it falls within the frequency range of the target tissue layer.
- Dielectric constant: This is a measure of the electrical permittivity of a material and determines how the material affects the propagation of electromagnetic waves. In medical applications, it is important to consider the dielectric constant of the human body.
- Type of tissue layer: There are different types of tissue layers in human body, such as skin, fat, muscle and bone, which have different electrical properties that can affect the performance of the antenna.

- Thickness of tissue layer: This is also an important factor to consider, as it can significantly impact the performance of the antenna. Thicker tissue layers can cause greater losses and reduce the efficiency of the antenna.

### **3.4 Planar Monopole Antenna Design**

a monopole antenna can be considered a planar monopole due to its structure, where the radiator is placed on one side of a substrate and the ground plane is on the opposite side, forming a planar arrangement.

A UWB monopole antenna with a notched band at (2.44 - 2.77 GHz) is presented in [44]. The band-notched characteristic of an antenna is made possible by the C-shaped slot in the round shape radiating patch, and the ground plane.

The slot helps to avoid this electromagnetic interference, as it is designed to reject specific frequency bands that cause interference. This can be done without significantly increasing the size or complexity of the system. Additionally, these slotted antennas can offer great radiation efficiency and low dispersion. Additionally, slots can help in reducing the size of the antenna by shifting its resonant frequency. The size and position of the slots determine whether the resonant frequency is shifted to a higher or lower value. The insertion of slots also helps to reduce the power lost to surface waves. Surface waves are generated in antennas, due to the interaction of the radiated field with the surface of the antenna. These waves can cause a significant reduction in the radiation efficiency of the antenna. By introducing slots, the path of the surface waves is disrupted, and this helps to reduce their impact on the efficiency of the antenna [45].

A 1 to 6 GHz bandwidth is the design goal, with a 10 dB return loss reference. The simulations are done by using electromagnetic simulators (CST) as a tool. The suggested elliptical band-notched UWB antenna's design as well as a picture of the constructed antenna is shown in Figure (3.1). The antenna is built using an FR4 substrate having a 1.6 mm thickness and a 4.3 dielectric constant. The type of materials used in UWB antenna design are listed in Table (3.1).

The suggested antenna consists of the elliptical radiating patch fed by a microstrip line of 50 ohms along the principal axis. The aspect ratio of an antenna is defined as the ratio of the length of its major axis to the length of its minor axis. An aspect ratio of 1.1 means that the length of the major axis is 1.1 times greater than the length of the minor axis to get the broadband characteristics. The parameters for the suggested antenna are listed in Table (3.2).

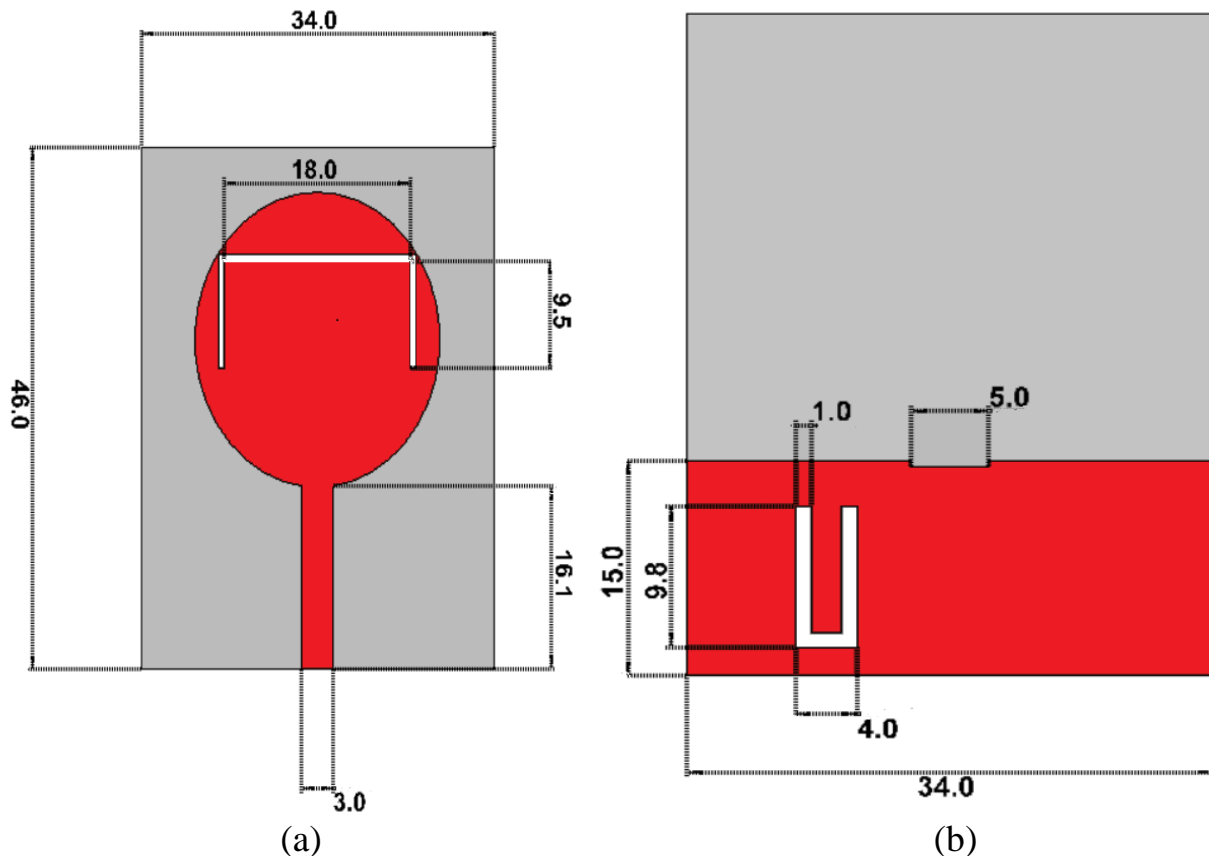


Figure 3.1: The suggested antenna's geometry in (a) front and (b) back views. All measurements are in millimeters.

Table 3.1: Material properties of antenna design.

component	Material name	Color
elliptical radiator	Perfect electrical conductor (PEC)	Red
ground plane	Perfect electrical conductor (PEC)	Red
Substrate	FR4	Grey
feedline	Perfect electrical conductor (PEC)	Red

Table 3.2: Design parameters of the proposed antenna.

Value (mm)	Parameters
<b>46*34</b>	Dimensions of the substrate, including its length and width
<b>13.1</b>	The major radius of the elliptical patch
<b>11.8</b>	The minor radius of the elliptical patch
<b>16.1*3</b>	Length and width of the feedline
<b>15*34</b>	Dimensions of the ground plane, including its length and width

The lowest frequency of the broadband antenna is  $f_L$  which is given in the following equation [46].

$$f_L = \frac{c}{\lambda} = \frac{7.2}{L+r+p} . \quad (3.3)$$

The cylindrical monopole antenna's length (L), and radius (r) are determined by equating the area of the antenna as follows:

$$2\pi rL = \pi ab . \quad (3.4)$$

$$\text{Let, } L = 2b . \quad (3.5)$$

$$\text{Then, } r = \frac{a}{4} . \quad (3.6)$$

Where 'p' is the gap between the ground plane and the radiating patch, *a* and *b* are the major axis and the minor axis of the radiating patch respectively.

Slots are utilized to get the band-notch characteristics, two slots are created: one on the radiating patch and one in the ground plane. The length of the slot is denoted by  $L_n$ , and is calculated by using the equation below.

$$L_n = \frac{c}{2f_r\sqrt{\epsilon_{eff}}} = \frac{\lambda}{2} . \quad (3.7)$$

where  $L_n$  denotes the length of the slot,  $\epsilon_{eff}$  the effective dielectric constant ( $\epsilon_{eff} = \frac{\epsilon_r+1}{2}$ ),  $\epsilon_r$  is the dielectric constant, and *c* denotes the light velocity,  $f_r$  is the resonant frequency [47].

The return loss for the designed UWB monopole antenna as a function of frequency is shown in Figure (3.2). The results demonstrate that the antenna's return loss performance is ultra-wideband, radiating at frequencies between 1 GHz and 6 GHz. It is noticed that at the resonance frequency =2.24 GHz the reflection loss (S11) is -40.5dB. The results of simulation of VSWR are illustrated in Figure (3.3). The VSWR is 1.0190 at f=2.24GHz.

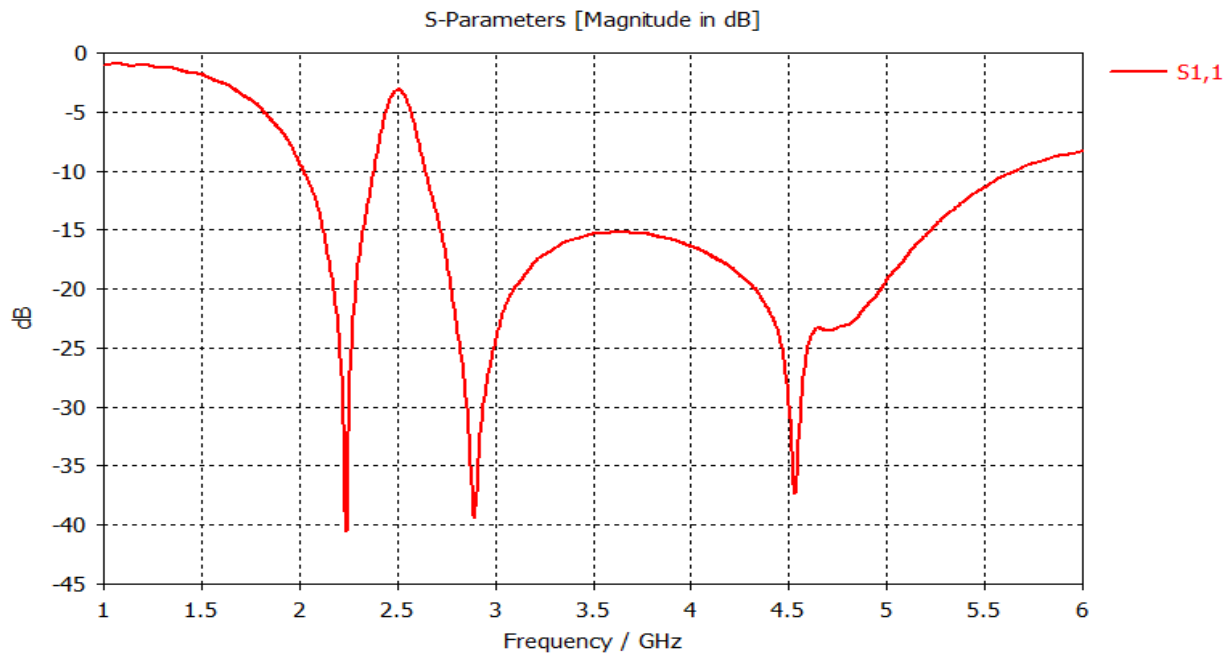


Figure 3.2: Simulated reflection coefficient results of UWB monopole antenna.

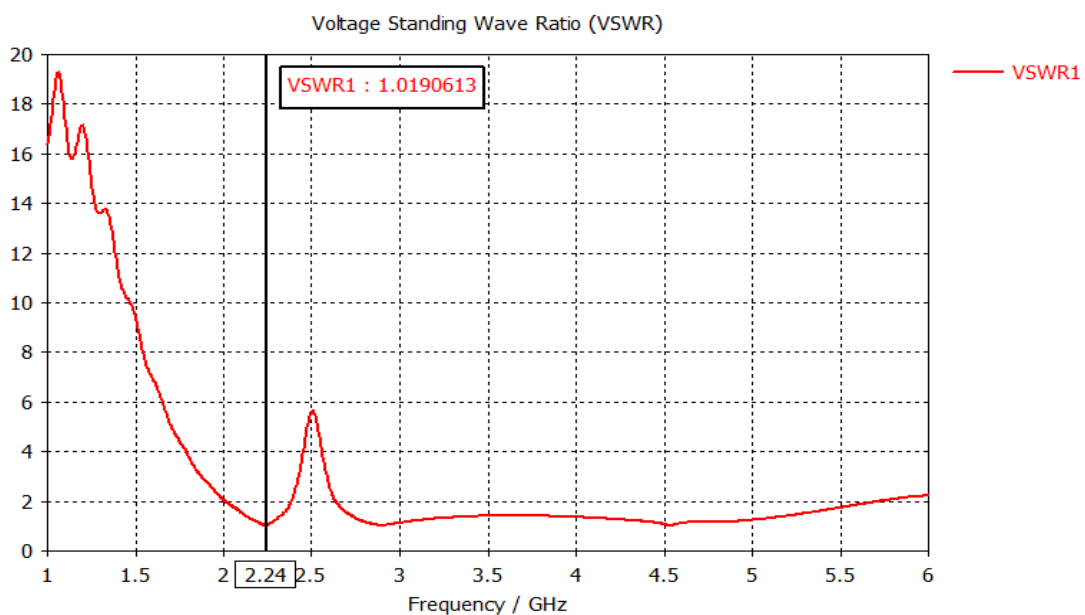


Figure 3.3: Simulated VSWR with frequency.

The simulated 3D radiation pattern of the proposed antenna at 2.24 GHz is shown in Figure (3.4). The antenna shows responsible power gain of 2.067dBi, and the directivity of 2.653 dBi at 2.24 GHz. The gain must be less or equal to the directivity, efficiency equal  $(\text{gain}/\text{directivity}) \times 100$ ,  $(2.067/2.653) \times 100 = 77.9\%$ .

The simulated E-Plane (y-z), and H-Plane (x-z) radiation patterns of proposed antenna at resonant frequency 2.24 GHz are shown in Figure (3.5). The E-Plane and H-Plane refer to two different cross-sectional views of the radiation pattern of an antenna. The E-Plane shows the electric field pattern, while the H-Plane shows the magnetic field pattern. In the x-z plane ( $\phi = 0^\circ$ ) and the y-z plane ( $\phi = 90^\circ$ ). While the E-Plane pattern has the same far-field field radiation pattern as a dipole antenna, the H-Plane pattern is almost omnidirectional, making it preferable to receive the signal from all directions.

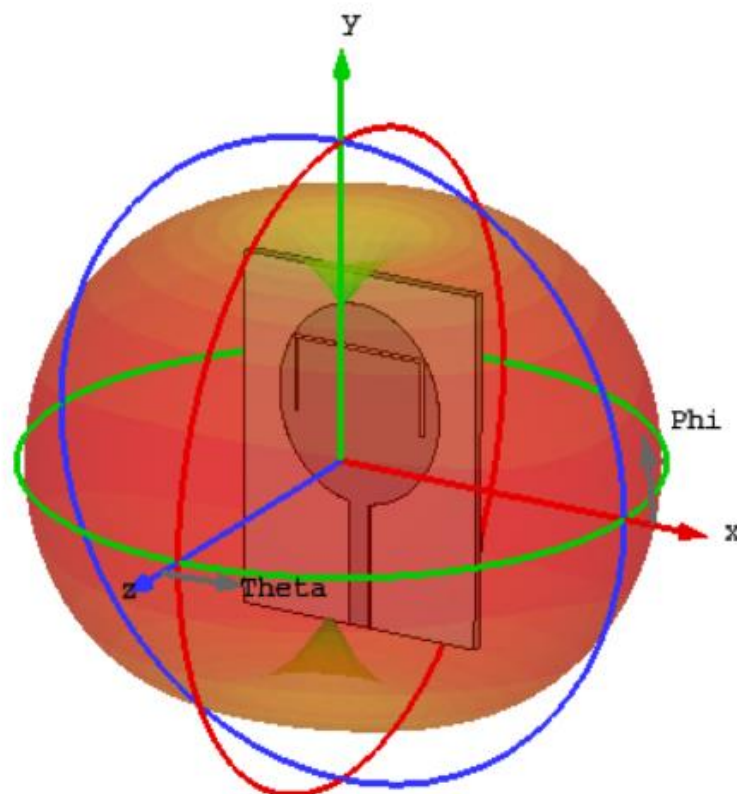


Figure 3.4: 3D Radiation plot at 2.24 GHz.

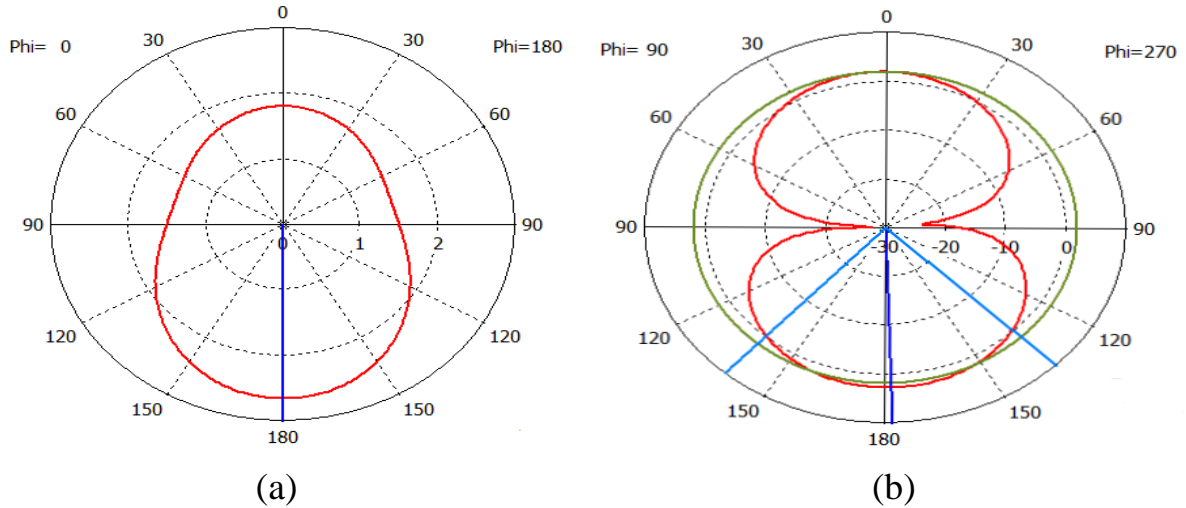


Figure 3.5: The proposed antenna's radiation patterns, (a) H-plane, and (b) E-plane.

### 3.5 Modeling Human Body Layers

In this work, the antenna's performance was simulated in simplified human body phantom layers created in CST Microwave Studio. The layers modeled the effect of the human body on the antenna's behavior, allowing for a detailed analysis of the antenna's performance when placed close to the human body.

A model that depicts the main layers of the human body can be used to validate any imaging approach. The model is made up of four layers: skin, fat, muscle and bone. The shrapnel is located inside. When an EM wave encounters a layer of human tissue, it interacts with the electric and magnetic fields of the tissue, causing the wave to scatter in multiple directions. The amount of scattering and the direction of the scattered wave depend on the size, shape, and material of the shrapnel, as well as the frequency and polarization of the incident wave.

In this model, the shrapnel is assumed to be aspherical shape, and the material of shrapnel is copper. Copper is a highly conductive metal, which means that it will strongly interact with the electric and magnetic fields of the incident EM wave.

The homogenous model of human layers that has been utilized in this work is built and depicted in Figure (3.6) which shows a side view in CST simulation and top cross section view. The model's dimensions were presumed to be those in table (3.3). The electrical and physical characteristics of several human tissues that has been in

this work are shown in table (3.4), where  $\epsilon_r$  is the relative dielectric constant,  $\sigma$  is conductivity (S/m), and  $\rho$  is the mass density of the tissue (kg/m<sup>3</sup>) [48]. The shrapnel radius size can range from 5 mm to 15 mm, additionally utilized different locations on the z-axis and on the x-axis.

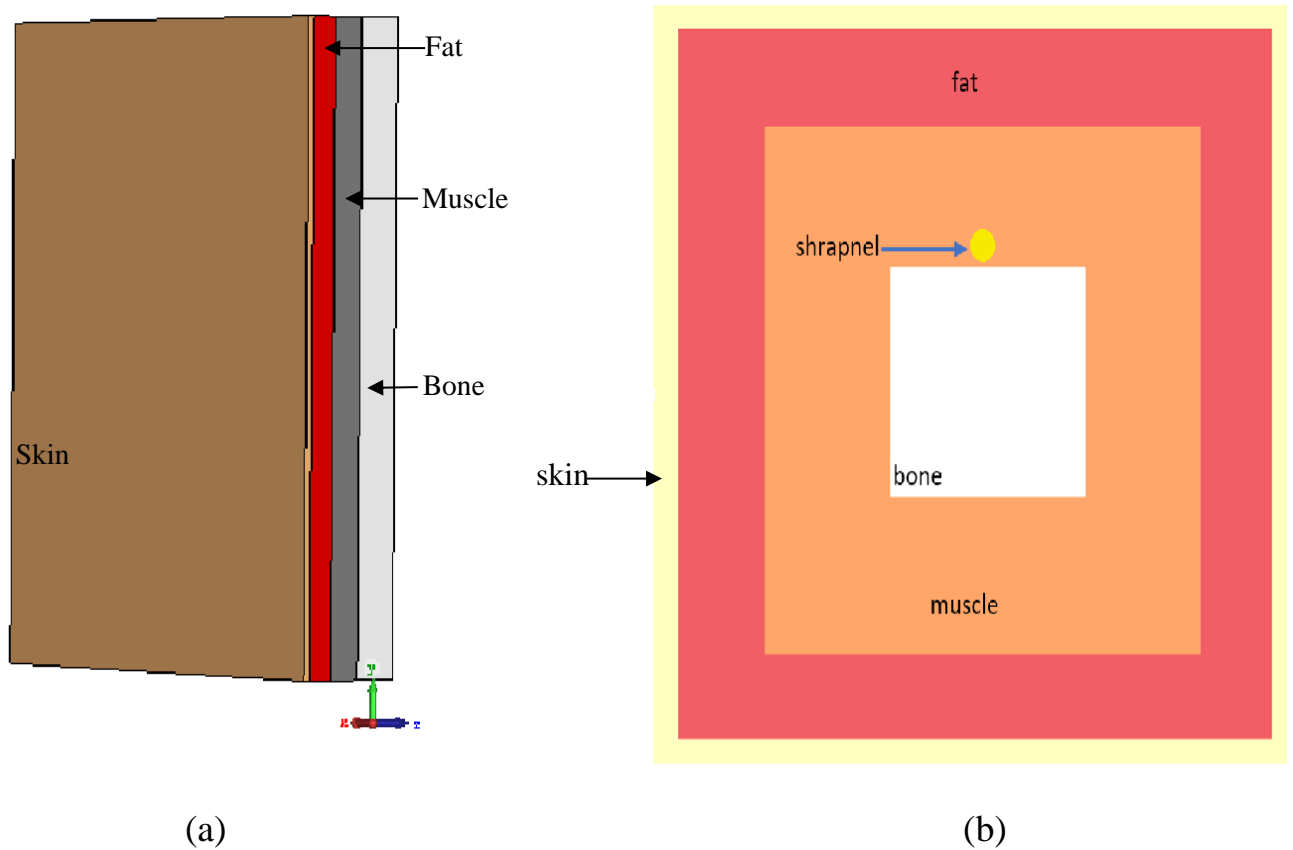


Figure 3.6: The designed model (a)side view in CST, (b) cross sectional view.

Table 3.3: The dimensions of the designed homogenous model.

component of a model	model dimensions mm
Model width	200
Model length	300
Skin thickness	3
Fat thickness	12
Muscle thickness	15
Bone thickness	20

Table 3.4: The electrical properties of the designed homogenous model.

Tissue type	$\epsilon_r$	$\sigma$ [S/m]	$\rho$ [kg/m <sup>3</sup> ]
Skin	38.00	1.46	1010
Fat	5.28	0.11	920
Muscle	52.73	1.74	1040
Bone	11.38	0.39	1850

### 3.6 Human Model Effect on Antenna Parameters

The human body can be considered as a lossy and dispersive medium, with its electrical properties varying with frequency. The high conductivity and permittivity of human body tissues can cause significant signal attenuation losses. The signal attenuation can be expressed mathematically using the following equation [49]:

$$L_\alpha = 20 \log_{10}(e^{-\alpha L}) . \quad (3.8)$$

Where  $\alpha$  (Np/m) is the attenuation constant, and  $L$  (m) the distance traveled by the signal through the body. The attenuation constant can be calculated by the following equation [49]:

$$\alpha = \omega \sqrt{\frac{\mu\epsilon}{2} \left( 1 + \left( \frac{\sigma}{\omega\epsilon} \right)^2 - 1 \right)} . \quad (3.9)$$

$$\omega = 2\pi f . \quad (3.10)$$

where  $\omega$ (rad/m) and  $\mu$ (H/m) are angular frequency and permeability of human body tissue, whereas the  $\epsilon$  and  $\sigma$  are the permittivity, and conductivity, respectively.

The imaginary part of permeability is equal to 0, because bodily tissues are not magnetic by nature. The losses due to reflections at the boundaries between tissues are calculated as a component of the total attenuation losses in the tissue. This takes into account the reduction in the intensity of the electromagnetic waves as they

pass through the tissue, and reflects off the boundaries between different tissue types. The losses due to the reflections at the boundary between the tissues is calculated as [49]:

$$L_r = 20 \log_{10}(\Gamma) . \quad (3.11)$$

$$\eta = \sqrt{\frac{j\omega\mu}{\sigma+j\omega\varepsilon}} . \quad (3.12)$$

$$\Gamma = \frac{\eta_2 - \eta_1}{\eta_2 + \eta_1} . \quad (3.13)$$

Where  $\eta$  is the intrinsic impedance and  $\Gamma$  is the tissue's boundary reflection coefficient.

Due to the difference in impedance, and electromagnetic characteristics of the two mediums, the transmitted signal is also reflected at the boundary between free space and the skin's outer layer. The received signal power by a receiver is calculated by the following equation [50]:

$$P_{RX} = P_{TX} + G_{TX} + G_{RX} - L_P - e_P - ML_{TX} - ML_{RX} . \quad (3.14)$$

Where  $P$ (dBm) is the power,  $G$ (dB) is the gain and  $ML$  (dB) is impedance mismatch loss. The subscript TX and RX represents transmitter and receiver.  $LP$ (dB) is the path loss and  $eP$  (dB) is the polarization mismatch factor. The path loss  $LP$  is the reduction in power density of an electromagnetic wave, as it propagates through human layer it can be calculated as [50]:

$$L_P = 10n \log\left(\frac{d}{d_0}\right) + 10 \log\left(\frac{4\pi d_0}{\lambda_0}\right)^2 + S . \quad (3.15)$$

where  $n$  is a path loss component that is dependent on the environment. The reference distance is  $d_0$  , and the wavelength is  $\lambda$ (m).  $S$  represents the mean's random scatter [51]. The gain of a conductive medium ( $G_{con}$ ) refers to the ability of the medium to amplify an electrical signal, as it passes through it, is given by [50]:

$$G_{con} = \frac{4\pi R g^2}{R_r} . \quad (3.16)$$

where  $R_r$  is the radiation resistance and  $R$  is the intrinsic resistance. The following equation can be used to compute the intrinsic resistance [51]:

$$R = \sqrt{\frac{\omega\mu}{2\sigma}} . \quad (3.17)$$

$g$  is a function involving the medium's parameters, and its value is provided by [51]:

$$g = \frac{|H|de^{\frac{d}{\delta}}}{I_i} . \quad (3.18)$$

$|H|$  is the magnetic field,  $d$  is the distance,  $I_i$  is the input current,  $\delta$  represents the skin depth. It is clear from equations (3.16) and (3.18) that the value of  $g$  will increase as, the magnetic field inside the human body increases. The antenna's gain will increase with a higher value of  $g$  [52].

The human body can affect the radiation efficiency and radiated power of an antenna. When an antenna is placed close to the human body, it can cause absorption and scattering of electromagnetic waves, which results in a reduction in the radiated power, and efficiency of the antenna. The radiation efficiency of antennas is given by the following equation [52]:

$$\eta = \frac{P_{rad}}{P_{in}} . \quad (3.19)$$

$P_{in}$  is the input power, which is made up of the three power components reflected, absorbed, and radiated ( $P_{ref} + P_{abs} + P_{rad}$ ). The near field coupling in the system causes the absorbed power to be larger than the reflected power, leading to low radiation efficiency, and reduced radiated power. The absorbed power is given by the following equation [53]:

$$P_{abs} = \frac{\omega}{2} \int \epsilon_0 \epsilon_r |E|^2 dv . \quad (3.20)$$

Increases in the absorbed power, and the specific absorption rate (SAR) has an effect on the antenna radiation efficiency. SAR is a measure of the amount of energy absorbed by a body, due to the exposure to electromagnetic fields, and high SAR levels can cause harmful effects on human tissue. The SAR is given by [53]:

$$SAR = \frac{P_L}{\rho} = \frac{\sigma|E|^2}{2\rho} . \quad (3.21)$$

where  $\rho$ (kg/m<sup>3</sup>) is the mass density, and  $E$ (V/m) is electric field. radiation resistance,

and loss resistance are used to represent the radiation efficiency of an antenna. Radiation resistance is a measure of the amount of power radiated by an antenna. Loss resistance is a measure of the power lost in the antenna structure, due to various causes such as dielectric, and conductor losses.

$$\eta = \frac{R_{rad}}{R_{rad}+R_L} . \quad (3.22)$$

Consequently, the antenna's gain would be [53]:

$$G = \eta D . \quad (3.23)$$

where  $D$  is the directivity of the radiated power. Directivity is a measure of the ability of an antenna to radiate power in a specific direction, and is defined as the ratio of the radiation intensity in a specific direction to the average radiation intensity in all directions. The average directivity is given by:

$$D = \frac{U(\theta,\phi)}{U(\theta,\phi)_{avg}} = \frac{4\pi U(\theta,\phi)}{p_t} . \quad (3.24)$$

where  $p_t$  represents the total power radiated. The antenna radiation efficiency also increases as the antenna radiation resistance increases. The radiated power of the antenna has a major effect on its radiation resistance. As a result of this connection between the antenna radiating element, and the body tissues, the antenna's radiation efficiency decreases inside human body tissues. The human body can have a significant effect on the radiation pattern of an antenna. When an antenna is placed near a human body, the body acts as a load, and influences the impedance, and radiation characteristics of the antenna [53].

When testing the performance of a monopole antenna near a simplified skin layer as shown in Figure (3.7). The dimensions of the simplified skin layer of the human body are (200×300× 3) mm. The electrical properties of the human skin tissue layer are  $\epsilon_r = 38$  and  $\sigma = 1.46$  S/m. The simulated return loss plot of the monopole antenna in free space and with skin layer is shown in Figure (3.8).

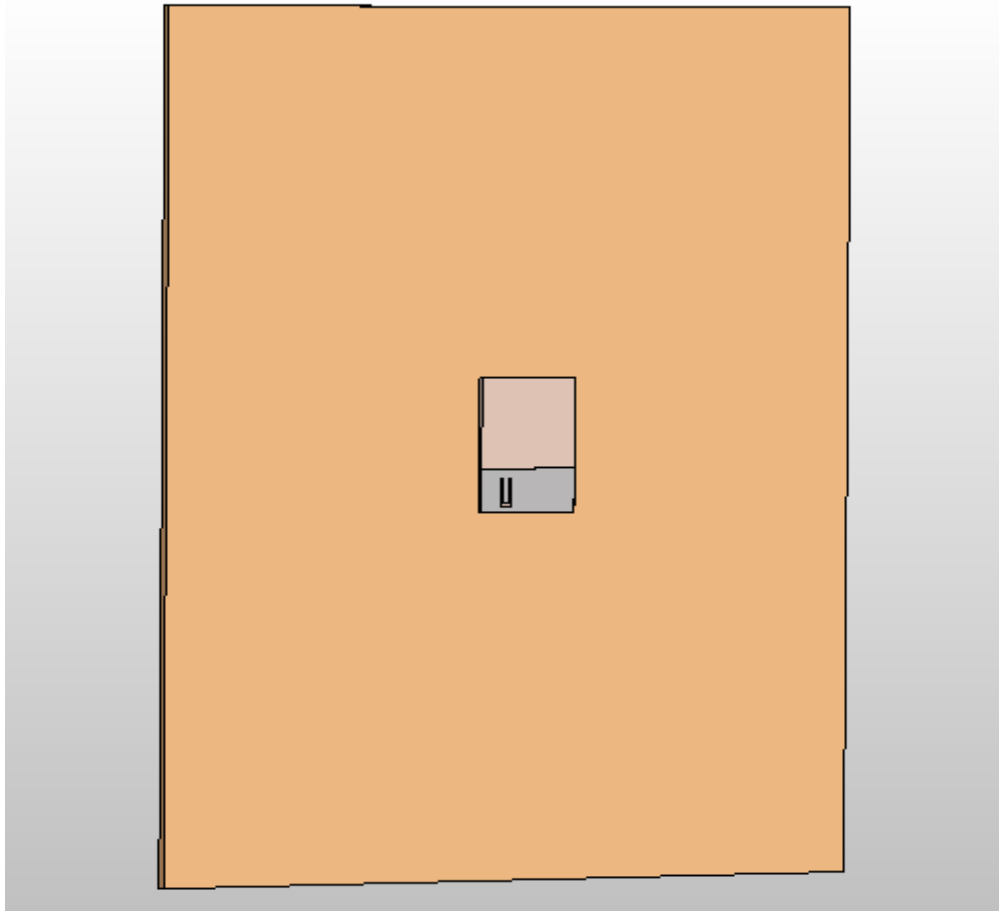


Figure 3.7: Block representation of monopole antenna near simplified skin layer.

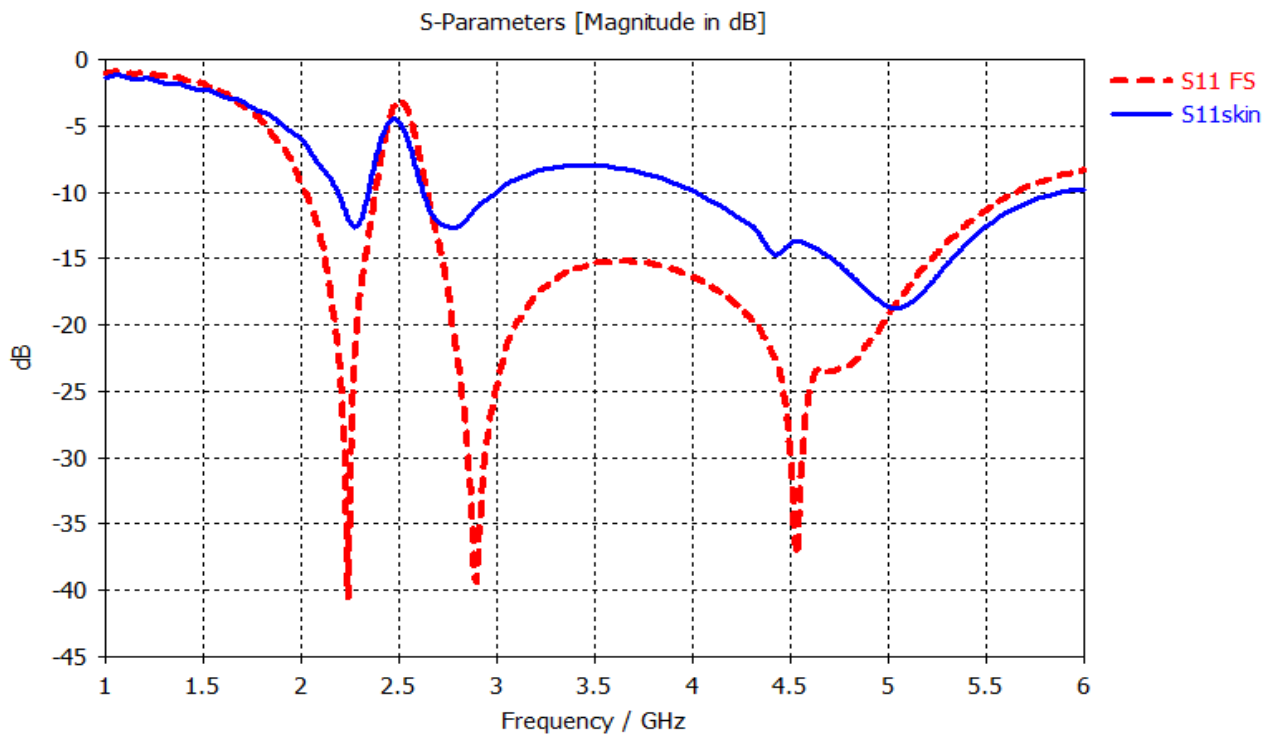


Figure 3.8: Return loss of monopole antenna in free space and with skin layer.

When testing the performance of a monopole antenna near a simplified fat layer as shown in Figure (3.9), the dimensions of the simplified skin layer of the human body are (200×300×12) mm. The electrical properties of the human fat tissue layer are  $\epsilon_r = 5.28$  and  $\sigma = 0.11$  S/m. The simulated return loss plot of the monopole antenna in free space, and with skin layer is shown in Figure (3.10).

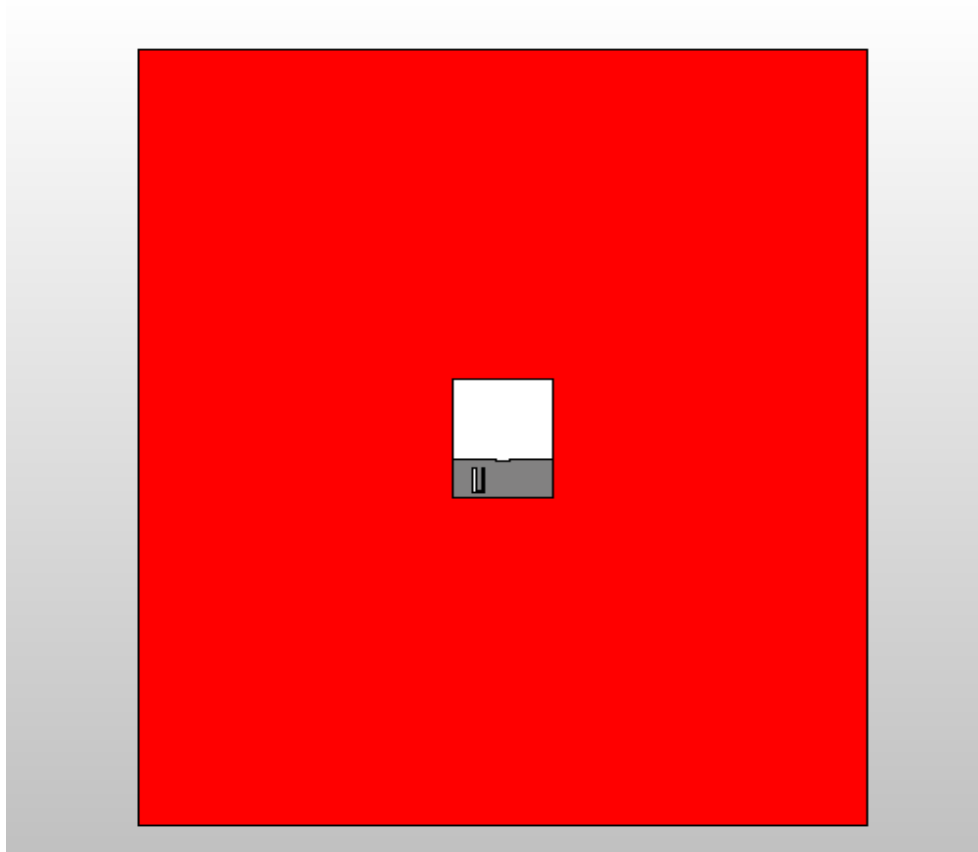


Figure 3.9: Block representation of monopole antenna near simplified fat layer.

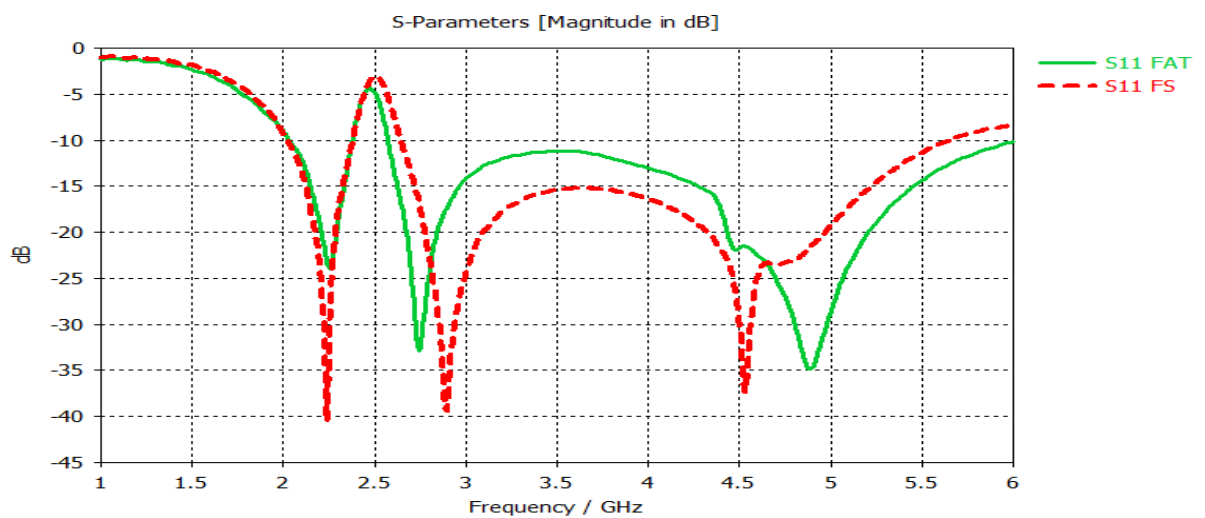


Figure 3.10: Return loss of monopole antenna in free space and with fat layer.

When testing the performance of a monopole antenna near a simplified muscle layer as shown in Figure (3.11). The dimensions of the simplified skin layer of the human body are (200×300×15) mm. The electrical properties of the human muscle tissue layer are  $\epsilon_r = 52.73$  and  $\sigma = 1.74$  S/m. The simulated return loss plot of the monopole antenna in free space and with muscle layer is shown in Figure (3.12).

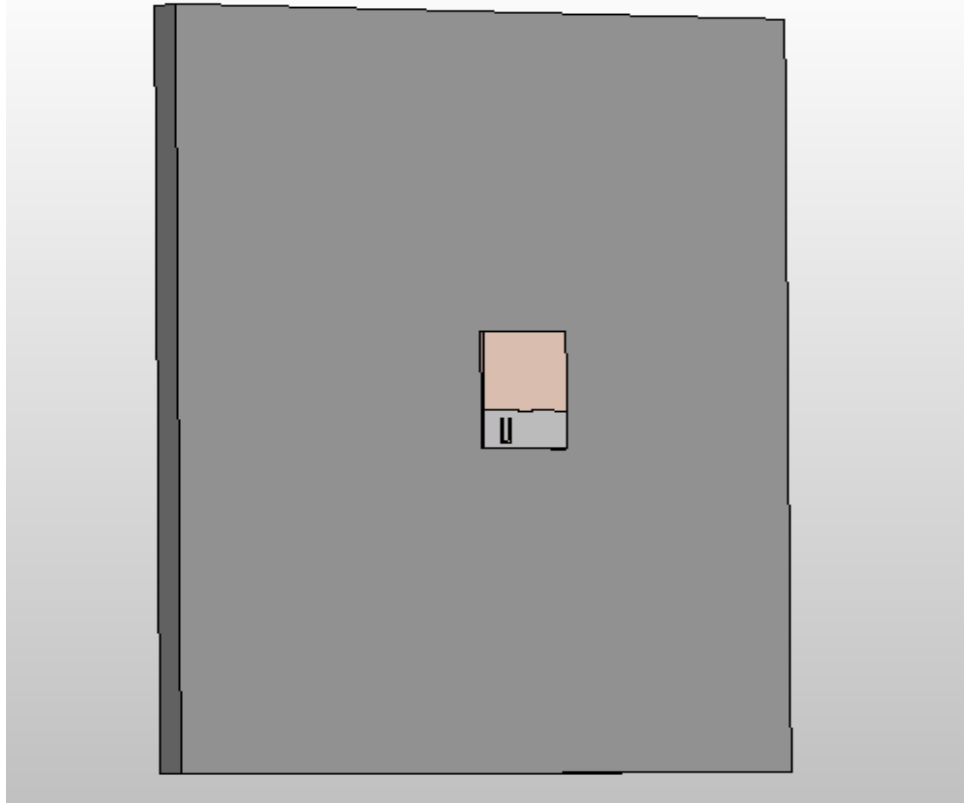


Figure 3.11: Block representation of monopole antenna near simplified muscle layer.

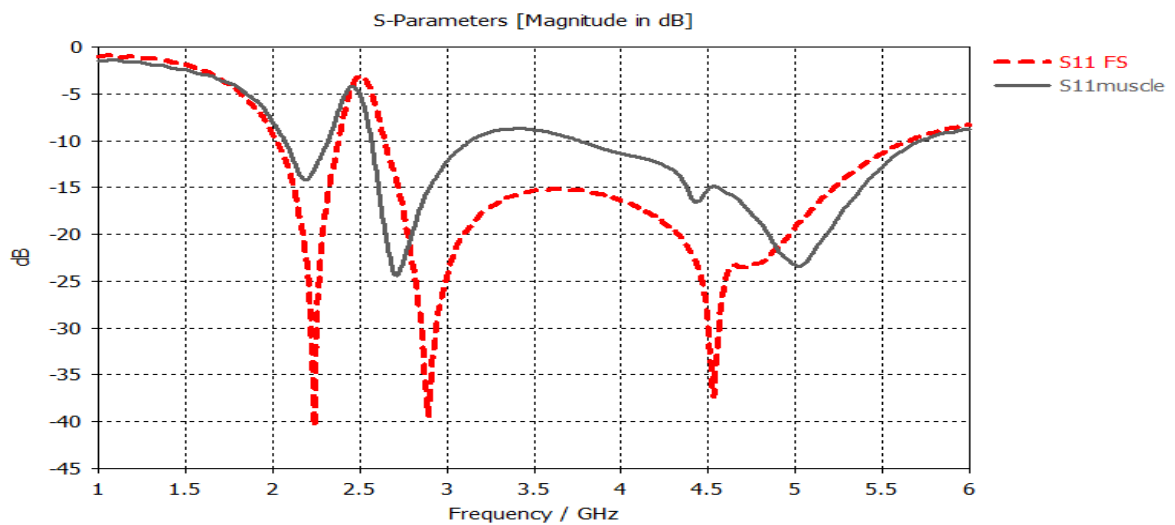


Figure 3.12: Return Loss of Monopole Antenna in Free Space and with Muscle.

When testing the performance of a monopole antenna near a simplified bone layer as shown in Figure (3.13), the dimensions of the simplified bone layer of the human body are (200×300×20) mm. The electrical properties of the human bone tissue layer are  $\epsilon_r = 11.38$  and  $\sigma = 0.39$  S/m. The simulated return loss plot of the monopole antenna in free space and with skin layer is shown in Figure (3.14).

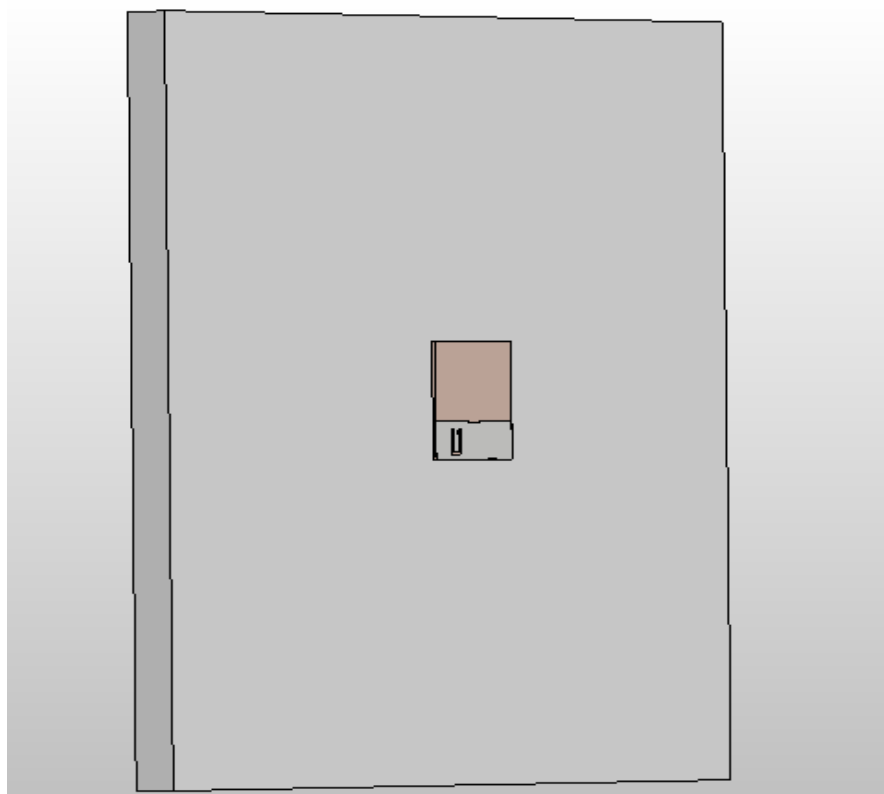


Figure 3.13: Block representation of monopole antenna near simplified bone layer.

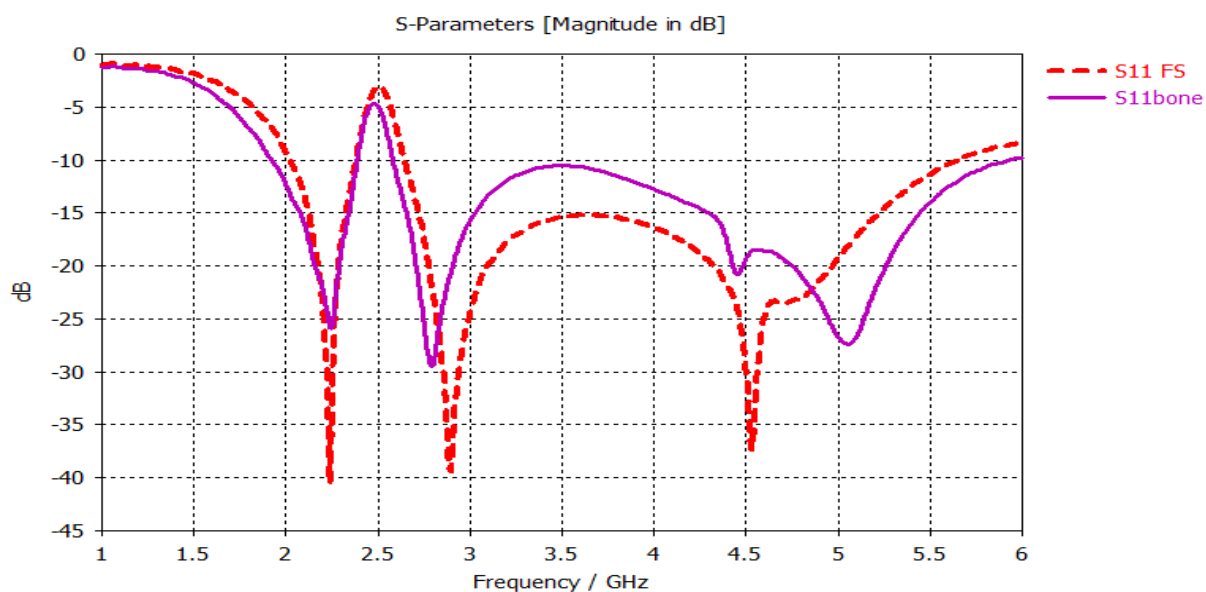


Figure 3.14: Return loss of monopole antenna in free space and with bone layer.

The planner monopole antenna was simulated in simplified multilayer tissue (skin, fat, muscle and bone) .The return loss of the antenna in four layers of the human body phantom is shown in Figure (3.15).

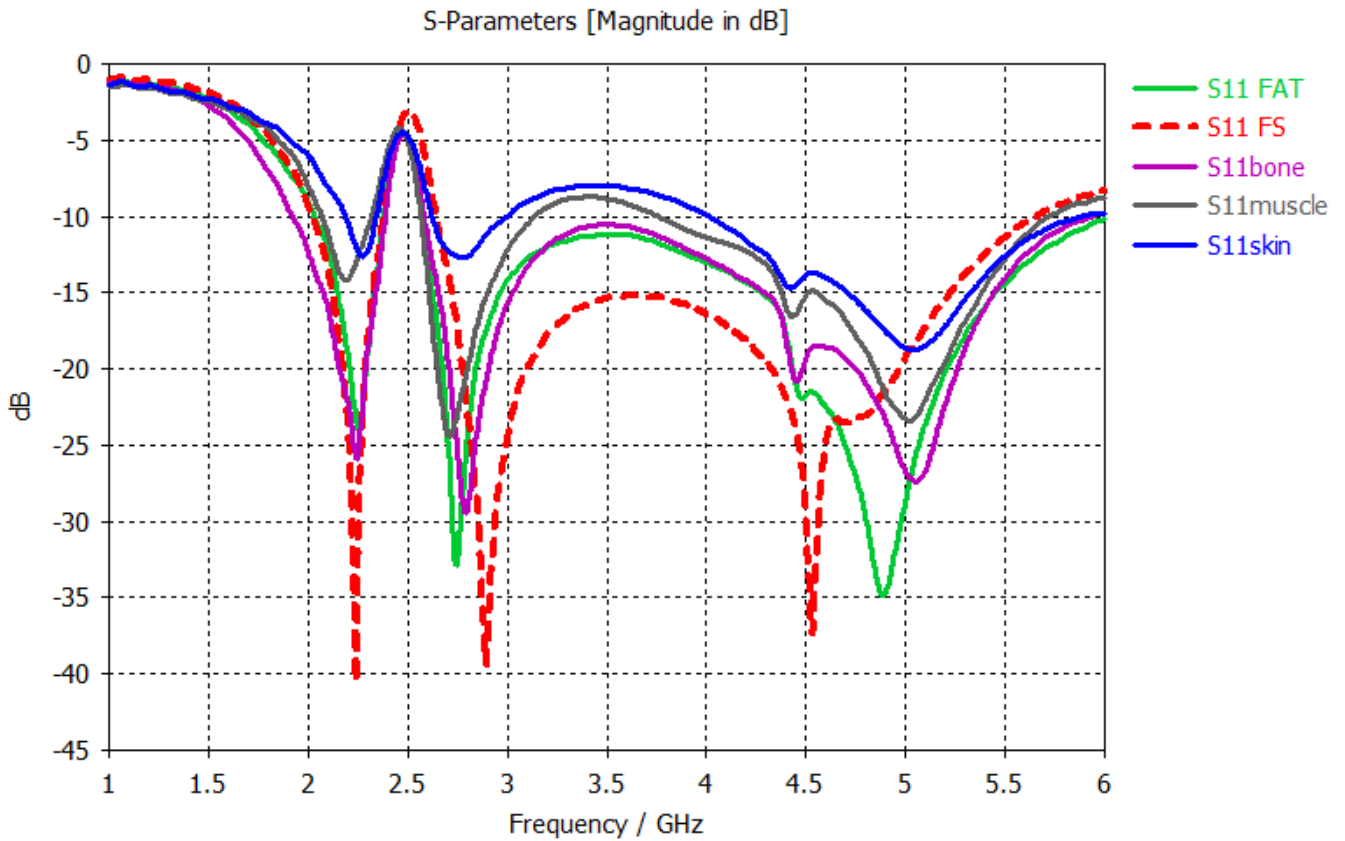


Figure 3.15: Monopole antenna return loss in multilayer tissues (skin, fat, muscle and bone).

The increase in return loss, when a layer of the model with a high relative permittivity is near the antenna, is due to the mismatch in impedance between the antenna and the layer. where the reflection coefficient is a measure of how much of the incident power is reflected at the interface between the antenna and the surrounding medium (in this case, the layer of the model). and a relative permittivity indicates that the layer has a much higher ability to store electrical energy in the presence of an electric field compared to free space (which has a relative permittivity of approximately 1).

The block representation of simplified multilayer tissue phantom, which is used to design and monopole antenna is near to the human layers model is

shown in Figure(3.16). The electrical properties of different tissues of the human body are given in Table (3.3). The simulated return loss of the monopole antenna with absence of body model is given in Figure (3.17)

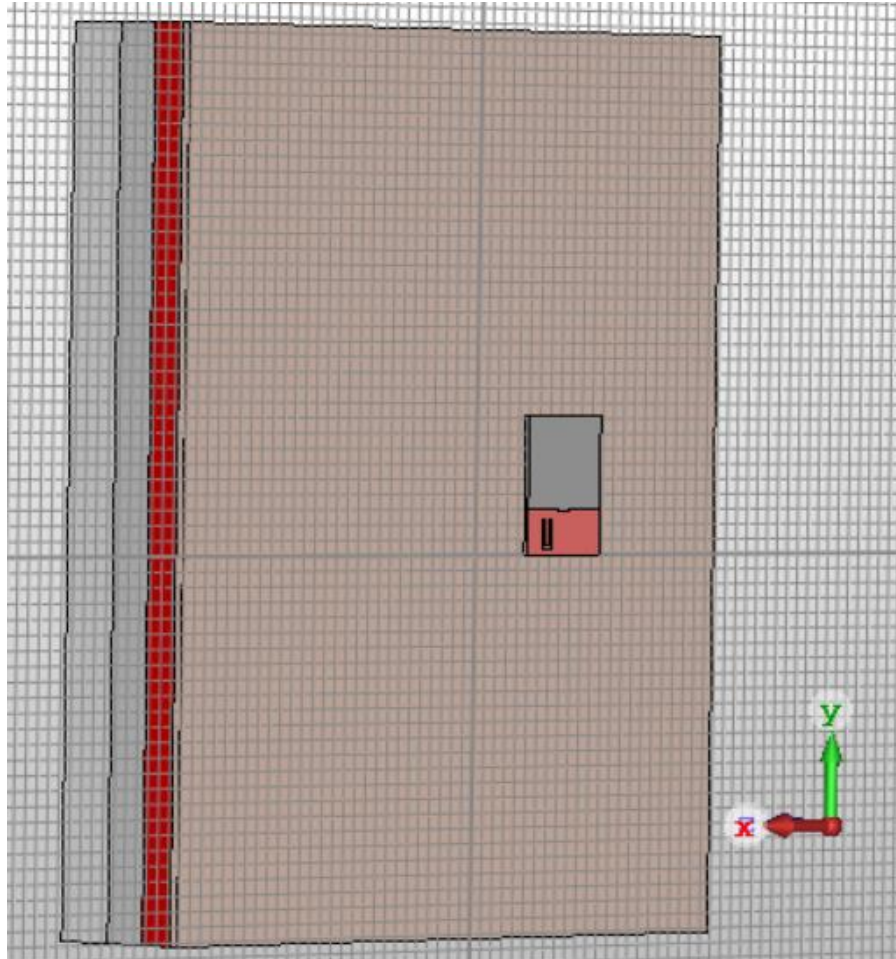


Figure 3.16: Block diagram of monopole antenna near layer of body model.

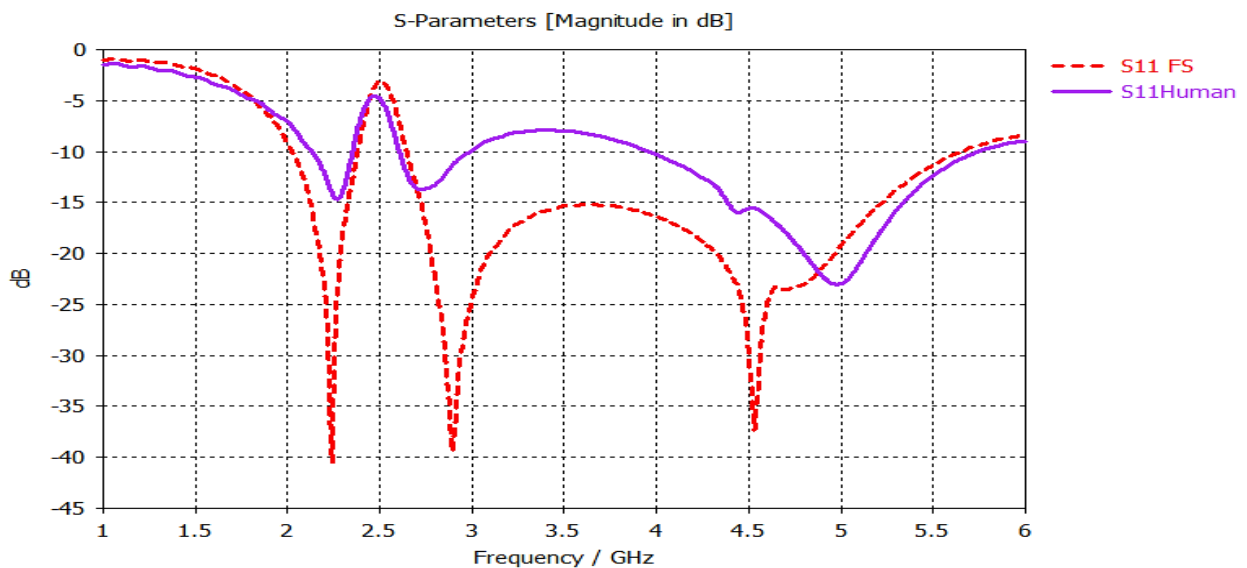


Figure 3.17: Return loss of the monopole antenna with absence of body model.

The received radiation pattern from the homogeneous model is shown in Figure (3.18). The model acts as a scatterer, causing the electromagnetic waves radiated by the antenna to interact with the surface of the model, causing changes in the radiation pattern. Figure (3.19) shows the E-plane and H-plane radiation pattern.

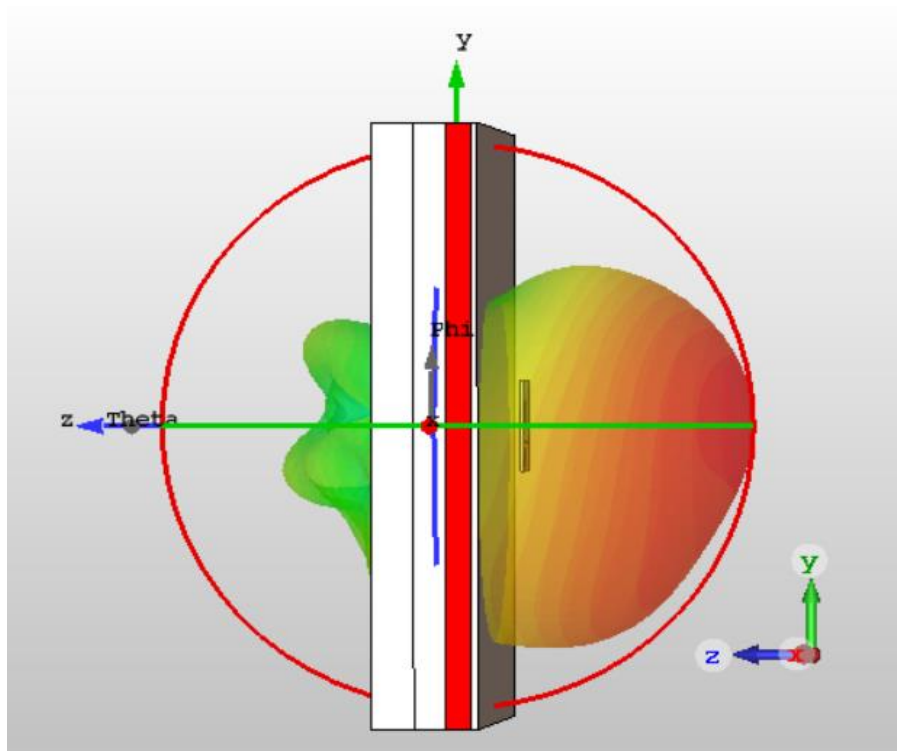


Figure 3.18: 3D radiation pattern received from the model.

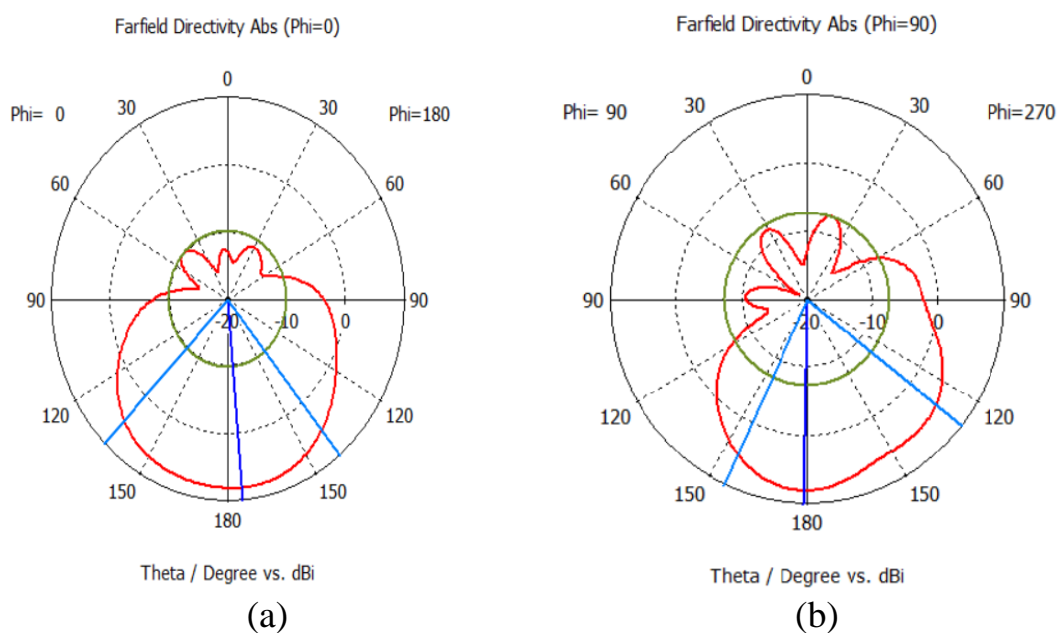


Figure 3.19: Received radiation pattern from the model (a) H-plane (b) E-plane.

# **CHAPTER FOUR**

## **NEURAL NETWORKS IMPLEMENTATION AND RESULTS**

### **4.1 Introduction**

In this chapter, a new approach for detecting hidden objects based on the use of a neural network is presented. Reflection coefficients will be used in combination with deep learning techniques to detect buried objects. In this approach, an UWB antenna is used to measure the reflection coefficients of the human body model with a shrapnel inside at various locations. The measured reflection data are then used as input data to a deep learning model, such as a convolutional neural network, to detect the presence of buried objects.

Deep learning can be trained on a dataset of measured reflection coefficients with known hidden objects to learn the relationship between the reflection coefficients and the presence of hidden objects. During the detection process, the DL takes the measured reflection coefficients as input, and produces a map of the probabilities of the presence of hidden objects.

From the perspective of a neural network, it is feasible to state that the differences between the scattering characteristics of healthy and injured humans indicate that the dispersed signals captured at various locations around the model carry the telltale signs of the presence of shrapnel. Table (4.1) shows the hypothesis for shrapnel detection using a neural network. The hypothesis assumes that dispersed signals collected at various locations around the model contain distinct features indicative of the presence of shrapnel.

It is important to note that the accuracy of this approach will depend on the quality and quantity of the data used to train the network, as well as the architecture, and training method used. The flow chart in Figure (4.1) illustrates how the process steps is done.

Table 4.1: Hypotheses and Rationale for shrapnel detection using a neural network.

<b>Hypothesis</b>	<b>Rationale</b>
<p>Dispersed signals collected at various locations around the model contain distinct features indicative of the presence of shrapnel.</p>	<p>It is assumed that when an EM wave encounters shrapnel within the human body model, the interaction with the electric and magnetic fields of the tissue causes the wave to scatter. This scattering behavior is influenced by the size, shape and material of the shrapnel, as well as the frequency and polarization of the incident wave. The hypothesis suggests that these scattering characteristics produce discernible features in the dispersed signals that can be captured and utilized by a neural network.</p>
<p>The neural network can learn to identify and extract the distinct features from the dispersed signals associated with the presence of shrapnel</p>	<p>Neural networks have the ability to learn complex patterns, and features from input data. By training on dispersed signals captured at various locations, the neural network can potentially learn to distinguish the patterns associated with the presence of shrapnel.</p>
<p>The neural network can accurately classify the presence of shrapnel with different radius sizes (5 mm, 10 mm, and 15 mm).</p>	<p>The neural network can generalize its learning to accurately classify the presence of shrapnel, regardless of its radius size.</p>
<p>The neural network can accurately pinpoint the location of shrapnel within the human body model based on received signals from various locations.</p>	<p>By comparing received signals collected at different locations, the neural network can potentially infer the location of the shrapnel within the human body model.</p>

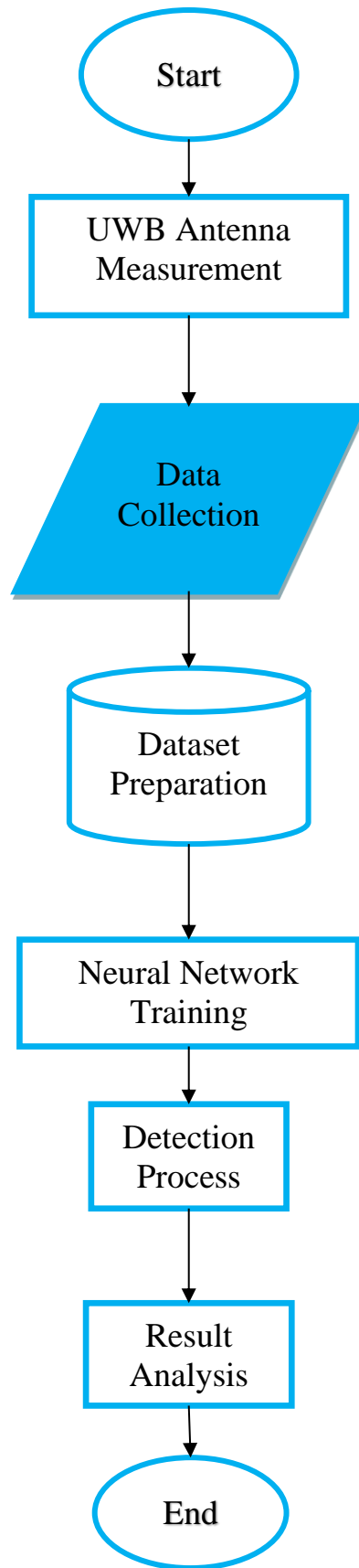


Figure 4.1: The flow chart of process steps.

The process begins with UWB Antenna Measurement to understand how electromagnetic waves interact with hidden objects. Data Collection gathers measured reflection coefficients. Dataset Preparation creates a dataset with reflection coefficients and labels (presence/absence of hidden objects). Neural Network Training uses a CNN to learn the relationship between coefficients and object presence. Detection Process inputs coefficients into the trained CNN for predicting probabilities. Deep Learning Inference yields an output map of probabilities for object presence. Result Analysis identifies likely locations of hidden objects. The process concludes with the End step.

## **4.2 Dataset Preparation for Homogenous Model**

To generate the dataset necessary for detection and recognition, an UWB monopole antenna is set at 10 mm from the model surface with a view to receive the scattered signals. The model has shrapnel in a variety of places. The antenna is shifted on the destination range in x coordinates, and at each 10mm the reflection coefficient (S11) is examined using the electromagnetic simulator CST Microwave Studio.

The reflection loss of a homogeneous model when shrapnel of different sizes is immersed is the amount of energy that is reflected back by the model and shrapnel as a result of the scattering process. The reflection loss is determined by the scattering properties of the shrapnel and the material of the model. The size of the shrapnel can affect the reflection loss, as larger shrapnel can scatter more energy than smaller shrapnel. When the shrapnel is immersed in the model at a depth of 30 mm, change the radius (5, 10, 15) and each time the reflection coefficient is measured. The information that depicts the scattered signals, as they were measured at each site is kept in a database. The simulated reflection loss (S11) of three different sized shrapnel is displayed in Figure (4.2).

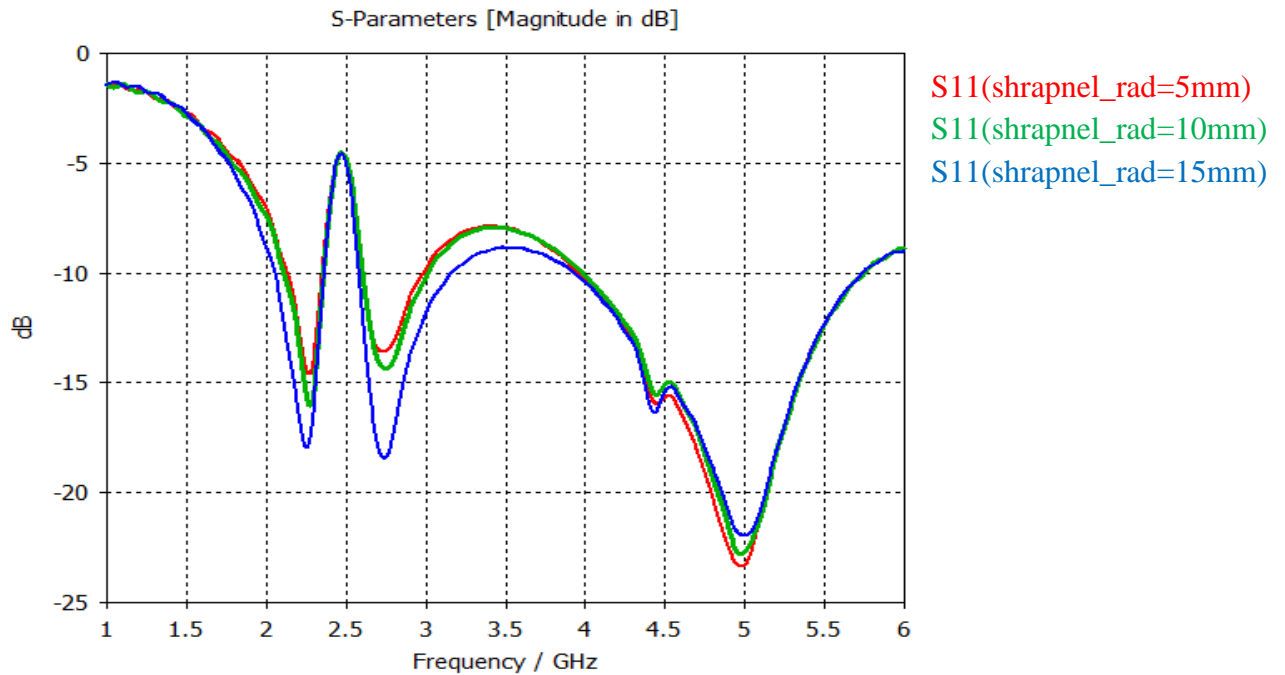


Figure 4.2: Simulated reflection loss for three different sizes.

### 4.3 Neural Network Designer in MATLAB

The Neural Network Designer in MATLAB is a graphical user interface (GUI) tool that allows users to create, design and train models in a visual and interactive manner. The tool enables users to easily experiment with different network architectures, hyperparameters and training options and provides visualization and performance metrics to monitor the training progress. To implement the design of a neural network in MATLAB:

- 1- Start the Neural Network Designer application in MATLAB typing `>> nnstart` in the MATLAB command prompt and pressing enter.
- 2- The Neural Network Designer application in MATLAB includes several wizards to help solving different types of deep learning problems. The wizards guide users through the process of loading data, defining the network architecture, training the network and providing visualizations and performance metrics to help in evaluating the network's performance as shown in Figure (4.3).

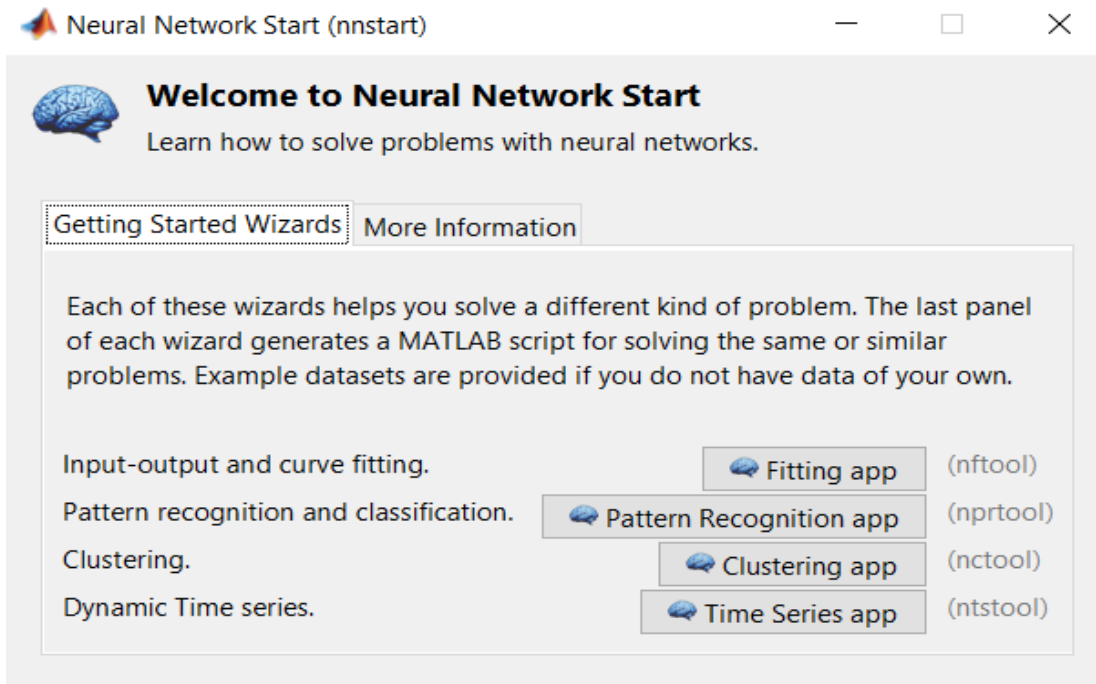


Figure 4.3: Neural network start in MATLAB.

- 3- Click on the pattern recognition application (nprtool), then select the data that are used as inputs that were generated using EM simulator.
- 4- Select the data that are used as target, split the data into training and validation sets. For example, if the validation ratio is set to 20%, then 20% of the data will be used for validation, and the remaining 80% will be used for training.
- 5- Choose the number of layers, neurons, as well as activation functions used by the hidden and output layers.
- 6- Set the training parameters such as the number of epochs, minimum accepted error, learning rate and the performance function.
- 7- Click the "Train" button to start the training process. The training process will run for the specified number of epochs, and the network's performance on the training and validation sets will be displayed.
- 8- After training, use the "Test" button to evaluate the network on a test set. The behavior of system can be monitored through the level of the output mean square error (MSE). In nnstart, the training error curve shows the MSE as a function of the number of epochs [56].

#### 4.4 One-Dimensional Locating of Shrapnel Using ANN

Whenever a shrapnel changes its position in the z direction (depth), a dataset of reflection coefficients is collected using a CST model. This dataset is then used to train an artificial neural network (ANN) to predict the absence or presence, as well as the size and location (depth) of any shrapnel. To train the ANN, the collected dataset of reflection coefficients would be needed to be labeled according to whether or not a shrapnel was present, and if so, the size and depth of the shrapnel.

In this work, "nnstart" in MATLAB is used to explore different network architectures and training strategies, and to experiment with different types of data and input/output mappings. "nnstart" is also used to compare the performance of different networks, and to optimize network's hyperparameters.

In the Neural Network Start GUI, can create a neural network by selecting a network type, such as feedforward or radial basis, and specifying the network architecture, such as the number of layers, neurons per layer, and activation functions. can also import data, preprocess it and split it into training, validation and test sets.

To determine the presence or absence of fragments, pattern recognition and classification tool is used. Pattern recognition involves identifying patterns or features in data, while classification involves assigning input data to one of several predefined categories or classes.

In "nnstart", pattern recognition and classification tasks can be created using the GUI by selecting the appropriate toolboxes, specifying the input and output data, and adjusting the network architecture and training parameters. Then training the network and evaluating its performance on new data can take place.

A two-layer feedforward neural network with sigmoid hidden neurons, an input layer with 1001 inputs and SoftMax output neurons, that is suitable for a classification task is designed. The inputs with 1001 features, where each feature represents the reflection coefficient at a specific frequency and antenna movement.

The Sigmoid activation function for the hidden neurons will introduce non-linearity into the network, allowing it to learn complex patterns in the data. The SoftMax activation in the output neurons will ensure that the output values represent probability distributions over the different classes, making it easier to interpret the network's predictions and make decisions based on those probabilities. The number of neurons will depend on the number of classes. In this case, equal 1 output neuron for predicting presence or absence of shrapnel. To train the neural network, a cost function is needed to measure the difference between the predicted output and the true output for each observation in the training set. For a classification task with SoftMax output neurons, a common cost function is the cross-entropy loss. it measures the dissimilarity between the predicted probabilities and the true class labels. As the network is trained, the cross-entropy loss is minimized, leading to improved performance on the classification task.

Next, an optimization algorithm is used, such as gradient descent or its variants, to minimize the cost function by updating the weights and biases of the neural network. Typically perform multiple iterations over the training set, which is referred to as epochs.

In this model, 130 observations are set for training and 23 observations are set for testing. The neural network pattern recognition is shown in Figure (4.4).

The performance plot of cross-entropy loss in pattern recognition neural networks typically shows the value of the loss function over the course of training. The x-axis represents the number of training iterations or epochs, while the y-axis represents the value of the cross-entropy loss. Figure (4.5) shows how the cross-entropy loss is decreased rapidly, as the network learns to make better predictions. This curve shows that after 84 epochs, the loss is approximately  $10^{-7}$ .

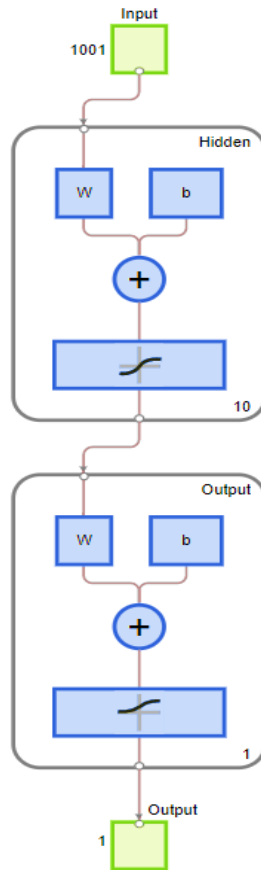


Figure 4.4: Pattern recognition neural network to predict the presence of shrapnel.

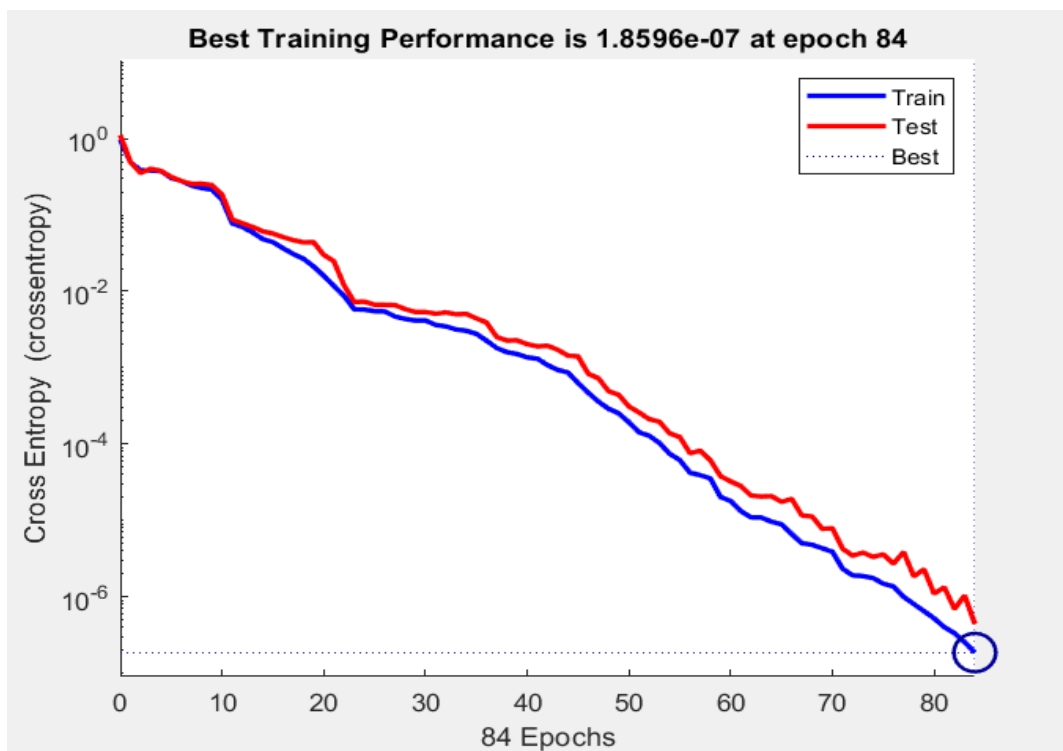


Figure 4.5: Cross entropy loss in training.

To determine the size of shrapnel, Neural network fitting tool is used. This tool uses an iterative process called backpropagation to adjust the weights and biases of the neural network to minimize the error between the predicted output and the actual output. A two-layer feedforward neural network with 10 sigmoid hidden neurons, an input layer with 1001 inputs and 1 linear output neurons suitable. The inputs with 1001 features, where each feature represents the reflection coefficient at a specific frequency and antenna movement. The linear output neuron allows the network to directly output continuous values for the regression task. The output is 1 to predict a single value (size). During the training, a loss function is used to measure the error between the predicted output values, and the actual output values, and an optimization algorithm such as gradient descent is used to adjust the weights and biases to minimize the loss function. One commonly used loss function for regression tasks is the mean squared error (MSE) function.

In this model 122 observations are set for training, and 31 observations are set for testing. The neural network fitting is shown in Figure (4.6).

The mean square error (MSE) is a common metric used to evaluate the performance of a neural network model. Typically, the MSE will decrease as the training progresses, indicating that the model is improving its fit to the data. The performance plot of MSE in fitting neural network is shown in figure (4.7). In this plot, the x-axis represents the number of training epochs, and the y-axis represents the MSE. This curve shows that after 11 epochs, the MSE is approximately  $10^{-21}$ .

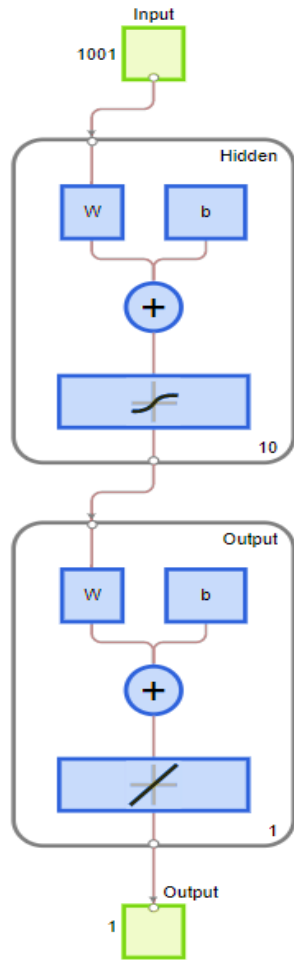


Figure 4.6: Fitting neural network to predict the size of shrapnel.

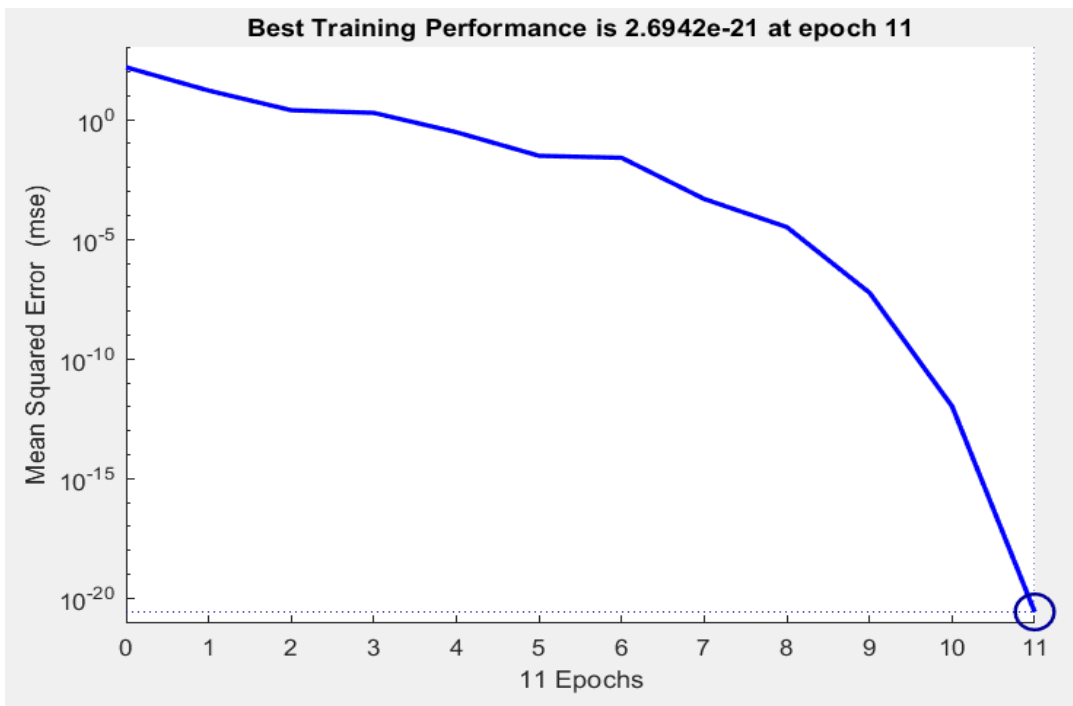


Figure 4.7: MSE in training process to predict size of shrapnel.

To determine the location (depth) of shrapnel, Neural network fitting tool is used. In this model 138 observations are set for training and 15 observations are set for testing. In the model, shrapnel was placed at various depths, and at a random location in the middle. Figure (4.8) shows how error varies with the number of trials (epochs). This curve shows that after 230 epochs, the MSE is approximately  $10^{-5}$ .

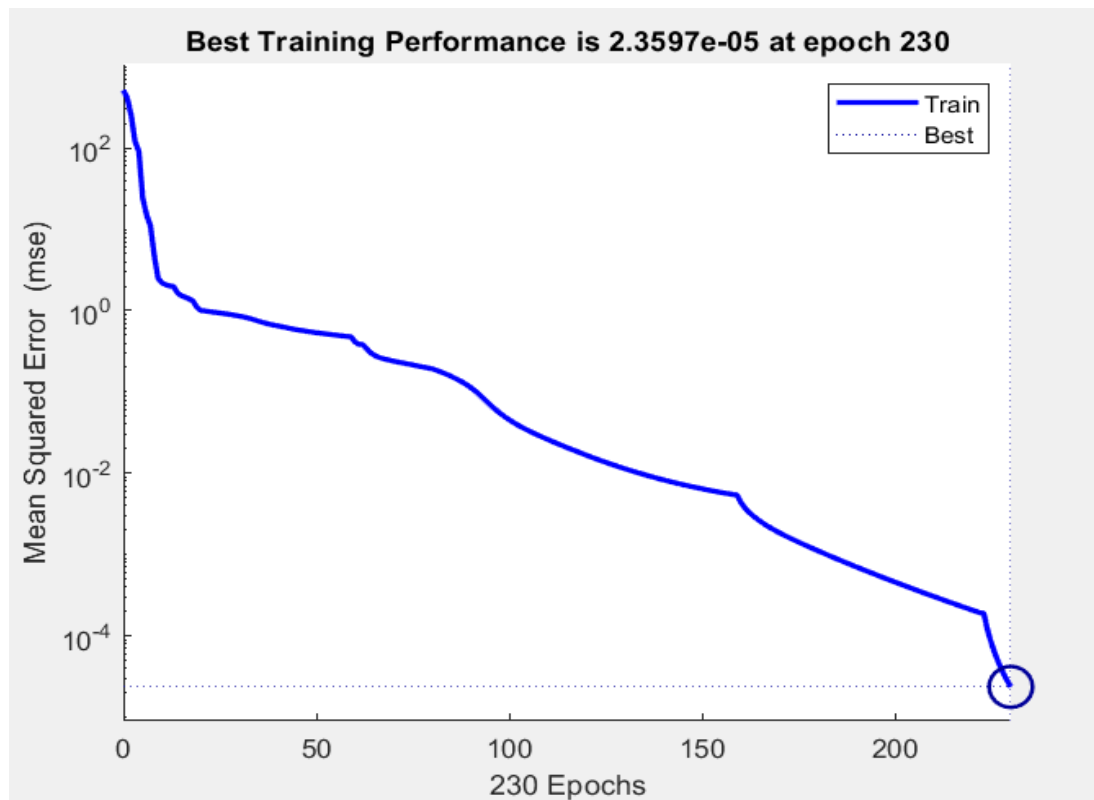


Figure 4.8: MSE in training process to predict depth of shrapnel.

When all targets are present (the presence or absence of shrapnel, and its size and location with one dimension (depth)), The feedforward neural network is used. The feedforward neural network is a type of neural network that consists of an input layer, one or more hidden layers, and an output layer. In this case, there are two hidden layers, with 10 and 6 neurons, respectively .an input layer with 1001 inputs, and an output layer with 3 outputs (presence or absence, size, location). The training parameters are then set using the property of the neural network object. The epochs parameter specifies the maximum number of training epochs, learning rate, and

minimum gradient, which determines when the training process will stop. Finally, the train function is called to train the neural network using the inputs and targets data. The structure of the feedforward neural network is shown in Figure (4.9).

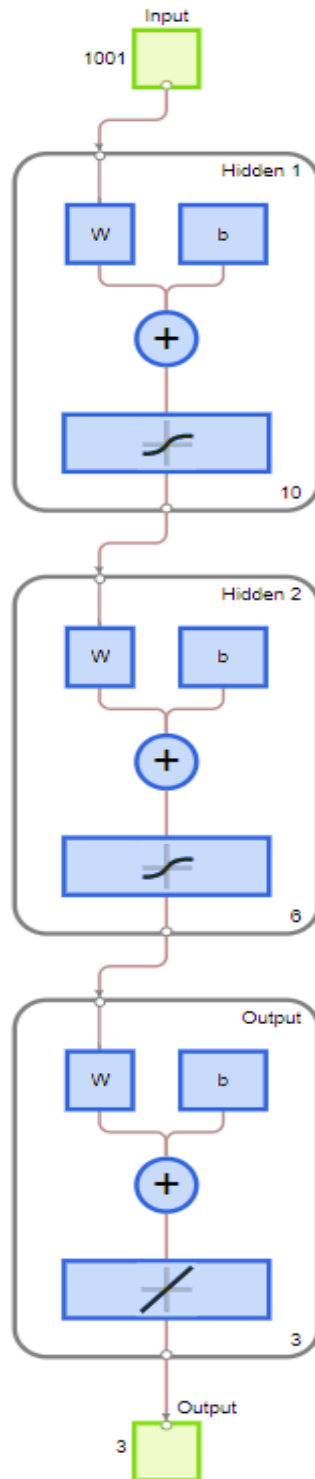


Figure 4.9: Feedforward neural network construction.

The goal of training the neural network is to adjust its weights and biases so that it can accurately predict the size and depth of the shrapnel given the input data. The weights and biases of the network are updated iteratively until the error reaches a minimum, or until a predetermined number of epochs (training iterations) have been completed.

At this point, the trained neural network can be used to make predictions on new data. The detection rate of shrapnel was (90%), while the results to size specification rate were (86%), and the results to the depth detection rate of the shrapnel were (78%). The relationship between the error and the number of epochs in neural network training is shown in Figure (4.10). This curve shows that after 75 epochs, the error is approximately  $10^{-4}$ .

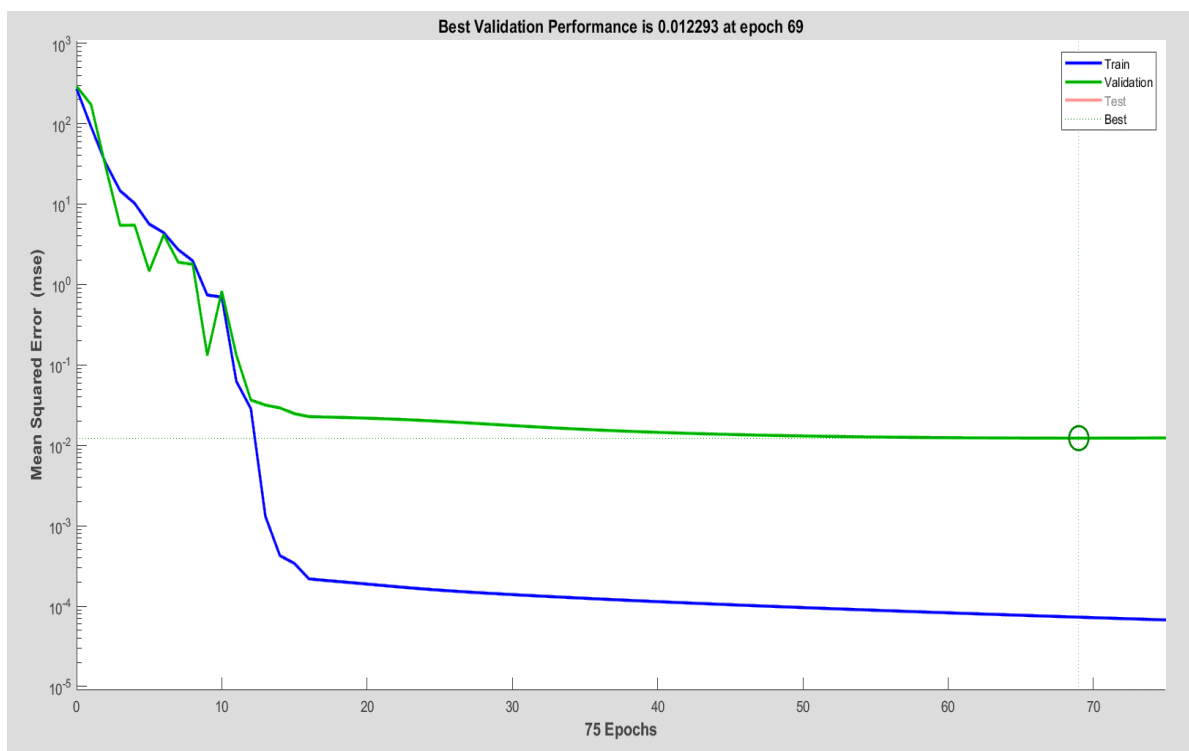


Figure 4.10: Error curves of training set and validation set performance across epochs.

Plotting regression in feedforward neural network involves visualizing the relationship between the predicted output values and the actual output values based on a set of input values. The neural network training regression is shown in Figure (4.11).

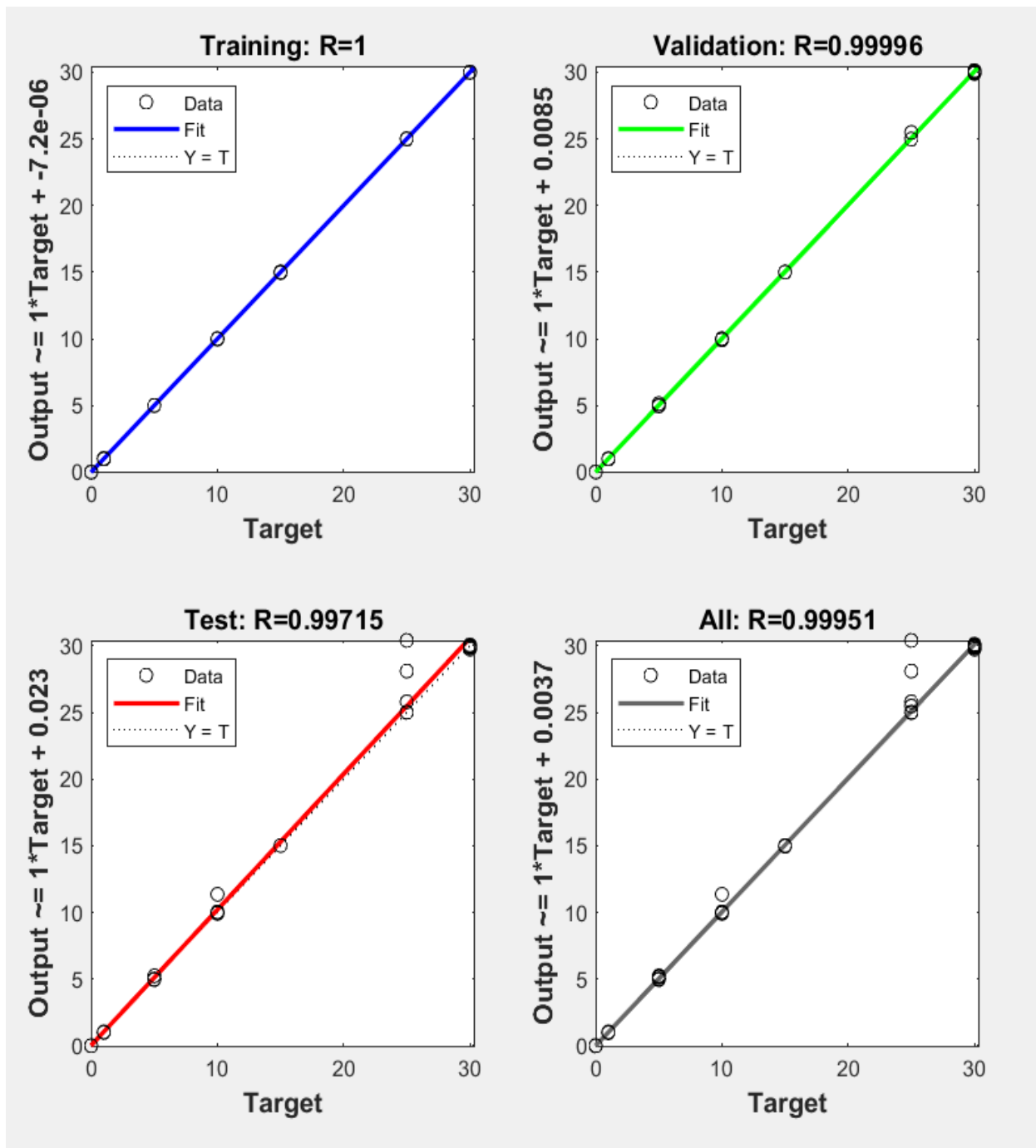


Figure 4.11: Regression in feedforward neural network.

## 4.5 Two-Dimensional Locating of Shrapnel Using ANN

Whenever a shrapnel changes its position in both the x and z directions, a dataset of reflection coefficients is collected using a CST model. This dataset is then used to train an ANN to predict the absence, or presence, as well as the size and location of shrapnel. To train the ANN, the collected dataset of reflection coefficients would be needed to be labeled according to whether or not shrapnel was present, and if so, the size and location of the shrapnel.

To predict the absence of shrapnel, pattern recognition and classification tool is used. In this model, 1980 observations are set for training and 349 observations are set for testing. the training performance is shown in Figure (4.12). This curve shows that after 107 epochs, the loss is approximately  $10^{-7}$ .

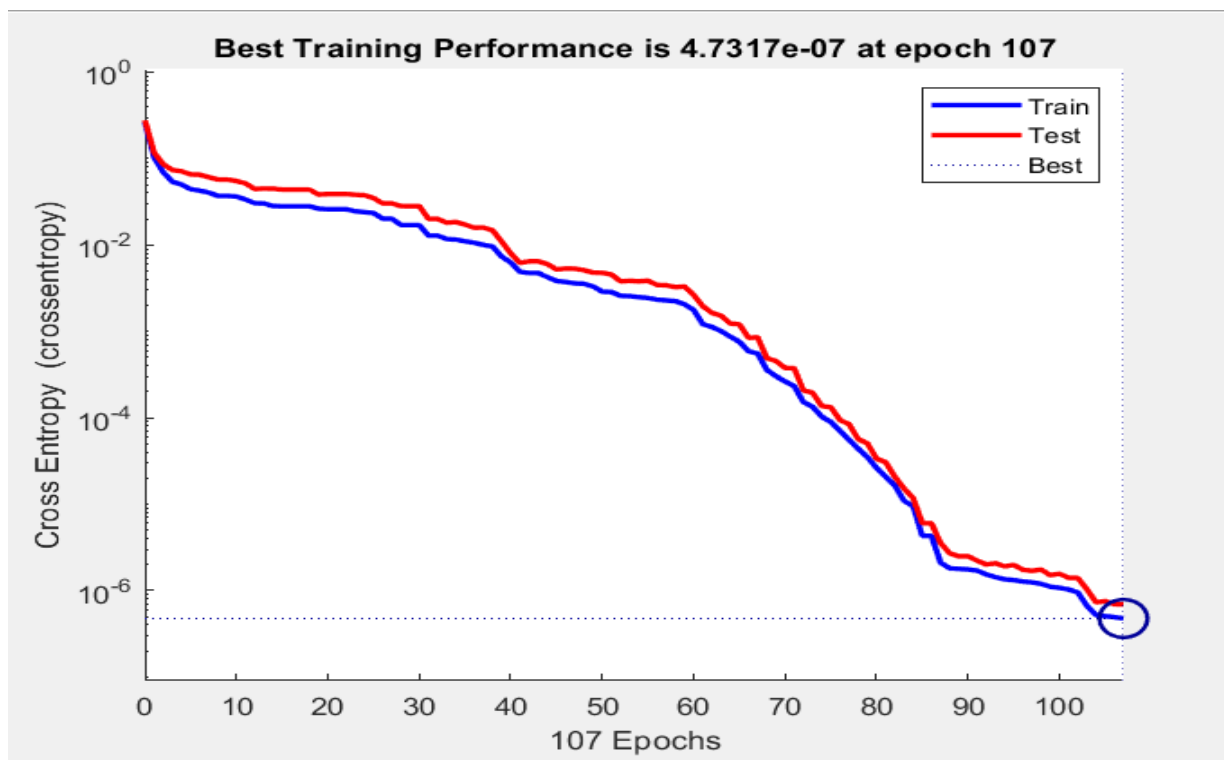


Figure 4.12: Training Performance of Pattern Recognition Neural Network.

To predict the size of shrapnel, Neural network fitting tool is used. After training the neural network on this data (two dimensions), the mean square error increased, and for this we resort to using an CNN to estimate the size of the fragment. Figure (4.13) shows how the MSE is approximately 0.1 after 67 epochs.

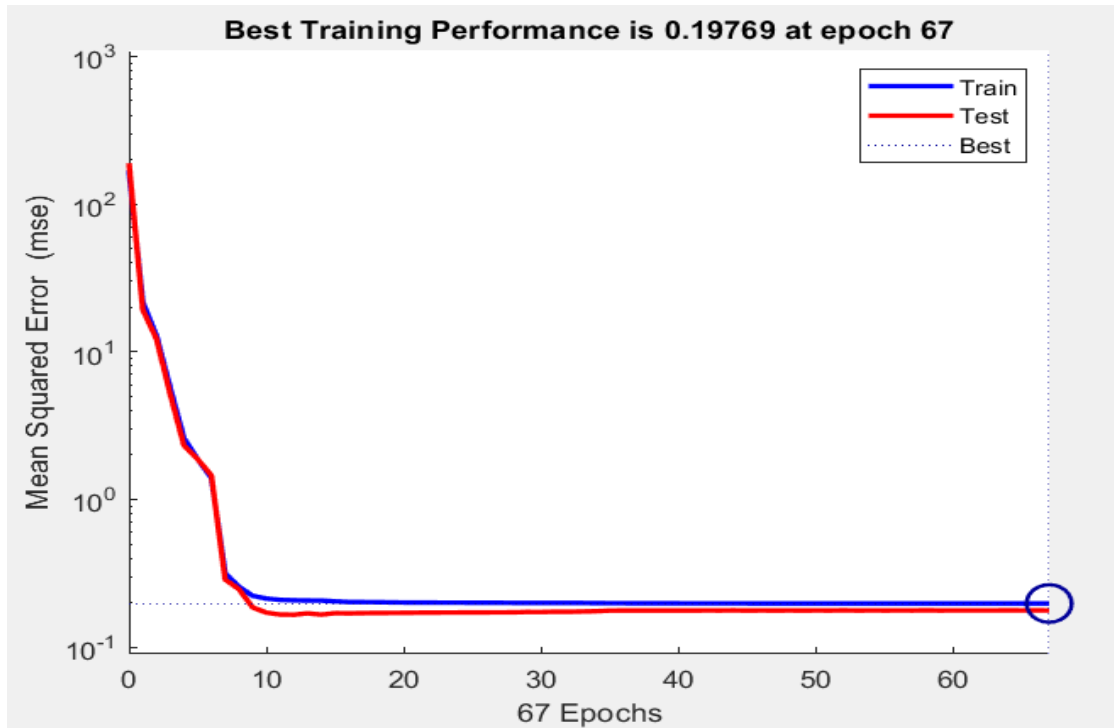


Figure 4.13: Training performance for predicting the size of shrapnel.

Well, when training the network for predicting the depth of shrapnel in the model, the curve shows how after 136 epochs the MSE is approximately 0.4 as shown in the Figure (4.14).

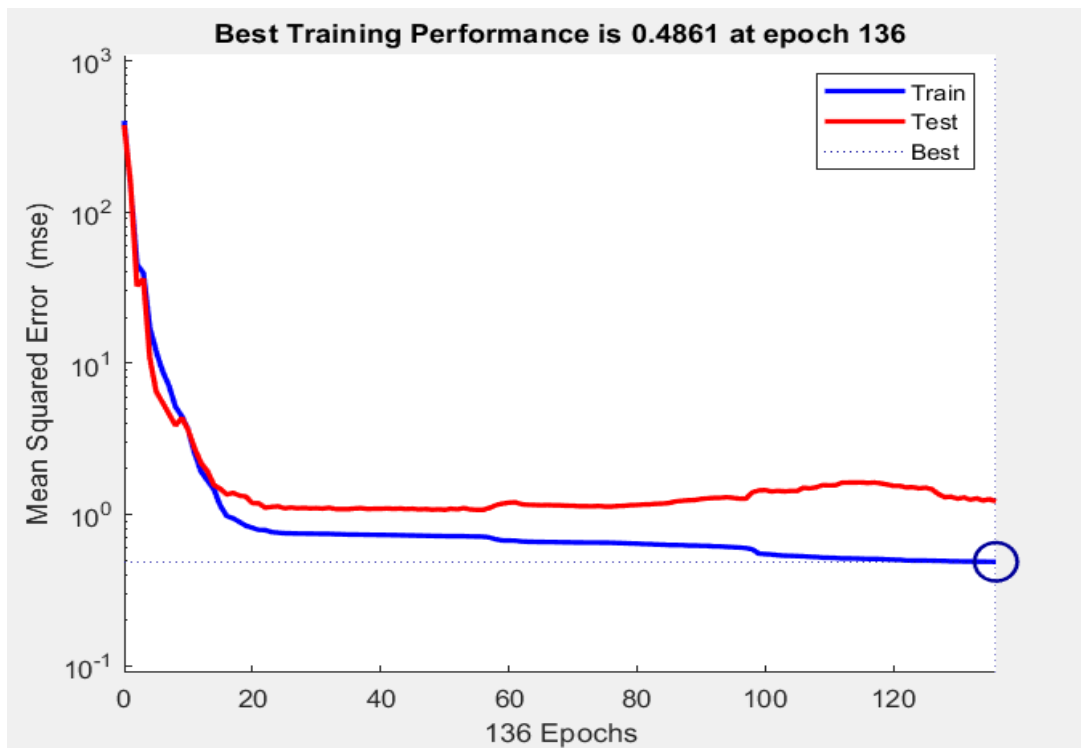


Figure 4.14: Training performance for predicting the depth of shrapnel.

## 4.6 Convolutional Neural Network (CNN) Training Results for Shrapnel Detection

If the MSE increases, it will indicate that the model is performing poorly and its predictions are further away from the actual values. One approach for building a machine learning model for this problem would be to use a convolutional neural network (CNN). A CNN is a type of neural network that is commonly used for imaging recognition tasks, but can also be used for other types of data, such as matrices. In a CNN, the input matrix is passed through a series of convolutional layers, which are able to identify patterns in the data. The output of the convolutional layers is then passed through a series of fully connected layers, which are used to make the final predictions.

The output of the machine learning model should be a set of four values, that describe the classification of the case, the size of the fragment, and the location of the fragment in X and Z.

**Classification:** The classification variable could be a categorical variable, that indicates the presence, or absence of a fragment in the body. In this case, it could be a value of 0 for no fragment, indicating the absence of a fragment, and 1 for the presence of a fragment.

**Size:** The size variable would have a limited set of possible values, which would be 0, 5, 10, and 15. The different possible size categories for the fragments that are being tried to be detected and classified would be represented by these values. During training, the machine learning model would be learned to associate specific input patterns with the different size categories, allowing it to predict the size of new fragments in future inputs.

**Location in Z:** The location in Z variable would have a limited set of possible values, which would be 25, 30, and 35. The different possible locations for the fragments along the Z-axis, which are being tried to be detected and classified, would be represented by these values.

Location in X: The location in X variable would have a limited set of possible values, which would be the values between 0 and 160 with increments of 10 (i.e., 0, 10, 20, 30, 40, 50, ..., 160). The different possible locations for the fragments along the X-axis, which are being tried to be detected and classified, would be represented by these values.

The machine learning model takes the input matrix as input and produces the four output values as its output, based on what it has learned from the labeled dataset during training. The data set is labeled in excel as shown in Figure (4.15).

The architecture of convolutional neural network consists of:

- 1- Sequence Input Layer: This layer specifies the input size of the network, which is the number of features in each input matrix. In this case, it is the number of rows in the input matrix, which is 1001.
- 2- convolution1dLayer: This layer performs a 1D convolution operation on the input sequence using a set of learnable filters. The first convolution layer has 128 filters of size 3, followed by a RELU activation function and layer normalization layer.
- 3- convolution1dLayer: This layer has 2\*num Filters (256) filters of size 3 followed by RELU activation function and layer normalization layer.
- 4- convolution1dLayer: This layer has 4\*num Filters (512) filters of size 3 followed by RELU activation function and layer normalization layer.
- 5- Global Average Pooling1dLayer: This layer calculates the meaning of each feature map across time steps, and returns a 1D output vector.
- 6- Fully Connected Layer: This layer connects every element of the input vector to every element of the output vector with learnable weights, followed by a SoftMax activation function to generate class probabilities.
- 7- Classification Layer: This layer computes the cross-entropy loss between the predicted probabilities, and the true labels, and backpropagates the gradient to update the weights of the network.

The network is trained using mini-batch stochastic gradient descent with the Adam optimizer. Adam optimization algorithm is a variant of stochastic gradient descent that is commonly used to train deep neural networks. Adam stands for "Adaptive Moment Estimation." The algorithm computes individual adaptive learning rates for each parameter in the network based on estimates of the first, and second moments of the gradients. The first moment is the mean of the gradient, and the second moment is the variance of the gradient. These moments are calculated for each parameter and used to update the learning rate and weight parameters during training. Adam is known for its efficiency in training deep neural networks, as it can automatically adjust the learning rate during training and converge to a good solution faster than other optimization algorithms.

The validation data is used for monitoring the performance of the network during training and preventing overfitting. The network is trained for a maximum of 250 epochs or until convergence, whichever occurs first. The final trained network is stored in the "net" variable.

For classification to indicate the presence or absence of a fragment, CNN is used. In this case, it could be a value of 0 for no fragment, indicating the absence of a fragment, and 1 for the presence of a fragment. The training process of CNN is shown in Figure (4.16).

	target data	reflection coefficient (S11) at specific frequency and antenna movement																					
		0	0	0	0	0	0	0	0	1	1	1	1	1	1	1	1	1	1	1	1		
	class(presence or absence)	0	0	0	0	0	0	0	0	1	1	1	1	1	1	1	1	1	1	1	1		
	size of shrapnel (radius in mm)	0	0	0	0	0	0	0	0	5	10	10	5	10	15	5	10	15	5	10	15	5	10
	location of shrapnel in z direction	0	0	0	0	0	0	0	0	10	10	-10	-10	-10	10	10	10	10	10	10	10	10	10
	location of shrapnel in x direction (in mm)	0	0	0	0	0	0	0	0	25	25	25	25	25	30	30	30	30	30	30	30	30	30
	location of antenna in x direction (in mm)	0	10	60	70	80	-10	-20	60	60	40	50	50	0	10	10	10	20	20	20	30	30	
	input data	-1.5328351	-1.523735	-1.5252398	-1.518603	-1.513419	-1.5327786	-1.533672	-1.52486	-1.53745	-1.5369	-1.52956	-1.53217	-1.29974	-1.52939	-1.40514	-1.4408	-1.53003	-1.4134	-1.30109	-1.53346	-1.53261	-1.41
		-1.5253314	-1.516659	-1.5180245	-1.5111183	-1.505502	-1.525322	-1.526284	-1.51739	-1.53043	-1.5311	-1.52227	-1.52637	-1.29603	-1.52179	-1.43008	-1.42395	-1.52244	-1.44108	-1.29749	-1.52586	-1.52713	-1.44
		-1.5138634	-1.505778	-1.5068632	-1.4996958	-1.493668	-1.5139109	-1.51493	-1.50604	-1.5194	-1.52164	-1.51109	-1.5169	-1.29713	-1.51029	-1.45429	-1.40535	-1.51101	-1.46781	-1.29869	-1.51438	-1.51806	-1.47
		-1.4991101	-1.491738	-1.4924353	-1.4850086	-1.478594	-1.499223	-1.500286	-1.49149	-1.50505	-1.5091	-1.49671	-1.50437	-1.30301	-1.49559	-1.47684	-1.38604	-1.49642	-1.49255	-1.30468	-1.4997	-1.50599	-1.49
		-1.4818845	-1.475321	-1.475549	-1.4678652	-1.461084	-1.4820699	-1.483165	-1.47456	-1.48817	-1.49423	-1.47994	-1.48951	-1.31347	-1.47849	-1.49689	-1.36708	-1.47948	-1.51437	-1.31526	-1.48266	-1.49162	-1.52
		-1.4630923	-1.457393	-1.4571111	-1.4491659	-1.442037	-1.4633524	-1.464469	-1.45616	-1.46967	-1.47783	-1.46168	-1.47313	-1.32812	-1.4599	-1.5137	-1.34951	-1.46109	-1.53246	-1.33001	-1.46416	-1.47575	-1.54
		-1.4436854	-1.43887	-1.4380732	-1.4298621	-1.422395	-1.4440234	-1.445153	-1.43723	-1.45053	-1.46078	-1.44288	-1.4561	-1.34639	-1.44077	-1.52672	-1.33426	-1.4422	-1.5462	-1.34839	-1.44515	-1.45923	-1.55
		-1.4246272	-1.420677	-1.4193963	-1.4109119	-1.403114	-1.4250411	-1.426179	-1.41874	-1.43171	-1.44396	-1.4245	-1.43931	-1.36757	-1.42205	-1.53556	-1.32215	-1.42376	-1.55521	-1.36968	-1.42658	-1.44293	-1.56
		-1.4068447	-1.403706	-1.4020086	-1.3932404	-1.385111	-1.4073331	-1.408474	-1.40159	-1.41413	-1.42822	-1.40744	-1.42361	-1.39083	-1.40467	-1.54006	-1.31384	-1.40668	-1.55931	-1.39305	-1.40938	-1.42767	-1.57
		-1.3911983	-1.388787	-1.3867697	-1.3777064	-1.369236	-1.3917554	-1.392897	-1.38665	-1.39869	-1.41436	-1.39256	-1.4098	-1.41526	-1.38947	-1.54026	-1.30981	-1.39179	-1.5586	-1.41758	-1.3944	-1.41424	-1.57
		-1.3784487	-1.376656	-1.3744417	-1.3650688	-1.356241	-1.379068	-1.38021	-1.37465	-1.38614	-1.40309	-1.3806	-1.39859	-1.43989	-1.37721	-1.53641	-1.31033	-1.37985	-1.55337	-1.44231	-1.38237	-1.40334	-1.5
		-1.3692344	-1.367926	-1.3656608	-1.3559663	-1.346757	-1.3699072	-1.37105	-1.36623	-1.37714	-1.39502	-1.37219	-1.39059	-1.46378	-1.36851	-1.52896	-1.3155	-1.37145	-1.54415	-1.46628	-1.37391	-1.39557	-1.56
		-1.3640487	-1.363078	-1.3609226	-1.3508925	-1.341271	-1.3647654	-1.365911	-1.36187	-1.3722	-1.39062	-1.36782	-1.38627	-1.48599	-1.36384	-1.51851	-1.32518	-1.36709	-1.53166	-1.48858	-1.36951	-1.3914	-1.54
		-1.3632326	-1.362441	-1.3605683	-1.3501912	-1.340117	-1.3639808	-1.365134	-1.36189	-1.37166	-1.39022	-1.36779	-1.38597	-1.50571	-1.36355	-1.50583	-1.33905	-1.36706	-1.51675	-1.50838	-1.36948	-1.39114	-1.53
		-1.3669605	-1.366185	-1.3647722	-1.3540368	-1.343468	-1.3677295	-1.368892	-1.36646	-1.3757	-1.394	-1.37229	-1.38985	-1.52223	-1.36778	-1.49174	-1.35661	-1.37154	-1.50037	-1.52498	-1.37397	-1.39498	-1.51
		-1.3752429	-1.374323	-1.373545	-1.3624446	-1.351331	-1.3760197	-1.377197	-1.37557	-1.38435	-1.40197	-1.3813	-1.39795	-1.53503	-1.37655	-1.47714	-1.37721	-1.38051	-1.48351	-1.53785	-1.38298	-1.40295	-1.50
		-1.3879236	-1.386704	-1.386731	-1.3752583	-1.363551	-1.3886957	-1.389891	-1.38905	-1.39745	-1.41402	-1.39466	-1.41014	-1.54378	-1.38968	-1.46292	-1.40004	-1.3938	-1.46718	-1.54665	-1.39634	-1.41493	-1.48
		-1.404689	-1.403027	-1.4040162	-1.3921728	-1.379815	-1.4054437	-1.406661	-1.40659	-1.4147	-1.42987	-1.41204	-1.42614	-1.54834	-1.40685	-1.44995	-1.42422	-1.41108	-1.45234	-1.55125	-1.4137	-1.43065	-1.46
		-1.4250818	-1.422852	-1.4249417	-1.4127309	-1.399668	-1.4258064	-1.427048	-1.4277	-1.43565	-1.4491	-1.43298	-1.44554	-1.5488	-1.4276	-1.43905	-1.44881	-1.43189	-1.43987	-1.55176	-1.4346	-1.44971	-1.45
		-1.4485112	-1.445609	-1.4489167	-1.4363462	-1.422527	-1.4491943	-1.450462	-1.45181	-1.45969	-1.47119	-1.45688	-1.46781	-1.54547	-1.45134	-1.43092	-1.47285	-1.45561	-1.43055	-1.54846	-1.45843	-1.4716	-1.44
		-1.4742782	-1.470626	-1.4752399	-1.4623253	-1.4477	-1.47491	-1.476205	-1.47818	-1.48612	-1.49549	-1.48303	-1.4923	-1.53884	-1.47735	-1.42615	-1.49542	-1.48156	-1.42499	-1.54184	-1.48448	-1.49569	-1.43
		-1.5015987	-1.497147	-1.5031274	-1.4898889	-1.474413	-1.5021707	-1.503491	-1.50605	-1.51417	-1.52128	-1.51066	-1.5183	-1.52955	-1.50485	-1.42519	-1.5157	-1.50895	-1.42368	-1.53256	-1.51197	-1.52127	-1.
		-1.5296358	-1.524363	-1.531737	-1.5181989	-1.501838	-1.5301395	-1.531483	-1.53457	-1.54298	-1.54779	-1.53891	-1.54503	-1.51838	-1.53302	-1.42832	-1.53297	-1.53695	-1.42692	-1.52139	-1.54004	-1.54761	-1.43
		-1.5575252	-1.551445	-1.5602039	-1.5464004	-1.529123	-1.5579563	-1.559316	-1.56288	-1.57168	-1.57423	-1.56693	-1.5717	-1.50618	-1.56098	-1.43569	-1.54669	-1.56469	-1.43482	-1.50919	-1.56784	-1.57391	-1.44
		-1.5844174	-1.577575	-1.5876756	-1.5736437	-1.555434	-1.5847745	-1.586143	-1.59012	-1.59941	-1.59981	-1.59387	-1.59751	-1.49385	-1.58791	-1.44725	-1.55653	-1.59135	-1.44732	-1.49685	-1.59453	-1.59941	-1.45

Figure 4.15: Samples from the labeled data set in Excel.

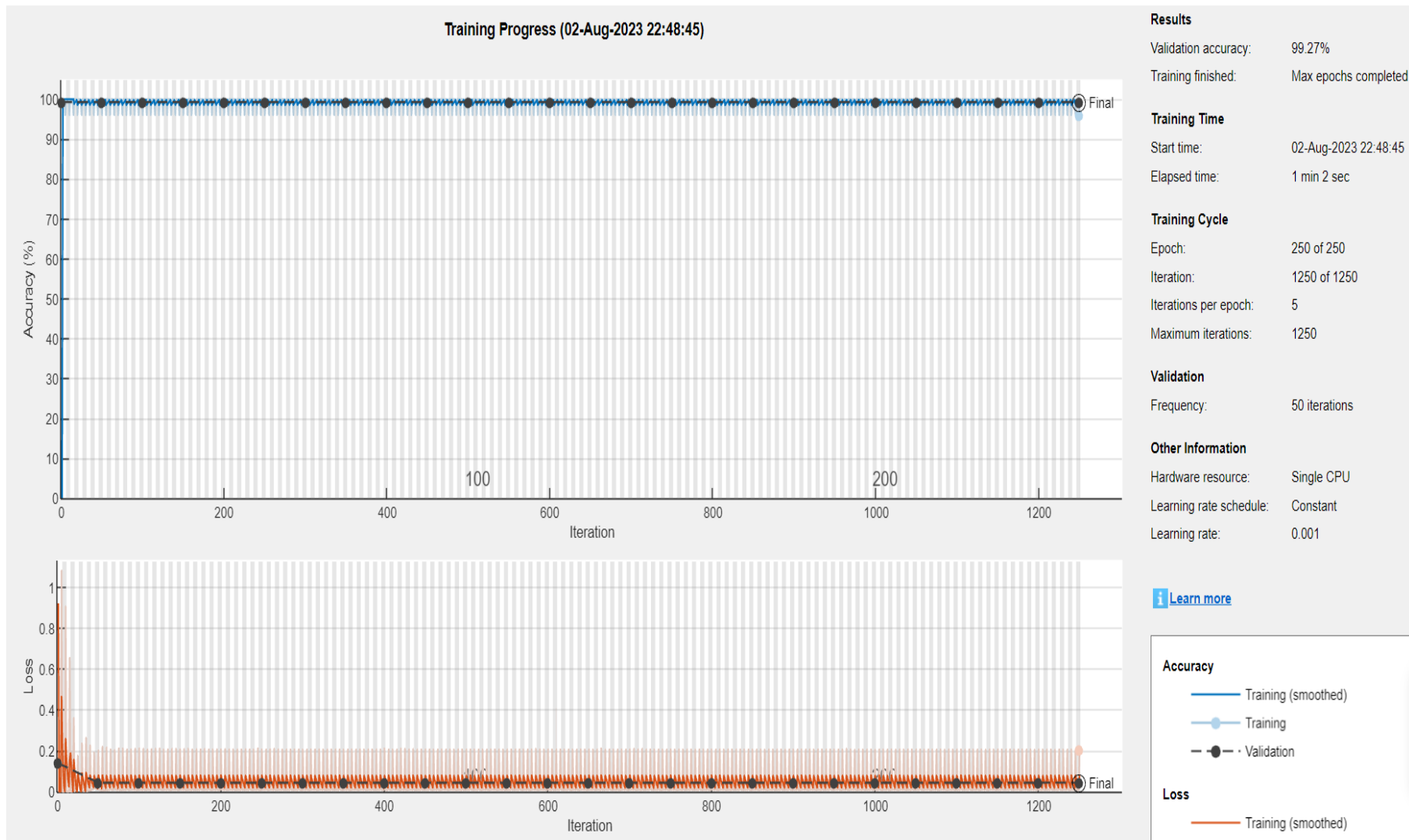


Figure 4.16: Training process for classification using CNN.

A validation accuracy of 99% indicates that the model is performing well on the validation set and is able to classify accurately the presence, or absence of a fragment.

To train the network to predict both the size and location of the fragment, it is required to modify output layer of the network. Instead of output that represents the presence or absence of a fragment, the output must be represent the size and location of the fragment. The training process for predicting the size and location are shown in Figure (4.17).

A validation accuracy of 88% after 900 epochs indicates that the model is able to accurately predict the size and location of the fragment.

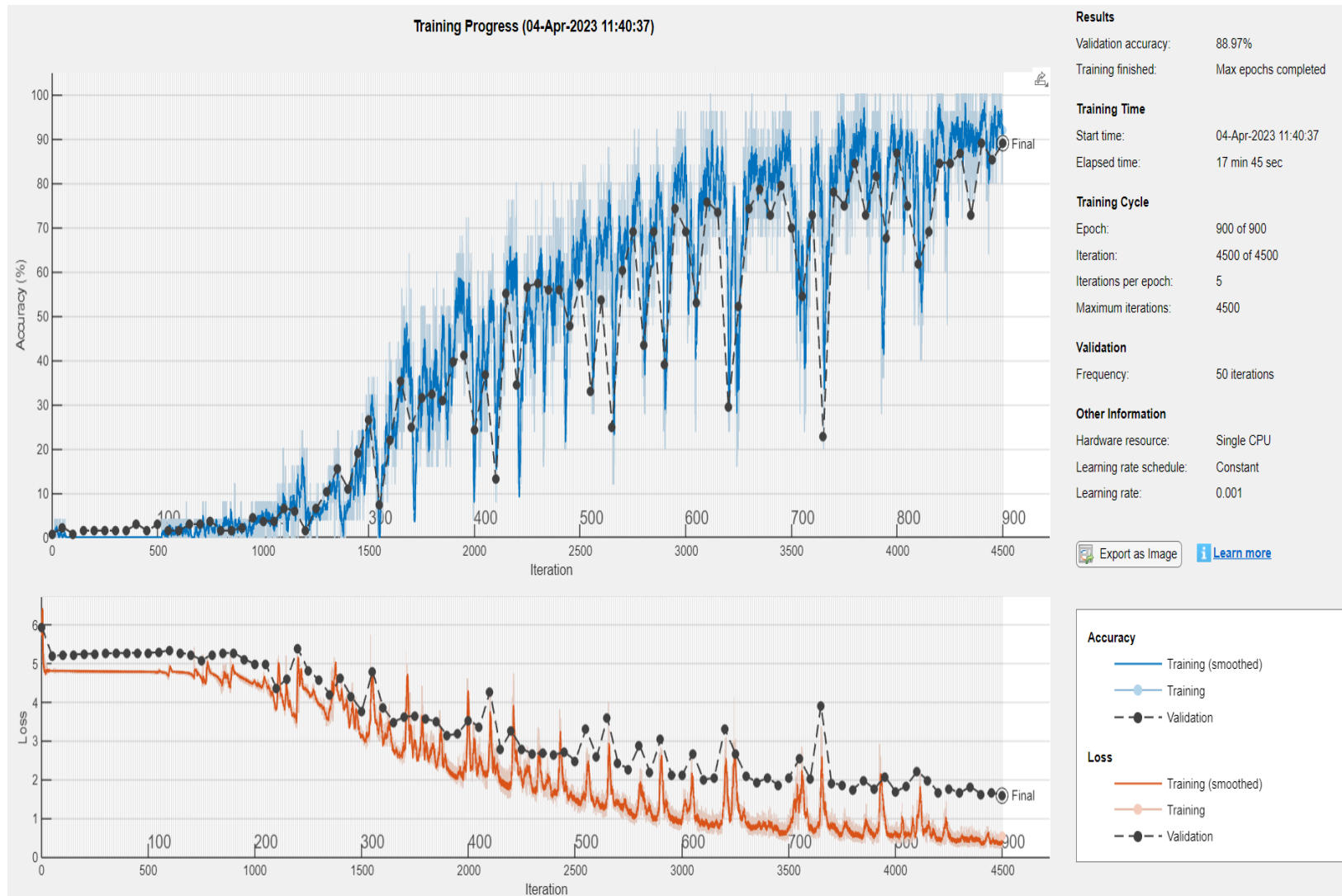


Figure 4.17: Training process for prediction size and location using CNN.

# CHAPTER FIVE

## CONCLUSIONS AND FUTURE WORK

### 5.1 Conclusions

Specifying the size and location of a shrapnel within the human body is a challenging task in the field of hidden object detection. There are several factors that contribute to this challenge, such as the variability of human tissue properties and the interaction of electromagnetic waves with them. to solve this problem:

- 1- A model depicting the main layers of the human body (skin, fat, muscle, and bone) was designed to represent the anatomical structure, and test detection methods. The fragment was incorporated into the model, assuming an aspherical shape, and using copper as its material representation.
- 2- It is possible to use a single antenna to detect hidden object by using the reflection coefficient. The antenna can transmit a signal toward the model, and the reflection of that signal can provide information about the presence of shrapnel.
- 3- The data which was collected from scattered signals at various locations around the model, and a neural network was employed to analyze this data, and determine the fragment's location and size.
- 4- It is possible to use neural networks for detecting shrapnel, and having a large number of trained data can be beneficial for improving the network's performance.
- 5- A CNN can be an effective approach for detecting and locating shrapnel in model, and can help to improve the accuracy, and reliability of the detection system.
- 6- In order to use a convolutional neural network (CNN), the input data is typically represented in the form of images, which can be thought of as matrices of pixel values. the input data for the CNN would be represented as dimensions of 1001\*17 (1001 represent frequency steps, 17 represent antenna movements).

- 7- During the training process of a CNN, the model can be trained to detect and locate the presence of shrapnel in two dimensions, as well as estimate their size.
- 8- From results, a convolutional neural network (CNN) improves the rate of detection and position determination as compared to regular neural network. The results were acquired utilizing the neural network with 90% success in shrapnel identification, 86% success in shrapnel sizing, and 78% success in shrapnel depth. Also, better results were obtained when using the CNN, where 99% was reached to determine the presence of the fragment and 88% to determine the size and location.

## **5.2 Future Work**

Based on the work done in this dissertation, there are several aspects that can be considered to extend the research further. Some of these aspects include:

- 1- Incorporating more complex network architectures: The dissertation discusses the use of a basic convolutional neural network for detecting hidden objects. However, more complex architectures such as ResNet, can be explored to further improve the performance of the network.
- 2- Increasing the size of the dataset: While the dataset used in this dissertation is sufficient to train the network, increasing the size of the dataset can help improve the accuracy of the model.
- 3- Investigating the use of multiple sensors: The dissertation uses a single antenna to detect hidden objects. However, the use of multiple sensors, such as a radar system, can potentially improve the accuracy of the detection, and locating of the hidden object.
- 4- Testing the model with various types of materials for initial tests can help to evaluate the performance of the model in detecting hidden objects under different conditions. This can help to improve the model's accuracy and reliability, and make it more effective in real-world scenarios.

## REFERENCES

- [1] Resch, M. D., et al. "Confocal microscopic evidence of increased Langerhans cell activity after corneal metal foreign body removal." *European Journal of Ophthalmology* 18.5 (2008): 703-707.
- [2] Jameii, M. Khak, and M. A. Nekoui. "Improving the performance of the PI systems through the use of neural network." 2010 Second International Conference on Computer Engineering and Applications. Vol. 1. IEEE, 2010.
- [3] Liang, Ding, et al. "Enhancement of microwave tomography using Kalman filter theory." *Proceedings 2013 International Conference on Mechatronic Sciences, Electric Engineering and Computer (MEC)*. IEEE, 2013.
- [4] Nordbeck, Peter, Georg Ertl, and Oliver Ritter. "Magnetic resonance imaging safety in pacemaker and implantable cardioverter defibrillator patients: how far have we come?" *European heart journal* 36.24 (2015): 1505-1511.
- [5] Bushong, Stewart C., and Geoffrey Clarke. *Magnetic resonance imaging: physical and biological principles*. Elsevier Health Sciences, 2003.
- [6] Wu, Jun-ru, and Wesley Nyborg, eds. *Emerging therapeutic ultrasound*. World Scientific, 2006.
- [7] K. M. Chew, R. Sudirman, N. H. Mahmood, N. Seman, and C. Y. Yong, "Human Brain Microwave Imaging Signal Processing: Frequency Domain (S-parameters) to Time Domain Conversion," *Engineering*, vol. 05, no. 05, 2013.
- [8] R. Chandra, H. Zhou, I. Balasingham, and R. M. Narayanan, "On the Opportunities and Challenges in Microwave Medical Sensing and Imaging," *IEEE Transactions on Biomedical Engineering*, vol. 62, no. 7. 2015. doi: 10.1109/TBME.2015.2432137.
- [9] M. Z. Mahmud, M. T. Islam, N. Misran, A. F. Almutairi, and M. Cho, "Ultra-wideband (UWB) antenna sensor-based microwave breast imaging: A

review,” *Sensors (Switzerland)*, vol. 18, no. 9. MDPI AG, Sep. 05, 2018. doi: 10.3390/s18092951.

- [10] Dumin, Oleksandr, et al. "Subsurface object identification by artificial neural networks and impulse radiolocation." 2018 IEEE Second International Conference on Data Stream Mining & Processing (DSMP). IEEE, 2018.
- [11] Chen, H., Zhang, Y., Zhang, W., Liao, P., & Li, K. "Thoracic disease identification and localization with limited supervision." *Proceedings of the IEEE conference on computer vision and pattern recognition (ICASSP)*. IEEE, 2018.
- [12] Al-Gburi, Ahmed Jamall Abdullah, Imran Ibrahim, and Zahriladha Zakaria. "A miniature raspberry shaped UWB monopole antenna based on microwave imaging scanning technique for kidney stone early detection." *Int. J. Psychosoc. Rehabil* 24.2 (2020): 1755-1763.
- [13] O. Dumin, O. Pryshchenko, V. Plakhtii, and G. Pochanin, "Landmine detection and classification using UWB antenna system and ANN analysis," in 2020 IEEE Ukrainian Microwave Week, (UkrMW).IEEE, 2020. doi: 10.1109/UkrMW49653.2020.9252574.
- [14] V. S. Bhadouria, Z. Akhter, M. J. Akhtar, and P. Munshi, "Automated microwave monitoring of hidden objects for strategic and security applications," *Journal of Electromagnetic Waves and Applications* 35.18 (2021): 2492-2509. doi: 10.1080/09205071.2021.1953404.
- [15] Hossain, A., Islam, M. T., Islam, M. S., Chowdhury, M. E., Almutairi, A. F., Razouqi, Q. A., & Misran., "A YOLOv3 Deep Neural Network Model to Detect Brain Tumor in Portable Electromagnetic Imaging System," *IEEE Access* 9 (2021): 82647-82660. doi: 10.1109/ACCESS.2021.3086624.
- [16] E. J. Snider, S. I. Hernandez-Torres, G. Avital, and E. N. Boice, "Evaluation of an Object Detection Algorithm for Shrapnel and Development of a Triage

- Tool to Determine Injury Severity,” *Journal of imaging* 8.9 (2022): 252. doi: 10.3390/jimaging8090252.
- [17] Boice, Emily N., Sofia I. Hernandez-Torres, and Eric J. Snider. "Comparison of Ultrasound Image Classifier Deep Learning Algorithms for Shrapnel Detection." *Journal of Imaging* 8.5 (2022): 140.
- [18] SJ, Gokul Nath, Athul O. Asok, and Sukomal Dey. "Metallic Object Detection Inside Human Stomach with Antipodal Vivaldi Antenna Utilizing Microwave Imaging Technique." 2022 IEEE Wireless Antenna and Microwave Symposium (WAMS). IEEE, 2022.
- [19] Patel, Jigneshkumar L., and Ramesh K. Goyal. "Applications of artificial neural networks in medical science." *Current clinical pharmacology* 2.3 (2007): 217-226.
- [20] H. U. Dike, Y. Zhou, K. K. Deveerasetty and Q. Wu, "Unsupervised Learning Based on Artificial Neural Network: A review," 2018 IEEE International Conference on Cyborg and Bionic Systems (CBS), IEEE, 2018. doi: 10.1109/CBS.2018.8612259.
- [21] Kurt, Hüseyin Burak, Murat Millidere, and Emrah Sezer. "Aerodynamic Database Simulation Implementation Based On Neural Network and Neural Network Parameter Selection Using Genetic Algorithms." *European Conference for Aeronautics and Space Sciences*. 2019.
- [22] Dongare, A. D., R. R. Kharde, and Amit D. Kachare. "Introduction to artificial neural network." *International Journal of Engineering and Innovative Technology (IJEIT)* 2.1 (2012): 189-194.
- [23] Da Silva, Ivan Nunes, et al. *Artificial neural network architectures and training processes*. Springer International Publishing, 2017., pp. 21–28. doi: 10.1007/978-3-319-43162-8\_2.
- [24] Jayawardana, R., and T. Sameera Bandaranayake. "Analysis of optimizing

neural networks and artificial intelligent models for guidance, control, and navigation systems." *International Research Journal of Modernization in Engineering, Technology and Science* 3.3 (2021): 743-759.

- [25] N. B. Shaik, S. R. Pedapati, S. A. Ammar Taqvi, A. R. Othman, and F. A. Abd Dzubir, "A feed-forward back propagation neural network approach to predict the life condition of crude oil pipeline," *Processes* 8.6 (2020): 661. doi: 10.3390/PR8060661.
- [26] Zhang, Y., D. Huston, and T. Xia. "Underground object characterization based on neural networks for ground penetrating radar data. In *Nondestructive characterization and monitoring of advanced materials, aerospace, and civil infrastructure 2016*." *International Society for Optics and Photonics* 9804 (2016): 980403. doi: 10.1117/12.2219345.
- [27] Sai, Yang, Ren Jinxia, and Li Zhongxia. "Learning of neural networks based on weighted mean squares error function." *2009 Second International Symposium on Computational Intelligence and Design*. Vol. 1. IEEE, 2009. doi: 10.1109/ISCID.2009.67.
- [28] Kim, Jonghoon, Jisu Hong, and Hyunjin Park. "Prospects of deep learning for medical imaging." *Precision and Future Medicine* 2.2 (2018): 37-52. doi: 10.23838/pfm.2018.00030.
- [29] Z. Q. Zhao, P. Zheng, S. T. Xu, and X. Wu, "Object detection with deep learning: A review." *IEEE transactions on neural networks and learning systems* 30.11 (2019): 3212-3232. doi: 10.1109/TNNLS.2018.2876865.
- [30] Goodfellow, Ian, Yoshua Bengio, and Aaron Courville. "Deep feedforward networks." *Deep learning* 1 (2016).
- [31] Scherer, Dominik, Andreas Müller, and Sven Behnke. "Evaluation of pooling operations in convolutional architectures for object recognition." *International*

conference on artificial neural networks. Berlin, Heidelberg: Springer Berlin Heidelberg, 2010.

- [32] Sardogan, Melike, Adem Tuncer, and Yunus Ozen. "Plant leaf disease detection and classification based on CNN with LVQ algorithm." 2018 3rd international conference on computer science and engineering (UBMK). IEEE, 2018. doi: 10.1109/UBMK.2018.8566635.
- [33] Semenov, Serguei Y., and Douglas R. Corfield. "Microwave tomography for brain imaging: Feasibility assessment for stroke detection." *International Journal of Antennas and Propagation* 2008 (2008). doi: 10.1155/2008/254830.
- [34] Liang, Qilian. "Biologically inspired target recognition in radar sensor networks." *EURASIP Journal on Wireless Communications and Networking* 2010 (2009): 1-8. doi: 10.1155/2010/523435.
- [35] Mohammed, Beadaa Jasem. Design and implementation of microwave imaging systems for medical applications. Diss. Ph. D. dissertation, The University of Queensland School of Information Technology and Electrical Engineering, Australia, 2014.
- [36] Jalilvand, Malyhe. Application-specific broadband antennas for microwave medical imaging. Vol. 85. KIT Scientific Publishing, 2017. doi: <https://doi.org/10.5445/KSP/1000069288>.
- [37] R. Chandra, H. Zhou, I. Balasingham, and R. M. Narayanan. "On the opportunities and challenges in microwave medical sensing and imaging." *IEEE transactions on biomedical engineering* 62.7 (2015): 1667-1682. doi: 10.1109/TBME.2015.2432137.
- [38] Pozar, David M. *Microwave engineering*. John Wiley & sons, 2011.
- [39] Gabriel, Camelia, and Azadeh Peyman. "Dielectric properties of biological tissues; variation with age." *Conn's Handbook of Models for Human Aging*

(2018): 939-952. doi: 10.1016/B978-0-12-811353-0.00069-5.

- [40] Zhurbenko, Vitaliy. "Challenges in the design of microwave imaging systems for breast cancer detection." *Advances in Electrical and Computer Engineering* 11.1 (2011): 91-96. doi: 10.4316/aece.2011.01015.
- [41] Singh, Sukhvinder, et al. "Sense through wall human detection using UWB radar." *EURASIP Journal on Wireless Communications and Networking* 2011.1 (2011): 1-11. doi: 10.1186/1687-1499-2011-20.
- [42] M. A. Aldhaeabi, K. Alzoubi, T. S. Almoneef, S. M. Bamatra, H. Attia, and O. M. Ramahi, "Review of microwaves techniques for breast cancer detection," *Sensors* 20.8 (2020): 2390. doi: 10.3390/s20082390.
- [43] Xu, Huilin, and Liuqing Yang. "Ultra-wideband technology: Yesterday, today, and tomorrow." *2008 IEEE Radio and Wireless Symposium*. IEEE, 2008.
- [44] Balanis, Constantine A. *Antenna theory: analysis and design*. John Wiley & sons, 2016.
- [45] CST. "CST Microwave Studio, Workflow and Solver Overview." (2020).
- [46] Sharma, Mahendra Mohan, et al. "Compact planar monopole UWB antenna with quadruple band-notched characteristics." *Progress In Electromagnetics Research C* 47 (2014): 29-36.
- [47] Rizvi, Syed Naheel Raza, et al. "A Compact Size Antenna for Extended UWB with WLAN Notch Band Stub." *Applied Sciences* 13.7 (2023): 4271. <https://doi.org/10.3390/app13074271>
- [48] Kumar, Girish, np Agrawall, and K. P. Ray. "Wide-band planar monopole antennas." (1998). doi: 10.1109/8.660976.
- [49] Rao, Devireddy Sreenivasa, and Govardhani Immadi. "A Penta band notched elliptical planar monopole antenna for UWB applications." *Progress In*

Electromagnetics Research M 93 (2020): 53-66.

- [50] Ali, Faruk, and Sudhabindu Ray. "SAR analysis for handheld mobile phone using DICOM based voxel model." *Journal of Microwaves, Optoelectronics and Electromagnetic Applications* 12 (2013): 363-375.
- [51] Zakavi, Parisa, Nemaï Chandra Karmakar, and Ian Griggs. "Wireless orthopedic pin for bone healing and growth: Antenna development." *IEEE transactions on antennas and propagation* 58.12 (2010): 4069-4074. doi: 10.1109/TAP.2010.2078459.
- [52] Kiourti, Asimina, and Konstantina S. Nikita. "A review of implantable patch antennas for biomedical telemetry: Challenges and solutions [wireless corner]." *IEEE Antennas and Propagation Magazine* 54.3 (2012): 210-228. doi: 10.1109/MAP.2012.6293992.
- [53] Alomainy, Akram, and Yang Hao. "Modeling and characterization of biotelemetric radio channel from ingested implants considering organ contents." *IEEE Transactions on Antennas and Propagation* 57.4 (2009): 999-1005. doi: 10.1109/TAP.2009.2014531.
- [54] Moore, R. "Effects of a surrounding conducting medium on antenna analysis." *IEEE Transactions on Antennas and Propagation* 11.3 (1963): 216-225. doi: 10.1109/TAP.1963.1138043.
- [55] Huang, Yi, and Kevin Boyle. "Antennas." *From Theory to Practice*. 2008. doi: 10.1002/9780470772911.
- [56] MathWorks, Inc. (2021). Matlab R2021a. <https://www.mathworks.com>.

## الخلاصة

يعد اكتشاف الشظايا في جسم الإنسان مهمة تصوير طبي يتم إجراؤها عادةً باستخدام الأشعة السينية أو التصوير المقطعي المحوسب (CT) أو الموجات فوق الصوتية أو التصوير بالرنين المغناطيسي (MRI). يمكن أن توفر تقنيات التصوير هذه صورًا مفصلة للأعضاء الداخلية والعظام، إلا أن هذه الطرق تعاني من عدم تمييز الشظايا غير المعدنية، الإشعاع المؤين، عدم التمييز بين الشظايا والعظام وتستغرق وقتًا طويلاً، على التوالي.

يتضمن التصوير الطبي بالميكروويف استخدام الموجات الكهرومغناطيسية لإنشاء صور للهياكل الداخلية لجسم الإنسان، ويتميز بأنه تصوير آمن وغير جراحي. يمكن دمج التصوير بالموجات الدقيقة مع الشبكات العصبية لتحليل وتفسير بيانات الميكروويف المجمعة.

في هذا البحث ، تم استخدام الشبكة العصبية العميقة للتعرف على وجود أو غياب وحجم ومواقع الشظايا. لبناء نموذج، تم استخدام جهاز محاكاة كهرومغناطيسي CST Microwave Studio. يتكون هذا النموذج من أربع طبقات (جلد ودهن وعضل وعظم) ذات موصلية وسماحية نسبية مختلفة. وتمتلك الشظايا الكروية أنصاف أقطار مختلفة (5 مم و10 مم و15 مم) في أماكن مختلفة في النموذج. تم توجيه الإشارة إلى النموذج باستخدام هوائي أحادي عريض النطاق، والذي استُخدم أيضًا لالتقاط الإشارات المنعكسة. تعمل الإشارة المرسله في نطاق تردد من 1 جيجاهرتز إلى 6 جيجاهرتز. من أجل تحديد ما إذا كانت الشظايا موجودة أم لا وحجمها وموقعها، تم تحليل الإشارات المجمعة باستخدام شبكة عصبية عميقة. من المهم تحديد التصميم المناسب وخوارزمية التعلم للشبكة العصبية لتحقيق أفضل النتائج. يمكن استخدام برنامج MATLAB لاختبار أحجام الشبكات العصبية المختلفة واستنتاج ما هو أفضل نموذج.

تم الحصول على نتائج استخدام الشبكة العصبية بنسبة نجاح 90% في تحديد الشظايا، و86% نجاح في تحديد حجم الشظايا، و78% نجاح في تحديد عمق الشظايا، كما تم الحصول على نتائج أفضل عند استخدام الـ CNN حيث تم التوصل الى 99% نجاح في تحديد وجود القطعة و88% في تحديد حجمها وموقعها.

بشكل عام، يُظهر الجمع بين التصوير بالموجات الدقيقة والشبكات العصبية، وتحديدًا شبكات CNN، إمكانات كبيرة في تحسين دقة وموثوقية أنظمة الكشف عن الشظايا، خاصةً مع وجود كمية كبيرة من البيانات المدربة. يمكن أن تؤدي المزيد من الأبحاث والتطورات في هذا المجال إلى تعزيز تقنيات التصوير الطبي وتحسين رعاية المرضى.

## إقرار المشرف

أشهد بأن هذه الرسالة الموسومة (اكتشاف الاجسام المعدنية باستخدام خوارزميات التعلم العميق للتصوير الطبي بالموجات الدقيقة) قد تم اعدادها من قبل الطالبة (نرمين حسين فتحي) تحت اشرافي في قسم هندسة الاتصالات/ كلية هندسة الالكترونيات / جامعة نينوى, كجزء من متطلبات نيل شهادة الماجستير - علوم في اختصاص هندسة الاتصالات

التوقيع:

التوقيع:

الاسم: أم.د. ضياء محمد علي

الاسم: أم.د. يونس محمود عبوش

التاريخ:

التاريخ:

## إقرار رئيس قسم هندسة الاتصالات

بناءً على التوصيات المقدمة من قبل المشرف والمقيم اللغوي اشرح هذه الرسالة للمناقشة.

التوقيع:

الاسم:

التاريخ:

## قرار المقوم اللغوي

أشهد بأنه قد تمت مراجعة هذه الرسالة من الناحية اللغوية وتصحيح ما ورد فيها من اخطاء لغوية وتعبيرية وبذلك أصبحت الرسالة مؤهلة للمناقشة بقدر تعلق الأمر بسلامة الاسلوب او صحة التعبير.

التوقيع:

الاسم:

التاريخ:

## إقرار رئيس لجنة الدراسات العليا

بناءً على التوصيات المقدمة من قبل المشرف والمقيم اللغوي ورئيس قسم هندسة الاتصالات أشرح هذه الرسالة للمناقشة.

التوقيع:

الاسم:

التاريخ:

اكتشاف الاجسام المعدنية باستخدام خوارزميات التعلم العميق للتصوير الطبي  
بالموجات الدقيقة

دراسة تقدمت بها

نرمين حسين فتحي

الى

مجلس كلية هندسة الالكترونيات

جامعة نينوى

كجزء من متطلبات نيل شهادة الماجستير

في هندسة الاتصالات

باشراف

الاستاذ المساعد الدكتور يونس محمود عبوش

الاستاذ المساعد الدكتور ضياء محمد علي



وزارة التعليم العالي والبحث العلمي

جامعة نينوى

كلية هندسة الالكترونيات

قسم هندسة الاتصالات

اكتشاف الاجسام المعدنية باستخدام خوارزميات التعلم العميق للتصوير الطبي بالموجات  
الدقيقة

نرمين حسين فتحي

رسالة ماجستير علوم في

هندسة الاتصالات

باشراف

الاستاذ المساعد الدكتور يونس محمود عبوش

الاستاذ المساعد الدكتور ضياء محمد علي

2023م

1445هـ

